CalVal Jason-2

Jason-2 validation and cross calibration activities (Annual report 2014)

Contract No 104685/00 - lot 1.2A

Reference : CLS.DOS/NT/15-010

Nomenclature : SALP-RP-MA-EA-22409-CLS

Issue : 1rev 1

Date : January 27, 2015

CLS - 8-10 Rue Hermès - Parc Technologique du Canal - 31520 Ramonville St-Agne - FRANCE
Telephone 33 5 61 39 47 00 / Fax 33 5 61 75 10 14

Chronology Issues:		
Issue:	Date:	Reason for change:
1rev0	January 27, 2015	Creation
1rev1	February 26, 2015	Revision after comments from N. Picot and J-D. Desjonqueres.

People involved in this issue :				
	AUTHORS	**COMPANY**	**DATE**	**INITIALS**
Written by:	H. Roinard P. Matton S. Philipps	CLS CLS CLS		
Checked by:		CLS		
Approved by:		CLS CLS		
Application authorised by:				

Index Sheet :	
Context:	
Keywords:	
Hyperlink:	

Distribution:		
Company	Means of distribution	Names
CLS/DOS	electronic copy	G.DIBARBOURE V.ROSMORDUC
CNES	electronic copy	thierry.guinle@cnes.fr emilie.bronner@cnes.fr jean-damien.desjonqueres@cnes.fr nicolas.picot@cnes.fr aqgp_rs@cnes.fr dominique.chermain@cnes.fr delphine.vergnoux@cnes.fr

List of tables and figures

List of Tables

List of Figures

List of items to be defined or to be confirmed

Applicable documents / reference documents

Contents

1. Introduction

This document presents the synthesis report concerning validation activities of Jason-2 GDRs under SALP contract (N° 104685/00 Lot 1.2A) supported by CNES at the CLS Space Oceanography Division. It covers several points: CAL/VAL Jason-2 activities, Jason-2 / Jason-1 cross-calibration (until mid-2013), particular studies and investigations.
The OSTM/Jason-2 satellite was successfully launched on June, 20th 2008. Since July, 4th, Jason-2 is on its operational orbit. Until January 2009, it was flying in tandem with Jason-1, only 55s apart. Note that from May 2012 onwards, Jason-1 was on a geodetic orbit (see note on Jason-1 geodetic mission [9]). Jason-1 sent its last measurement on 21st June 2013, after about 11.5 years in orbit. Since the beginning of the mission, Jason-2 data have been analyzed and monitored in order to assess the quality of Jason-2 products. Cycle per cycle reports are available on AVISO webpage (http://www.aviso.altimetry.fr/en/data/calval/systematic-calval.html).
This present report assesses the Jason-2 data quality. Missing and edited measurements are monitored. Furthermore relevant parameters derived from instrumental measurements and geophysical corrections are analyzed.
During 2012, the whole Jason-2 mission was reprocessed in GDR-D standard. For more details, please refer to the reprocessing report ([16]), spanning the reprocessing period (cycles 001 to 145), which contains comparisons between previous GDR-T and current GDR-D standard, as well as comparison between Jason-2 GDR-D and Jason-1 and Envisat data. Another report ([15]) focuses on the comparison of Jason-2 GDR-T and GDR-D with Jason-1 data during the first 20 Jason-2 cycles (the formation flight phase, when both satellites were on the same ground-track only 55s apart).

Hereafter, analyzes focus on Jason-1/Jason-2 cross-calibration. During the formation flight configuration (4th July 2008 to 26th January 2009) both satellites were on the same ground track. This allowed to precisely assess parameter discrepancies between both missions in order to detect geographically correlated biases, jumps or drifts. The SLA performances and consistency with Jason-1 are also described. But even after the end of the flight formation phase, and after Jason-1 moved to its geodetic orbit, comparison were still possible until the end of the Jason-1 mission in June 2013. Even if only low order statistics are mainly presented here, other analyzes including histograms, plots and maps are continuously produced and used in the quality assessment process. It is now well recognized that the usefulness of any altimeter data only makes sense in a multi-mission context, given the growing importance of scientific needs and applications, in particular for operational oceanography. One major objective of the Jason-2 mission is to continue the Jason-1 and T/P high precision altimetry and to allow combination with other missions (ENVISAT, Jason-1, SARAL/AltiKa). This kind of comparisons between different altimeter missions flying together provides a large number of estimations and consequently efficient long term monitoring of instrument measurements.
An ISRO (Indian Space Research Organization)/CNES satellite, SARAL (Satellite with ARgos and ALtika), embarks the AltiKa altimeter (working in Ka-band, 35 GHz), built by CNES, as well as an Argos instrument. The launch of this mission on 25th of February 2013 allows to complete the altimetry constellation from 2013 onwards, re-occupying the long-term ERS and Envisat ground track. Comparisons between AltiKa and Jason-2 data are available in [22].

2. Processing status

2.1. Processing

End of 2008 Jason-2 data were already available to end users in OGDR (3h data latency) and IGDR (1-2 days data latency). They were first released in version T and switched at cycle 015 to version C. They stayed in this version till cycle 149 (till 2012/07/31 12:01:59 for OGDR), this is the same version (concerning the geophysical standards) as Jason-1 data (for better compatibility). GDR data were released in version T during August 2009. During 2012 the whole GDR dataset was reprocessed in GDR-D version. **In this report, GDR-D from cycle 1 to 230 are used (until 09/10/2014)**. A description of the different Jason-2 products is available in the OSTM/Jason-2 Products handbook ([52]). Note that since 5th of April 2013 (cycle 175), platform moduleB has been used. During cycle 226 and 227, the precise orbit ephemeris (orbit in GDR) was based on DORIS and SLR only due to payload GPS unavailability. Since cycle 228, GPS-B (instead of GPS-A) is operational.
The purpose of this document is to report the major features of the data quality from the Jason-2 mission. As Jason-2 was in formation flight with Jason-1 (only 55 s apart) until January 2009, this report also uses results from intercalibration with Jason-1.

2.2. CAL/VAL status

2.2.1. List of events

The following table shows the major planned events during the Jason-2 mission.

Dates	Events	Impacts
4 July 2008 5h57	Start of Jason-2 Cycle 0	
4 July 2008 12h15	Start of Poseidon3 altimeter. Tracking mode : autonomous acquisition, median	Start of level2 product generation.
04 July 2008 13:47:52 to 04 July 2008 14:13:36	Poseidon3 altimeter. Tracking mode : Diode acquisition, median	
04 July 2008 14:14:39 to 17 July 2008 15:30:22	Poseidon3 altimeter. Tracking mode : Diode acquisition, SGT	
8 July 2008 4h45 - 5h25	Poseidon3 altimeter. Dedicated period for validation of tracking mode performances	small data gaps on corresponding passes [Cycle 0]
.../...		

Dates	Events	Impacts
11 July 2008 13h00-13h01 and 13h04-13h12	Poseidon3 altimeter. Tracking mode : Diode-DEM (functional)	Functional test of DIODE-DEM tracking mode while onboard DEM was not correct, leading to wrong waveforms and so impacts on altimeter retracking outputs.
12 July 2008 1h20	Start of Jason-2 Cycle 1	
16 July 2008 7h10-17h08	upload POS3 - DEM	Data gap on corresponding passes [Cycle 1, Pass 108-144]
17 July 2008 7h29-11h30	upload POS3 - DEM	Data gap on corresponding passes [Cycle 1, Pass 108-144]
17 July 2008 15:30:22 to 31 July 2008 21:17:08 UTC	Poseidon3 altimeter. Tracking mode : Diode acquisition, median	
21 July 2008 23h18	Start of Jason-2 Cycle 2	
31 July 2008 21:17:09 to 10 August 2008 19:15:39	Jason-2 Cycle 3: Poseidon3 altimeter. Tracking mode : Diode-DEM	
10 August 2008 19:15:40 to 20 August 2008 17:14:10	Jason-2 Cycle 4: Poseidon3 altimeter. Tracking mode : Diode acquisition, median	
20 August 2008 17:14:11 to 30 August 2008 15:12:43	Jason-2 Cycle 5: Poseidon3 altimeter. Tracking mode : Diode-DEM	
30 August 2008 15:12:43 to 9 September 2008 13:11:15	Jason-2 Cycle 6: Poseidon3 altimeter. Tracking mode : Diode acquisition, median	
9 September 2008 13:11:15 to 19 September 2008 11:09:47	Jason-2 Cycle 7: Poseidon3 altimeter. Tracking mode : Diode-DEM	
19 September 2008 11:09:47 to 29 September 2008 09:08:19	Jason-2 Cycle 8: Poseidon3 altimeter. Tracking mode : Diode acquisition, median	
11 Mai 2009 12:09 to 14 Mai 2009 13:09	Upload POS3 (new DEM)	data gaps (northern hemisphere) for passes 154 to 231
		.../...

Dates	Events	Impacts
2 February 2009 06:55:11 to 15:58:05	software upload to Poseidon-3	data gap between passes 204 and 213
4 June 2009 06:31:27 to 14 June 2008 04:29:59	Jason-2 Cycle 34: Poseidon3 altimeter. Tracking mode : Diode-DEM	
12 February 2010	Upload of Doris V8.0 flight software	improved OGDR orbit accuracy
16 September 2010	Jason-2 Cycle 81: Upload of DEM patch for Gavdos transponder calibration	data gap for passes 087 and 237
17 February 2011	GPSP OBS revert upload	
12-14 September 2012	DORIS OBS upload (DORIS restart on 19th September)	OGDR data gap (during the DORIS restart)
15 May 2013	update on Usingen receiver was done on 15-May-2013 at 11:05Z in order to solve a problem with the TM receiver	
5-15 March 2014	Tracking mode : Diode-DEM	gain of available measurements on earth
18 March 2014	Update of TRIODE software (for OGDR).	Reduction of 14days signal in OGDR SLA.
22 June-2 July 2014	Tracking mode : Diode-DEM	gain of available measurements on earth
9 September 2014	switch to GPS-B (instead of GPS-A)	

Table 1: Planned events

2.2.2. Missing measurements

This section presents a summary of major satellite or ground segment events that occurred from cycle 0 to 230. Table 2 gives a status about the number of missing passes (or partly missing) for GDRs, as well as the associated events for each cycle.
During 2014, cycles 196 to 230 were analyzed. Few altimetry data were missing due to technical or operator problems (mainly network problems between Fairbanks and SOCC). Except these cases, missing measurements are mostly due to scheduled events (like altimeter expert calibrations performed every 6 month or software upload).
The following table gives an overview over missing data and why it is missing.

Jason-2 Cycles/Pass	Dates	Events
000/222-224	10/07/2008 - 18:28:02 to 20:25:04	Missing telemetry (Usingen station pb)
000/232	11/07/2008 - 03:57:08 to 04:30:30	Partly missing due to altimeter calibration (long LPF)
000/235	11/07/2008 - 07:01:28 to 07:27:41	Partly missing due to altimeter calibration (CNG step)
001/44-46	13/07/2008 - 17:40:00 to 19:37:30	Missing telemetry (Usingen station pb)
001/48-50	13/07/2008 - 21:37:02 to 23:30:00	Missing telemetry (NOAA station pb)
001/108-144		several passes partly missing due to upload of new DEM (planned unavailability)
003/032-035	02/08/2008 - 02:23:45 to 05:46:30	Passes 32 and 35 are partly missing, passes 33 and 34 are completely missing due to missing telemetry (Usingen)
005/236-241	29/08/2008 - 21:44:56 to 30/08/2008 02:52:07	Missing telemetry (Usingen station pb): passes 237 to 240 completely missing, passes 236 and 241 partly missing
006/232	08/09/2008 - 15:48:00 to 16:21:22	pass 232 partially missing due to altimeter calibration (long LPF)
006/235	08/09/2008 - 18:53:00 to 19:19:10	pass 235 partially missing due to altimeter calibration (CNG step)
016/73	10/12/2008 - 15:11:19 to 15:13:27	pass 73 partially missing due to 1) upload of correction for low signal tracking anomaly and 2) memory dumps (planned unavailability)
026/33	18/03/2009 - 05:09:15 to 05:10:44	pass 33 has approximately 90 seconds of missing ocean measurements in gulf of guinea (probably due to missing telemetry)
029/209-210	23/04/2009 - 20:18:36 to 20:35:11	data gap over land (on transition between passes 209 and 210) due to missing telemetry
031/154-231	11/05/2009 12:09 to 14/05/2009 13:09	Upload of new DEM leading to missing portions (northern hemisphere) for passes 154 to 231
		.../...

Jason-2 Cycles/Pass	Dates	Events
033/204-213	02/06/2009 - 06:55:11 to 15:58:05	Passes 205 to 212 are completely missing. Passes 204 and 213 are partly missing with respectively 100% and 96% of missing measurements over ocean. This is due to software upload to Poseidon-3.
034/232	13/06/2009 - 07:07:03 to 07:40:23	Due to long calibration, pass 232 is partly missing with 65% of missing measurements over ocean.
034/235	13/06/2009 - 10:11:41 to 10:37:50	Due to calibration CNG step, pass 235 is partly missing with 8% of missing measurements over ocean.
037/54	06/07/2009 - 02:33:12 to 02:34:33	pass 054 has a small data gap due to missing PLTM
053/57	11/12/2009 - 20:38:19 to 21:29:43	passes 57 and 58 have a data gap due to Gyro calibration
053/232	18/12/2009 - 16:39 to 17:12	pass 232 has a data gap due to CAL2 calibration
053/235	18/12/2009 - 19:43	pass 235 has a 26 minutes data gap due to CNG calibration (mostly over land)
072/199	23/06/2010 - 19:15:37 to 19:16:59	pass 199 has small data gap due to missing telemetry
073/232	05/07/2010 - 00:09:33 to 00:42:54	pass 232 has a data gap due to CAL2 calibration
073/235	05/07/2010 - 03:14:11 to 03:40:20	pass 235 has a data gap due to CNG calibration (mostly over land)
081/087	16/09/2010 - 16:40:22 to 16:52:48	pass 087 has a data gap due to upload of DEM update (for GAVDOS transponder calibration)
081/237	22/09/2010 - 13:07:27 to 13:18:12	pass 237 has a data gap due to upload of DEM update (for GAVDOS transponder calibration)
084/031	14/10/2010 - 06:02 to 06:11:15	Calibration (I2 and Q2)
084/031-032	14/10/2010 - 06:12 to 06:21:15	Calibration (I and Q)
084/043	14/10/2010 - 17:00:57 to 17:02:39	pass 043 has a small data gap due to missing PLTM
094/231	29/01/2011 - 04:50 to 04:55	Calibration CAL1 (14% of missing ocean data)
094/232	29/01/2011 - 05:38 to 06:11	Calibration CAL2 (65% of missing ocean data)
		.../...

Jason-2 Cycles/Pass	Dates	Events
094/235	29/01/2011 - 08:37 to 09:03	Calibration CNG (mostly over land, 9% of missing ocean data)
101/133-135	04/04/2011 - 18:49:08 to 21:03:48	Telemetry outage at Usingen, passes 133 to 135 have respectively 23%, 100%, and 91% of missing ocean data
110/158-159	04/07/2011 - 00:27:29 to 01:27:29	Gyro calibration. Passes 158 and 159 have respectively 18% and 88% of missing ocean data
115/232	25/08/2011 - 11:07:35 to 11:40:56	Calibration CAL2: 65% of missing ocean data
115/235	25/08/2011 - 14:12 to 14:38	Calibration CNG: mostly over land, 8% of missing ocean data
132/232	10/02/2012 - 00:42:26 to 01:14:03	Calibration CAL2: 65% of missing ocean data
132/235	10/02/2012 - 03:47:11 to 04:13:20	Calibration CNG: mostly over land, 8% of missing ocean data
135/105	05/03/2012 - 19:54:49 to 20:26:14	technical problem and operator error: 25% of missing ocean data
136/191	19/03/2012 - 02:15:18 to 02:50:11	problem of ACK: 56% of missing ocean data
145/143	14/06/2012 - 11:41:15 to 11:42:58	pass 143 has a small data gap due to missing telemetry
145/248	18/06/2012 - 13:20:10 to 13:21:29	pass 248 has a small data gap
147/022	29/06/2012 - 13:45:30 to 13:49:46	pass 022 has a small data gap due to missing telemetry (8% of missing ocean data)
147/134	03/07/2012 - 22:41:25 to 22:43:58	pass 134 has a small data gap due to operator error (5% of missing ocean data)
154/210	14/09/2012 - 07:45:08 to 07:46:07	pass 210 has a small portion of missing data in central Pacific
156/232	05/10/2012 - 00:07:08 to 00:40:30	Calibration CAL2: 66% of missing ocean data
156/235	05/10/2012 - 03:11:47 to 03:37:57	Calibration CNG: mostly over land, 9% of missing ocean data
		.../...

Jason-2 Cycles/Pass	Dates	Events
168/158-159	29/01/2013 - 03:08:20 to 04:02:37	Gyro calibration. Passes 158 and 159 have respectively 14% and 100% of missing ocean data
172/96-97	07/03/2013 - 08:18:37 to 09:30:49	Operator error. Passes 96 and 97 have respectively 72% and 52% of missing ocean data
174/43-161	25/03/2013 - 02:42 to 29/03/2013 17:53	First Safe Hold Mode. Pass 43 has 63% of missing ocean data and passes 44 to 161 are entirely missing
174-191/175-83	30/03/2013 - 21:57 to 05/04/2013 14:49	Second Safe Hold Mode. About cycle 174, pass 191 has 9% of missing ocean data and passes 192 to 254 are entirely missing. About cycle 175, passes 1 to 82 are entirely missing and pass 83 has 90% of missing measurements over ocean.
178/234		Due to a problem with TM receiver, pass 234 is partly missing (north of pacific) and has 10% of missing measurements over ocean
179/ 38		Due to a problem with TM receiver, pass 38 has 6.8% of missing measurements over ocean
182/235	19/06/2013 from 22 :33 :29 to 22 :59 :37	pass 235 has a data gap due to CNG calibration (mostly over land)
190/185 - 191/116	05/09/2013 at 07 :44 :17 to 12/09/2013 at 12 :25 :52	Third Safe Hold Mode. Concerning cycle 190, pass 185 has 10.2% of missing measurements over sea and passes 186 to 254 are entirely missing. Concerning cycle 191, passes 1 to 115 are missing.
197/035	07/11/2013 - 20:45	Pass 35 has a small data gap.
198/235	25/11/2013 - 14:04:02 to 14:37:35	Calibration (I and Q) with 8% of missing ocean data
207/178	20/02/2014 - 14:30:33 to 14:43:50	24.6% of global missing data and 11.8% missing data over ocean due to DEM upload
208/027	24/02/2014 - 14:38:26 to 14:52:07	40.7% missing data over ocean due to recurring network problems between Fairbanks and SOCC
218/235	11/06/2014 - 21:34:36 to 22:13:13	Poseidon3/Jason2 special calibration. 9% missing data over ocean
222/114	16/07/2014 - between 20:05:19 and 20:10:34 and between 20:23:21 and 20:34:51	Gyro calibration. Pass 114 has 73% of missing ocean data
		.../...

Jason-2 Cycles/Pass	Dates	Events

Table 2: Missing pass status

2.2.3. Edited measurements

Table 3 indicates particular high editing periods (see section 3.2.1.). Most of the occurrences correspond to radiometer wet troposphere correction at default value (due to AMR unavailability) or altimeter low signal tracking anomaly (AGC anomaly), though the latter concerns only few measurements and was corrected during cycle 16.
There is no particular event between cycle 197 and cycle 230.

Jason-2 Cycles/Passes	Date	Comments
000/89	05/07/08 - 14:22:07 to 14:23:38	Partly edited by several parameters out of threshold (AGC anomaly)
000/134	07/07/08 - 08:06:37 to 08:28:57	Partly edited by several parameters out of threshold (AGC anomaly)
000/156	08/07/08 - 04:35:12 to 05:31:01	rain flag is set (dotted), probably related to start/stop sequence (from 04:45 to 05:24)
000/234	11/07/08 - 05:45:12 to 05:49:03	Partly edited by several parameters out of threshold (AGC anomaly)
000/241	11/07/08 - 13:04:27 to 13:09:11	Partly edited by ice flag (number of elementary Ku-band measurements at 0, AGC=16.88) due to test of altimeter DEM mode
001/		several passes partly edited by several parameters out of threshold (AGC anomaly)
002/		several passes partly edited by several parameters out of threshold (AGC anomaly)
004/		several passes partly edited by several parameters out of threshold (AGC anomaly)
006/		several passes partly edited by several parameters out of threshold (AGC anomaly)
008/		several passes partly edited by several parameters out of threshold (AGC anomaly)
		.../...

Jason-2 Cycles/Passes	Date	Comments
009/		several passes partly edited by several parameters out of threshold (AGC anomaly)
010/		several passes partly edited by several parameters out of threshold (AGC anomaly)
011/		several passes partly edited by several parameters out of threshold (AGC anomaly)
012/		several passes partly edited by several parameters out of threshold (AGC anomaly)
013/		several passes partly edited by several parameters out of threshold (AGC anomaly)
014/		several passes partly edited by several parameters out of threshold (AGC anomaly)
015/		several passes partly edited by several parameters out of threshold (AGC anomaly)
019/024-042	07/01/ 11:00:35 to 08/01/2009 03:23:34	radiometer wet troposphere correction at default value due to AMR unavailability
019/119-161	11/01/ 03:56:38 to 12/01/2009 19:26:14	radiometer wet troposphere correction at default value due to AMR unavailability
110/047	29/09/2011 16:14 to 16:20	a portion of pass 47 is edited by radiometer wet troposphere correction out of threshold or at default values (radio-frequency interference from a ground based source)
168/141-144	28/01/2013 10:50 to 13:22	radiometer wet troposphere correction at default value due to AMR unavailability
169/176-181	08/02/2013 17:37 to 22:44	radiometer wet troposphere correction at default value due to AMR unavailability
174/162-163	29/03/2013 17:53 to 29/03/2013 19:36	radiometer wet troposphere correction at default value after first Safe Hold Mode
175/83-85	05/04/2013 14:18 to 16:27	radiometer wet troposphere correction at default value after second Safe Hold Mode
191/116-125	12/09/2013 12:25:52 to 21:56:39	radiometer wet troposphere correction at default value after third Safe Hold Mode
		.../...

Jason-2 Cycles/Passes	Date	Comments
194/227	16/10/2013 15:02:08 to 15:04:17	a part of pass 227 is rejected near Kamchatka Peninsula because of ice flag (linked to high radiometer minus model wet troposphere difference, and probably related to typhoon WIPHA that happened in the region between the 15th and 17th October 2013)

Table 3: Edited measurement status

2.3. Models and Standards History

Three versions of the Jason-2 Operational Geophysical Data Records (OGDRs) and Interim Geophysical Data Records (IGDRs) have been generated up to now. These three versions are identified by the version numbers "T" (for test), "c" and "d" in the product filename. For example, version "T" IGDRs are named "JA2_IPN_2PT", version "c" IGDRs are named "JA2_IPN_2Pc", and version "d" IGDRs are named "JA2_IPN_2Pd". All three versions adopt an identical data record format as described in Jason-2 User Handbook ([52]). Versions "T" and "c" differ only slightly (names of variables are corrected and 3 variables added). Version "T" O/IGDRs were the first version released soon after launch and was disseminated only to OSTST community. Version "c" O/IGDRs were first implemented operationally from data segment 141 of cycle 15 for the OGDRs (3rd December 2008) and cycle 15 for the IGDRs. Version "c" of Jason-2 data is consistent with version "c" of Jason-1 data. Version "d" O/IGDRs were first implemented operationally from data segment 78 of cycle 150 for the OGDRs (31st July 2012) and cycle 150 for the IGDRs. GDR data switched to version "d" from cycle 146 onwards, but previous cycles 1 to 145 were reprocessed in version "d" during 2012. Therefore the whole Jason-2 mission is available in GDR version "d". The tables 4 and 5 below summarize the models and standards that are adopted for versions "T" / "c" and "d" of Jason-2 data. More details on some of these models are provided in Jason-2 User Handbook document ([52]).
Impact of GDR reprocessing can be found in the reprocessing reports [16] and [15].

From cycle 170 to 178, the flag "qual_inst_corr_1hz_sig0_ku" was wrongly set to one because of an out of thresholds criterion. From cycle 179 onwards, the flag "qual_inst_corr_1hz_sig0_ku" won't constantly be set as the threshold used to set this flag has been adjusted in the processing chain, in order to take into account the natural instrumental drift.

Model	Product version "T" and "c"
Orbit	Based on Doris onboard navigator solution for OGDRs. DORIS tracking data for IGDRs (DORIS + SLR tracking for cycles 20 to 78) DORIS+SLR+GPS tracking data for GDRs. Using POE-C
Altimeter Retracking	<u>"Ocean" retracking</u>: MLE4 fit from 2nd order Brown model: MLE4 simultaneously retrieves the following 4 parameters from the altimeter waveforms: • Epoch (tracker range offset) → altimeter range • Composite Sigma → SWH • Amplitude → Sigma0 • Trailing Edge slope → Square of mispointing angle
	.../...

Model	Product version "T" and "c"
	"Ice" retracking: Geometrical analysis of the altimeter waveforms, which retrieves the following parameters: • Epoch (tracker range offset) → altimeter range • Amplitude → Sigma0
Altimeter Instrument Corrections	Consistent with MLE4 retracking algorithm.
Jason-2 Advanced Microwave Radiometer (AMR) Parameters	Using calibration parameters derived from long term calibration tool developed and operated by NASA/JPL.
Dry Troposphere Range Correction	From ECMWF atmospheric pressures and model for S1 and S2 atmospheric tides
Wet Troposphere Range Correction from Model	From ECMWF model
Ionosphere correction from model	Based on Global Ionosphere TEC Maps from JPL
Sea State Bias Model	Empirical model derived from 3 years of MLE4 Jason-1 altimeter data with version "b" geophysical models.
Mean Sea Surface Model	CLS01
Mean Dynamic Topography Model	MDT_RIO_2005
Geoid	EGM96
Bathymetry Model	DTM2000.1
Inverse Barometer Correction	Computed from ECMWF atmospheric pressures after removing S1 and S2 atmospheric tides
Non-tidal High-frequency De-aliasing Correction	Mog2D high resolution ocean model on I/GDRs. None on OGDRs. Ocean model forced by ECMWF atmospheric pressures after removing S1 and S2 atmospheric tides.
Tide Solution 1	GOT00.2 + S1 ocean tide . S1 load tide ignored
Tide Solution 2	FES2004 + S1 and M4 ocean tides. S1 and M4 load tides ignored
Equilibrium long-period ocean tide model.	From Cartwright and Taylor tidal potential.
	.../...

Model	Product version "T" and "c"
Non-equilibrium long-period ocean tide model.	Mm, Mf, Mtm, and Msqm from FES2004
Solid Earth Tide Model	From Cartwright and Taylor tidal potential.
Pole Tide Model	Equilibrium model
Wind Speed from Model	ECMWF model
Altimeter Wind Speed	Wind speed table derived from Jason-1 data (Collard, [39]).

Table 4: Models and standards adopted for the Jason-2 version "T" and "c" products. Adapted from [52]

Model	Product version "d"
Orbit	Based on Doris onboard navigator solution for OGDRs. DORIS tracking data for IGDRs (expect for cycles 20 to 78 : DORIS + SLR tracking) DORIS+SLR+GPS-A tracking data for GDRs cycles 1 to 225. DORIS + SLR tracking for GDRs for cycles 226 and 227) DORIS+SLR+GPS-B tracking data for GDRs from cycle 228 onwards.
Altimeter Retracking	"Ocean MLE4" retracking: MLE4 fit from 2nd order Brown analytical model: MLE4 simultaneously retrieves the 4 parameters that can be inverted from the altimeter waveforms: • Epoch (tracker range offset) → altimeter range • Composite Sigma → SWH • Amplitude → Sigma0 • Square of mispointing angle (Ku band only, a null value is used in input of the C band retracking algorithm)

.../...

Model	Product version "d"
	"Ocean MLE3" retracking: MLE3 fit from 1st order Brown analytical model: MLE3 simultaneously retrieves the 3 parameters that can be inverted from the altimeter waveforms: • Epoch (tracker range offset) → altimeter range • Composite Sigma → SWH • Amplitude → Sigma0 "Ice" retracking: Geometrical analysis of the altimeter waveforms, which retrieves the following parameters: • Epoch (tracker range offset) → altimeter range • Amplitude → Sigma0
Altimeter Instrument Corrections	Two sets: • on set consistent with MLE4 retracking • on set consistent with MLE3 retracking
Jason-2 Advanced Microwave Radiometer (AMR) Parameters	Using calibration parameters derived from long term calibration tool developed and operated by NASA/JPL.
Dry Troposphere Range Correction	From ECMWF atmospheric pressures and model for S1 and S2 atmospheric tides
Wet Troposphere Range Correction from Model	From ECMWF model
Ionosphere correction from model	Based on Global Ionosphere TEC Maps from JPL
Sea State Bias Model	Two empirical models: • MLE4 version derived from 1 year of MLE4 Jason-2 altimeter data with version "d" geophysical models • MLE3 version derived from 1 year of MLE3 Jason-2 altimeter data with version "d" geophysical models
Mean Sea Surface Model	MSS_CNES_CLS11
	.../...

Model	Product version “d”
Mean Dynamic Topography Model	MDT_CNES-CLS09
Geoid	EGM96
Bathymetry Model	DTM2000.1
Inverse Barometer Correction	Computed from ECMWF atmospheric pressures after removing S1 and S2 atmospheric tides
Non-tidal High-frequency De-aliasing Correction	Mog2D high resolution ocean model on I/GDRs. None on OGDRs. Ocean model forced by ECMWF atmospheric pressures after removing S1 and S2 atmospheric tides.
Tide Solution 1	GOT4.8 + S1 ocean tide. S1 and M4 load tide included.
Tide Solution 2	FES2004 + S1 and M4 ocean tides. S1 and M4 load tides ignored
Equilibrium long-period ocean tide model.	From Cartwright and Taylor tidal potential.
Non-equilibrium long-period ocean tide model.	Mm, Mf, Mtm, and Msqm from FES2004
Solid Earth Tide Model	From Cartwright and Taylor tidal potential.
Pole Tide Model	Equilibrium model
Wind Speed from Model	ECMWF model
Altimeter Wind Speed	Wind speed table derived from Jason-1 data (Collard, [39]). In addition, a calibration bias of 0.32 is applied to JA2 Ku-band sigma0 prior wind speed computation.
Rain flag	Derived from comparisons to thresholds of the radiometer-derived integrated liquid water content and of the difference between the measured and the expected Ku-band backscatter coefficient
Ice flag	Derived from comparison of the model wet tropospheric correction to a dual-frequency wet tropospheric correction retrieved from radiometer brightness temperatures, with a default value issued from a climatology table

Table 5: Models and standards adopted for the Jason-2 version “d” products. Adapted from [52]

The differences between GDR-T and GDR-D products are listed in the table 6.

Model	Product Version "T"	Product Version "d"
Orbit	EIGEN-GL04S with time-varying gravity (annual and semi-annual terms up to deg/ord 50) + ITRF 2005 DORIS+SLR+GPS	EIGEN-GRGS_RL02bis_MEAN_FIELD with time-varying gravity (annual, semi-annual, and drifts up to deg/ord 50) + ITRF 2008 DORIS+SLR+GPS (increased weight for GPS)
Altimeter Retracking	MLE4 + 2nd order Brown model : MLE4 simultaneously retrieves the 4 parameters that can be inverted from the altimeter waveforms: epoch, SWH, Sigma0 and mispointing angle. This algorithm is more robust for large off-nadir angles (up to 0.8°).	Identical to version "T", in addition altimeter parameters are also available for MLE3 retracking
Altimeter Instrument Corrections	Consistent with MLE4 retracking algorithm.	One consistent with MLE4 retracking + One consistent with MLE3 retracking
Jason-2 Microwave Radiometer Parameters	Using calibration parameters derived from long term calibration tool developed and operated by NASA/JPL	Using calibration parameters derived from long term calibration tool developed and operated by NASA/JPL + enhancement in coastal regions + correction of anomaly in 34 GHz channel addition of radiometer rain and ice flag addition of radiometer 18.7 GHz/ 23.8 GHz/ 34 GHz antenna gain weighted land fraction in main beam
Dry Troposphere Range Correction	From ECMWF atmospheric pressures and model for S1 and S2 atmospheric tides.	Identical to version "T"
Wet Troposphere Range Correction from Model	From ECMWF model.	Identical to version "T"
Back up model for Ku-band ionospheric range correction.	Derived from JPL's Global Ionosphere Model (GIM) maps	Identical to version "T"
		.../...

Model	Product Version "T"	Product Version "d"
Sea State Bias Model	Empirical model derived from 3 years of Jason-1 MLE4 altimeter data with version "b" geophysical models	Empirical models derived from Jason-2 data (One consistent with MLE4 retracking + One consistent with MLE3 retracking)
Mean Sea Surface Model	CLS01	CNES_CLS_2011
Geoid	EGM96	Identical to version "T"
Bathymetry Model	DTM2000.1	Identical to version "T"
Mean Dynamic Topography	Rio 2005 solution	CNES_CLS2009 solution
Inverse Barometer Correction	Computed from ECMWF atmospheric pressures after removing model for S1 and S2 atmospheric tides.	Identical to version "T"
Non-tidal High-frequency De-aliasing Correction	Mog2D high resolution ocean model. Ocean model forced by ECMWF atmospheric pressures after removing model for S1 and S2 atmospheric tides.	Identical to version "T"
Tide Solution 1	GOT00.2 + S1 ocean tide . S1 load tide ignored.	GOT4.8 (S1 ocean tide and S1 load tide are included).
Tide Solution 2	FES2004 + S1 and M4 ocean tides. S1 and M4 load tides ignored	Identical to version "T"
Equilibrium long-period ocean tide model.	From Cartwright and Taylor tidal potential.	Identical to version "T"
Non-equilibrium long-period ocean tide model.	Mm, Mf, Mtm, and Msqm from FES2004.	Mm, Mf, Mtm, and Msqm from FES2004 + correction for a bug
Solid Earth Tide Model	From Cartwright and Taylor tidal potential.	Identical to version "T"
Pole Tide Model	Equilibrium model.	Equilibrium model + correction of error which was present over lakes and enclosed seas.
Wind Speed from Model	ECMWF model	Identical to version "T"
		.../...

Model	Product Version “T”	Product Version “d”
Altimeter Wind Speed	Table derived from Jason-1 GDR data.	Table is identical to version “T”, but the inputs differ.
Altimeter Rain Flag	Set to default values	Derived from Jason-2 sigma naught MLE3 values
Altimeter Ice Flag	Flag based on the comparison of the model wet tropospheric correction and of a radiometer bi frequency wet tropospheric correction (derived from 23.8 GHz and 34.0 GHz), accounting for a backup solution based on climatologic estimates of the latitudinal boundary of the ice shelf, and from altimeter wind speed.	Identical to version “T”
Update of the altimeter characterization file		PRF value is no longer truncated (2058.513239 Hz) Bias of 18.092 cm applied for Ku- and C-band range (corrects the value of the distance between center of gravity and the reference point of the altimeter antenna) Antenna aperture angle (at 3 dB) changed to 1.29 deg MQE setting is applied during 20 Hz to 1 Hz compression Tracker_range_res at a more precise value
other	LTM calculated over 1 day	LTM calculated over 7 days (sliding window) and applied for one day. the origin of the constant part of the time tag bias was found and is directly corrected in the Gdr-D datation.

Table 6: Models and standards adopted for the Jason-2 product version “T”, and “d”

3. Data coverage and edited measurements

3.1. Missing measurements

3.1.1. Over land and ocean

Determination of missing measurements relative to the theoretically expected orbit ground pattern is an essential tool to detect missing telemetry or satellite events for instance. Applying the same procedure for Jason-1 and Jason-2, the comparison of the percentage of missing measurements has been performed. Jason-2 can use several onboard tracking modes: Split Gate Tracker (ie the Jason-1 tracking mode, and used for cycle 0 and half of cycle 1), Diode/DEM (used for cycles 3, 5, 7, 34, 209 and 220) and median tracker (used for the other cycles). These different tracking modes are described by [44]. Thanks to the new modes of onboard tracking (median tracker and Diode/DEM), the data coverage over land surface was dramatically increased in comparison with Jason-1 depending on the tracker mode and the period. Figure 1 shows the percentage of missing measurements for Jason-2 and Jason-1 (all surfaces) computed with respect to a theoretical possible number of measurements. Due to differences between altimeter tracking algorithms, the number of available data is greater for Jason-2 than for Jason-1. Differences appear on land surfaces as shown in figure 2. The missing data are highly correlated with the mountains location. The monitoring shows a slight annual signal. The slight increase of Jason-2 missing measurements end of 2008 (during cycle 16) is related to the correction of the low signal tracking anomaly. During 2013, Jason-2 entered safe hold mode twice in March (from 25/03/2013 to 29/03/2013 and from 30/03/2013 until 05/04/2013, during cycles 174 and 175) and a third time in September (from 05/09/2013 to 12/09/2013, during cycles 190-191).

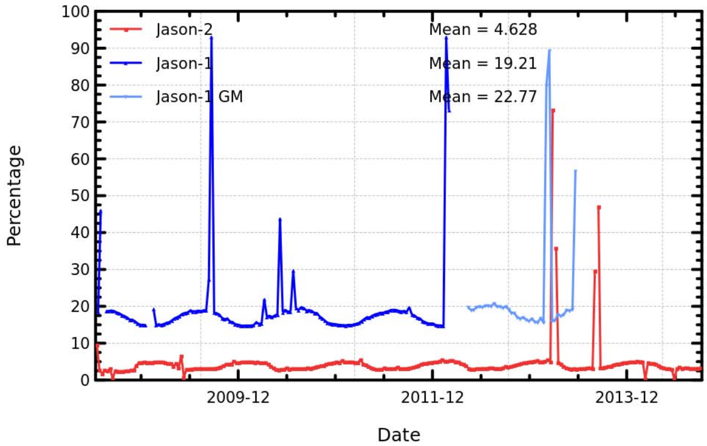

Figure 1: Percentage of missing measurements over ocean and land for JA2 and JA1

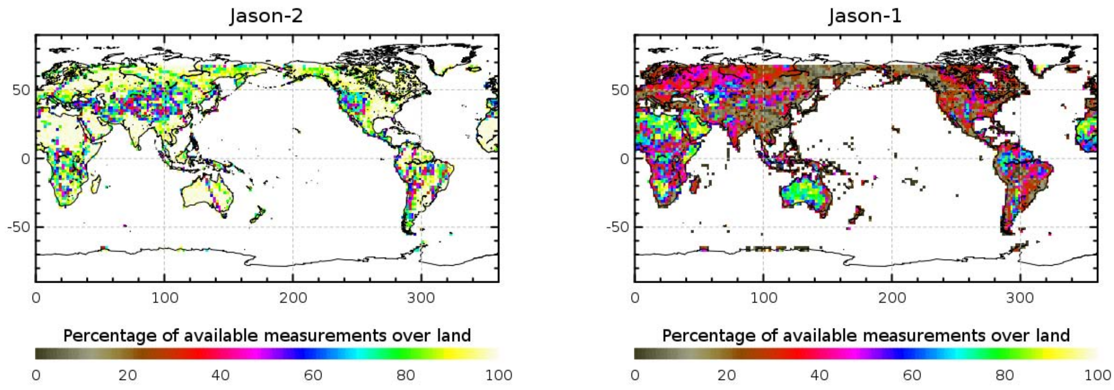

Figure 2: Map of percentage of available measurements over land for Jason-2 on cycle 154 (left) and for Jason-1 on cycle 511 (right)

3.1.2. Over ocean

When considering ocean surface, the same analysis method leads also to an improvement of Jason-2 data coverage, as plotted on the top left figure 3. It represents the percentage of missing measurements relative to the theory, when limited to ocean surfaces. The mean value is about 0.8% for Jason-2, 4.6% for Jason-1 on its repeat ground-track and 7.7% for Jason-1 on its geodetic ground-track. Note that since Jason-1 is on a geodetic ground-track, it is roughly once per month during about 2 h in INIT mode (no science data), due to Jason-2 overflight. Even if already very low, this figure of missing measurements is not significant due to several events where the measurements are missing. All these events are described on table 2.

On figure 3 on the top right, the percentage of missing measurements is plotted without taking into account the cycles where instrumental events or other big anomalies occurred. The mean value of missing measurements lowers down to 0.03% for Jason-2 and 1.9% (2.4%) for Jason-1 (Jason-1 geodetic). These additional Jason-1 missing measurements are mainly located over sea ice and near the coasts and are related to the altimeter tracking method. Indeed, selecting latitudes lower than 50° and bathymetry area lower than -1000m (see bottom of figure 3), the Jason-1 percentage becomes very weak (close to 0.02%) which represents less than 100 missing measurements per cycle over open ocean. For Jason-2, the same statistic is smaller with around 0.007% of missing measurements over open ocean. This weak percentage of missing measurements is mainly explained by the rain cells and sigma0 blooms. These sea states can disturb significantly the Ku band waveform shape leading to an altimeter lost of tracking.

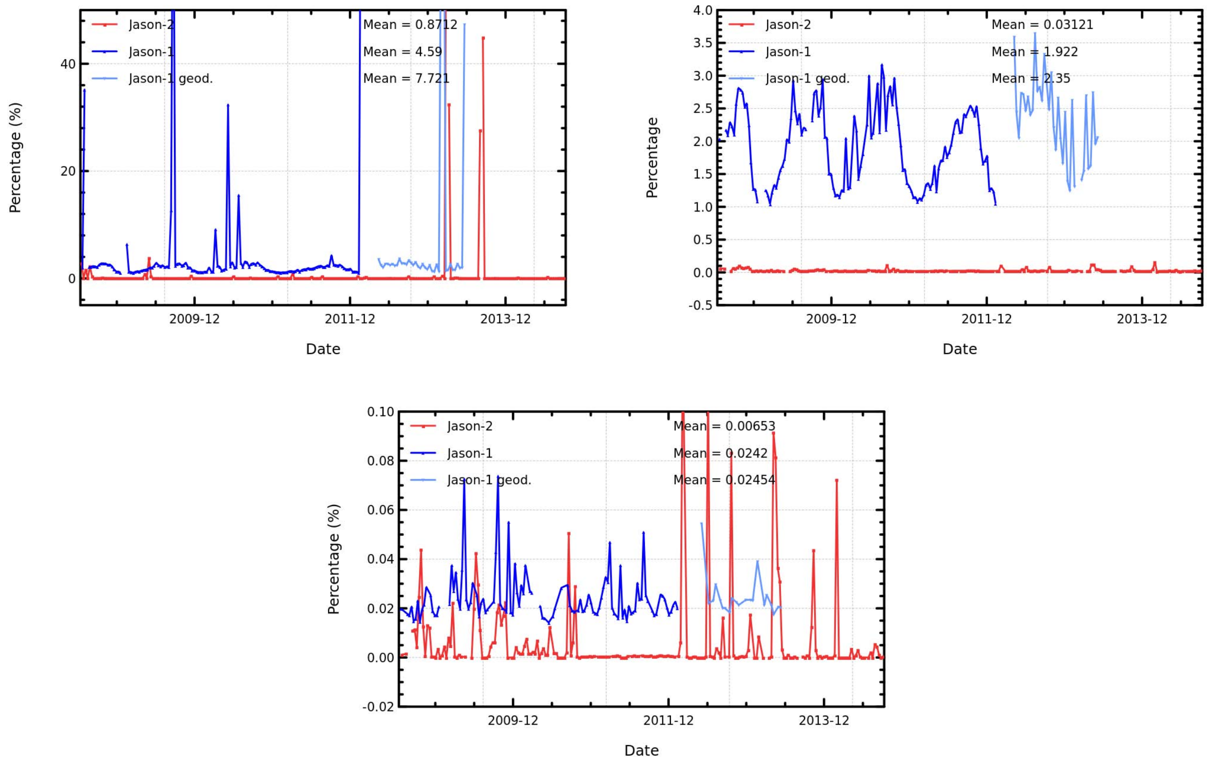

Figure 3: Cycle per cycle percentage of missing measurements over ocean (top left), without anomalies (top right), without anomalies and with geographical selections (bottom).

3.2. Edited measurements

3.2.1. Editing criteria definition

Editing criteria are used to select valid measurements over ocean. The editing process is divided into 4 parts. First, only measurements over ocean and lakes are kept (see section 3.2.2.). Second, some flags are used as described in section 3.2.3.. Note that though the altimeter rain flag is now available in the current release of GDR (D), it is not used hereafter in the editing procedure. But measurements corrupted by rain are well detected by other altimeter parameter criteria. Then, threshold criteria are applied on altimeter, radiometer and geophysical parameters and are described in the table 7. Except for the dual frequency ionosphere correction, only Ku-band measurements are used in this editing procedure, as they mainly represent the end user dataset. Moreover, a spline criterion is applied to remove the remaining spurious data. For each criterion, the cycle per cycle percentage of edited measurements has been monitored. This allows detection of anomalies in the number of removed data, which could come from instrumental, geophysical or algorithmic changes.

Parameter	Min thresholds	Max thresholds	mean edited
Sea surface height	$-130\,m$	$100\,m$	0.77%
Sea level anomaly	$-10\,m$	$10.0\,m$	1.04%
Number measurements of range	10	*Not applicable*	1.04%
Standard deviation of range	0	$0.2\,m$	1.40%
Squared off-nadir angle	$-0.2\,deg^2$	$0.64\,deg^2$	0.59%
Dry troposphere correction	$-2.5\,m$	$-1.9\,m$	0.00%
Inverted barometer correction	$-2.0\,m$	$2.0\,m$	0.00%
AMR wet troposphere correction	$-0.5m$	$-0.001\,m$	0.23%
Ionosphere correction	$-0.4\,m$	$0.04\,m$	1.18%
Significant wave height	$0.0\,m$	$11.0\,m$	0.65%
Sea State Bias	$-0.5\,m$	$0.0\,m$	0.62%
Number measurements of Ku-band Sigma0	10	*Not applicable*	1.03%
Standard deviation of Ku-band Sigma0	0	$1.0\,dB$	1.95%
Ku-band Sigma0 [1]	$7.0\,dB$	$30.0\,dB$	0.60%
Ocean tide	$-5.0\,m$	$5.0\,m$	0.01%
Equilibrium tide	$-0.5\,m$	$0.5\,m$	0.00%
Earth tide	$-1.0\,m$	$1.0\,m$	0.00%
Pole tide	$-15.0\,m$	$15.0\,m$	0.00%
Altimeter wind speed	$0\,m.s^{-1}$	$30.0\,m.s^{-1}$	1.02%
All together	-	-	3.27%

Table 7: Editing criteria

3.2.2. Selection of measurements over ocean and lakes

In order to remove data over land, a land-water mask is used. Only measurements over ocean or lakes are kept. This allows to keep data near the coasts and so to detect potential anomalies in these areas. Furthermore, there is no impact on global performance estimations since the most significant results are derived from analyzes in deep ocean areas. Figure 4 shows the cycle per

[1] The thresholds used for the Ku-band Sigma0 are the same than for Jason-1 and T/P, but the same sigma0 bias as between Jason-1 and T/P (about 2.4 dB) is applied.

cycle percentage of measurements eliminated by this selection. The signal shows mainly a seasonal cycle, due to changing properties of land reflection. But it also reveals the impact of the different altimeter tracking modes: SGT (split gate tracking), Median and DIODE/DEM (digital elevation model). SGT mode, the nominal mode for Jason-1, was used for Jason-2 during cycle 0 and half of cycle 1. This mode does not perform very well over land (as also depicted on right side of figure 2), therefore a comparable small percentage of measurements are edited over land for cycle 1 (approximately 24%). Most of Jason-2 cycles (cycles 2, 4, 6, 8 to 33, 35 to 208, 210 to 219 and from cycle 221 onwards) were operated in Median mode (also used by Envisat). This mode is more adapted for tracking over land than SGT and provides therefore more measurements over land (as also seen on left side of figure 2) and so more measurements are edited (between 25.5% and 27% depending on season) due to the ocean/land criteria. A new tracking mode, DEM, was used during cycles 3, 5, 7, 34, 209 and 220. It has been designed to provide more data over inland water surfaces and coastal areas. It provides a continuous data set over land but some are not meaningful (in areas where the DEM is not accurate enough like in the major mountains). Therefore during these cycles, almost 29% of measurements are removed by the selection. Since 10th of December, 2008 the onboard altimeter configuration was modified to correct for the low signal tracking anomaly, which led to a more strict control of acquisition gain loop (to avoid the tracking of low signal anomalies). This explains the quite steep decrease of land measurements edited around cycle 16.

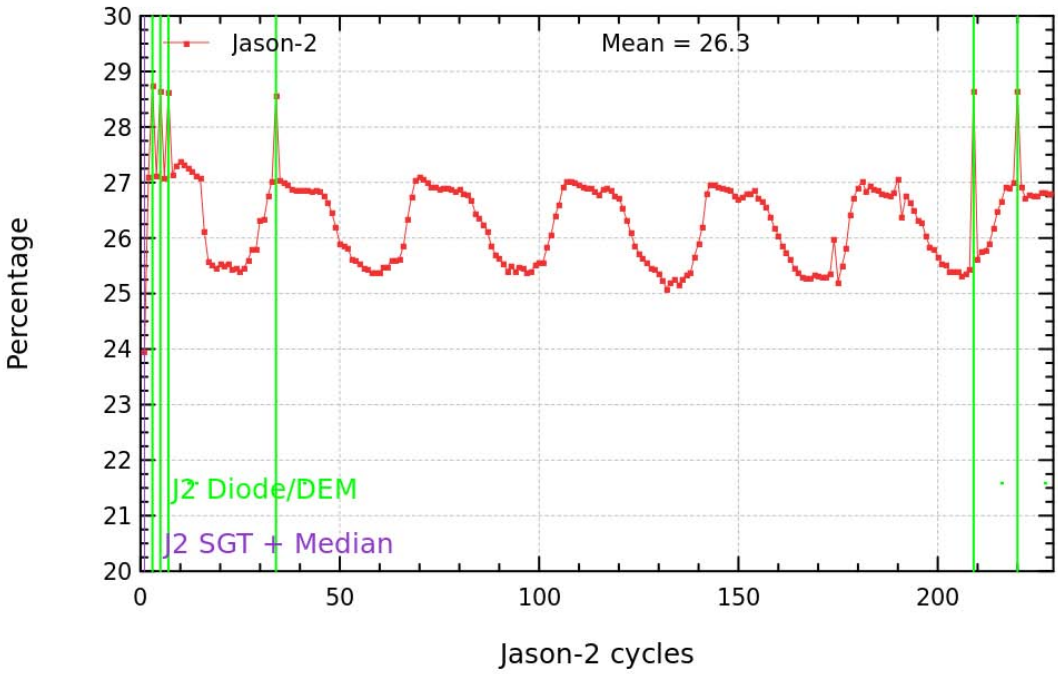

Figure 4: Cycle per cycle percentage of eliminated measurements during selection of ocean/lake measurements.

3.2.3. Flagging quality criteria: Ice flag

The ice flag is used to remove the sea ice data. Figure 5 shows the cycle per cycle percentage of measurements edited by this criterion. Over the shown period, no anomalous trend is detected (figure 5 left) but the nominal annual cycle is visible. Indeed, the maximum number of points over ice is reached during the southern winter (i.e. July - September). As Jason-2 takes measurements between 66° north and south, it does not detect thawing of sea ice (due to global warming), which takes place especially in northern hemisphere over 66°N. The percentage of measurements edited by ice flag is plotted in the right of figure 5 for a period of 1 year.

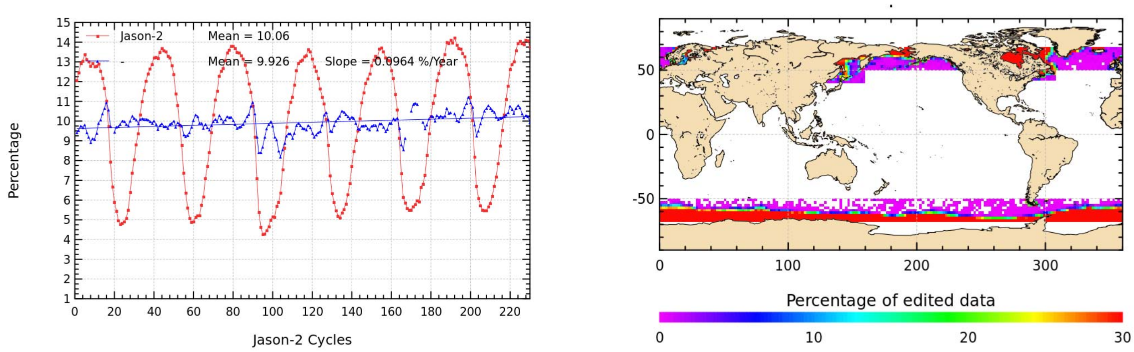

Figure 5: Percentage of edited measurements by ice flag criterion. Left: Cycle per cycle monitoring. The blue curve shows the trend of edited measurements after adjusting for annual and semi-annual signals. Right: Map over a one year period (cycles 193 to 230).

3.2.4. Flagging quality criteria: Rain flag

Though the altimeter rain flag is now present in GDR-D release, it is not used hereafter during the editing procedure. The percentage of measurements where rain flag is set to 1 is plotted in figure 6 over cycles 193 to 230 (covering 12 months). It shows that measurements are especially edited near coasts, but also in the equatorial zone and open ocean. The altimeter rain flag seems to be slightly too strict, using it would lead to edit 6.6% of additional measurements (for location see right part of figure 6).

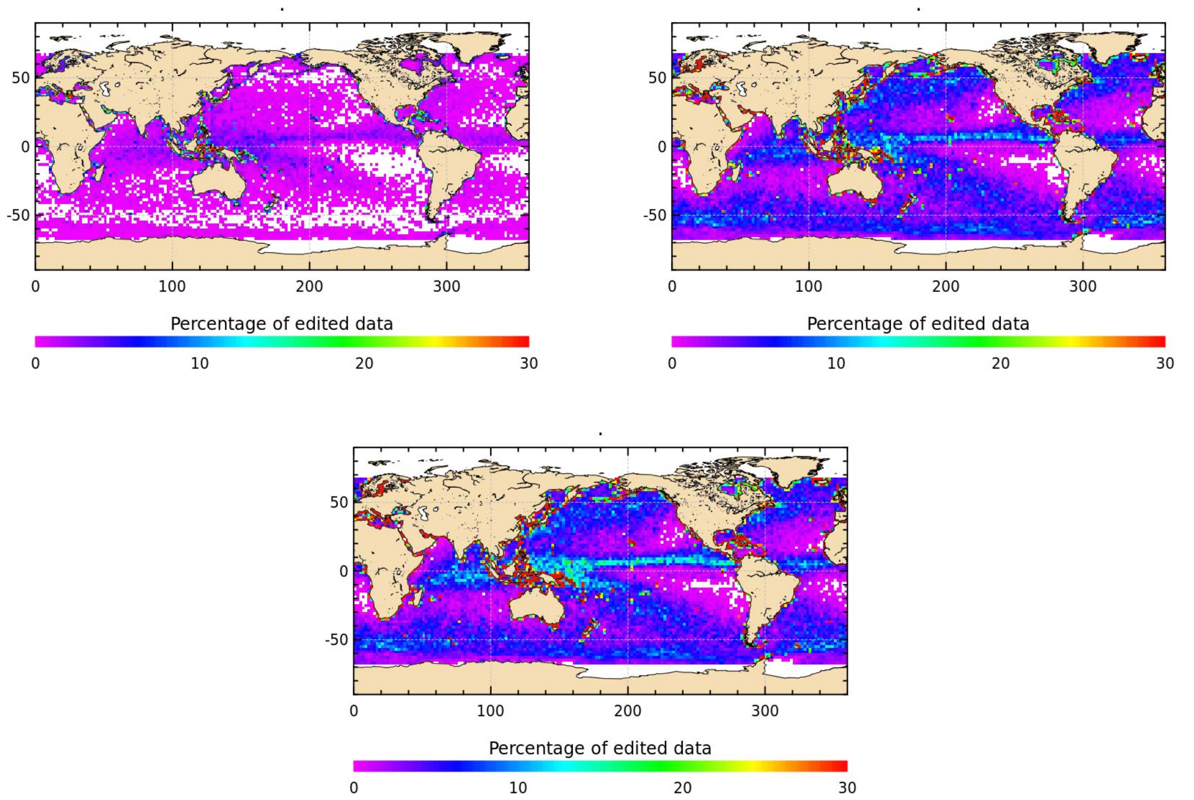

Figure 6: Percentage of edited measurements by altimeter rain flag criterion (all figures computed after iced flagged points remove). Map over a one year period (cycles 193 to 230). Left: rejected measurements where rain flag is also activated . Right: valid measurements where rain flag is activated. Bottom: All points where rain flag is activated.

3.2.5. Threshold criteria: Global

Instrumental parameters have also been analyzed from comparison with thresholds, after having selected only ocean/lakes measurements and applied flagging quality criteria (ice flag). Therefore measurements appear not as edited by thresholds, when they were already edited by land or sea ice flag. Note that no measurement is edited by the following corrections : dry troposphere correction, inverted barometer correction (including DAC), equilibrium tide, earth and pole tide. Indeed these parameters are only verified in order to detect data at default values, which might happen during a processing anomaly.

The percentage of measurements edited using each criterion is monitored on a cycle per cycle basis (figure 7). The mean percentage of edited measurements is about 3.3%. A small annual cycle is visible. The high percentage of edited measurements of cycles 019, 168 and 169 are explained by an AMR anomaly, which resulted in defaulted radiometer values during several passes. Concerning cycles 174 and 191, it is explained by the time lag between the altimeter restart and the radiometer restart after safe hold modes.

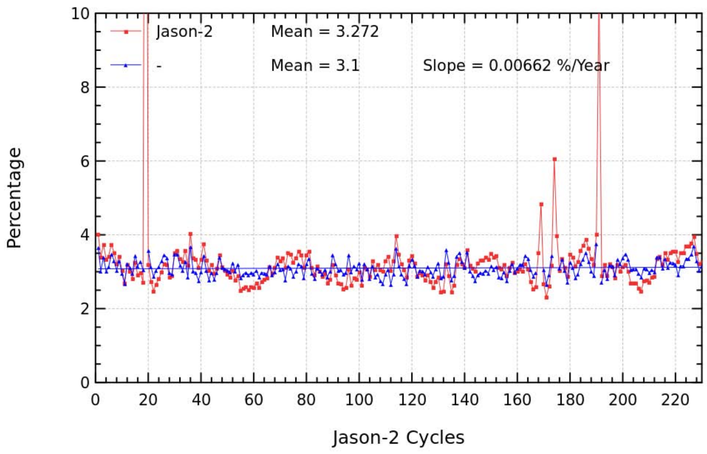

Figure 7: Cycle per cycle percentage of edited measurements by threshold criteria. The blue curve shows the trend of edited measurements after adjusting for annual and semi-annual signals.

3.2.6. Threshold criteria: 20-Hz measurements number

The percentage of edited measurements because of a too low number of 20-Hz measurements is represented on left side of figure 8. No trend neither any anomaly has been detected.
The map of measurements edited by 20-Hz measurements number criterion is plotted on right side of figure 8 and shows correlation with heavy rain and wet areas (in general regions with disturbed sea state). Indeed waveforms are distorted by rain cells, which makes them often meaningless for SSH calculation. As a consequence, edited measurements due to several altimetric criteria are often correlated with wet areas.

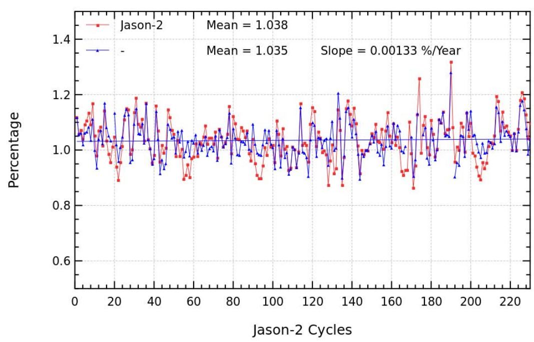

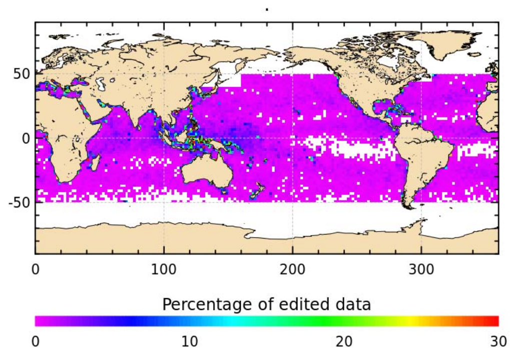

Figure 8: Percentage of edited measurements by 20-Hz measurements number criterion. Left: Cycle per cycle monitoring. The blue curve shows the trend of edited measurements after adjusting for annual and semi-annual signals. Right: Map over a one year period (cycles 193 to 230).

3.2.7. Threshold criteria: 20-Hz measurements standard deviation

The percentage of edited measurements due to 20-Hz measurements standard deviation criterion is shown in figure 9 (left). During cycle 1, slightly more measurements are edited by 20-Hz measurements standard deviation criterion than during other cycles. This is likely due to low signal tracking anomaly which impacted especially this cycle. The right side of figure 9 shows a map of measurements edited by the 20-Hz measurements standard deviation criterion. As in section 3.2.6., edited measurements are correlated with wet areas.

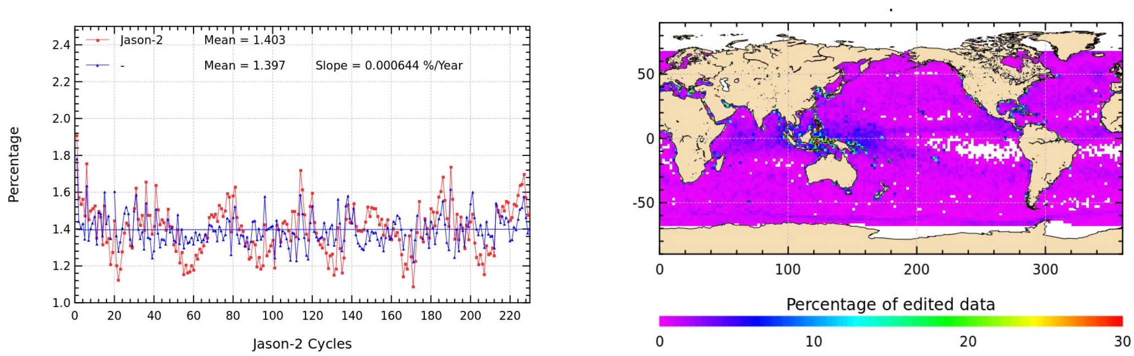

Figure 9: Percentage of edited measurements by 20-Hz measurements standard deviation criterion. Left: Cycle per cycle monitoring. The blue curve shows the trend of edited measurements after adjusting for annual and semi-annual signals. Right: Map over a one year period (cycles 193 to 230).

3.2.8. Threshold criteria: Significant wave height

The percentage of edited measurements due to significant wave height criterion is represented in figure 10. It is about 0.65%. In the beginning of the mission, the curve of measurements edited by SWH threshold criterion is quite irregular, as low signal tracking anomalies occurred during SGT and Median tracking modes, whereas there are no low signal tracking anomalies during DEM tracking modes (cycles 3, 5, and 7). Indeed during periods of low signal tracking anomaly, parameters like significant wave height, backscattering coefficient and squared off-nadir angle from waveforms are out of thresholds and therefore edited. Figure 10 (right part) shows that measurements edited by SWH criterion are especially found near coasts in the equatorial regions and in the Mediterranean Sea.

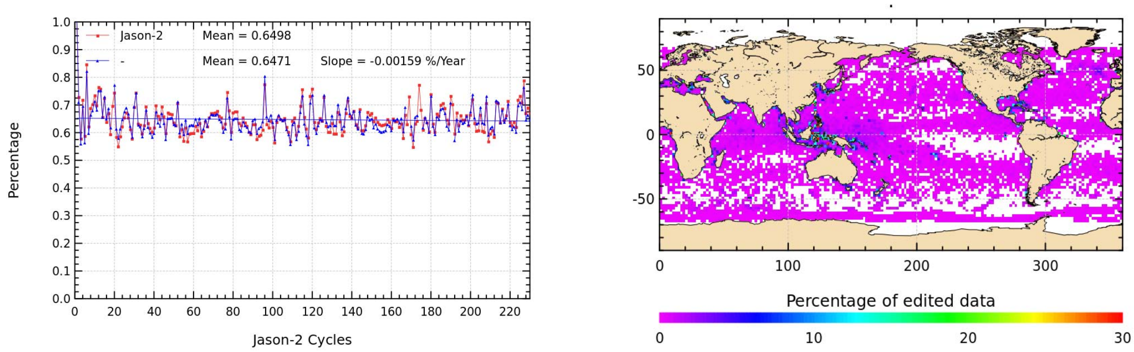

Figure 10: Percentage of edited measurements by SWH criterion. Left: Cycle per cycle monitoring. The blue curve shows the trend of edited measurements after adjusting for annual and semi-annual signals. Right: Map over a one year period (cycles 193 to 230).

3.2.9. Backscatter coefficient

The percentage of edited measurements due to backscatter coefficient criterion is represented in figure 11. It is about 0.60% It is also impacted by low signal tracking anomalies, especially during cycle 1. The right part of figure 11 shows that measurements edited by backscatter coefficient criterion are especially found near coasts in the equatorial regions and enclosed sea (Mediterranean).

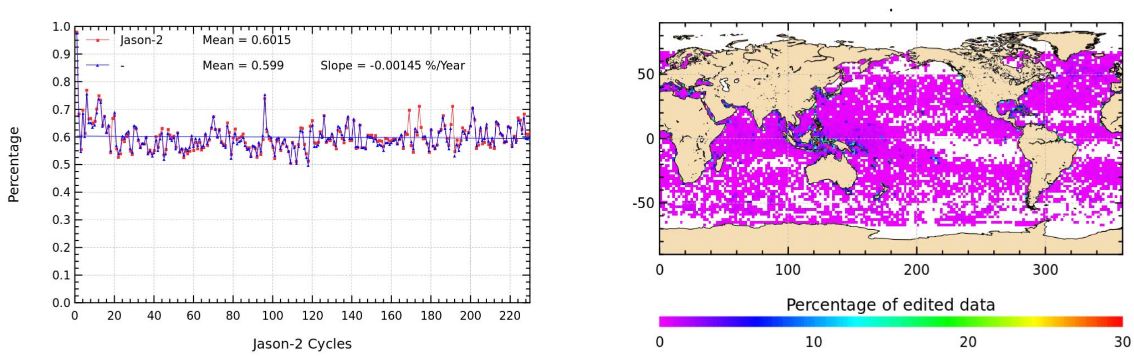

Figure 11: Percentage of edited measurements by Sigma0 criterion. Left: Cycle per cycle monitoring. The blue curve shows the trend of edited measurements after adjusting for annual and semi-annual signals. Right: Map over a one year period (cycles 193 to 230).

3.2.10. Backscatter coefficient: 20 Hz standard deviation

The percentage of edited measurements due to 20 Hz backscatter coefficient standard deviation criterion is represented in figure 12. It is about 1.9%. The right part of figure 11 shows that measurements edited by 20 Hz backscatter coefficient standard deviation criterion are especially found in regions with disturbed waveforms.

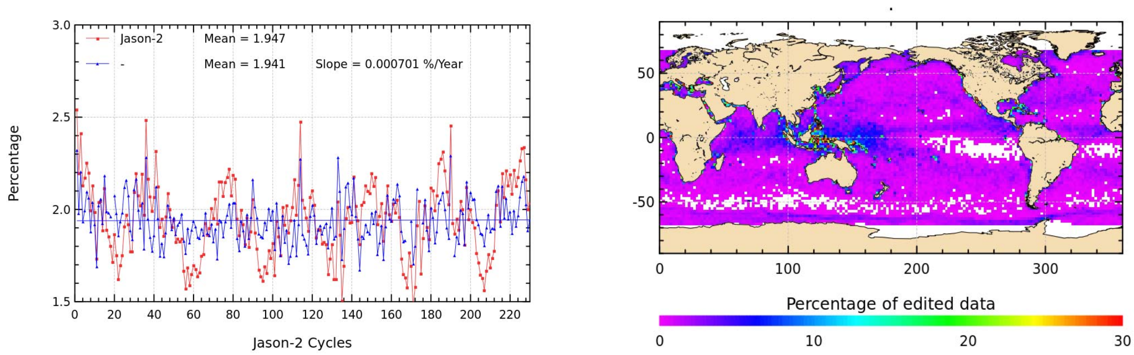

Figure 12: Percentage of edited measurements by 20 Hz Sigma0 standard deviation criterion. Left: Cycle per cycle monitoring. The blue curve shows the trend of edited measurements after adjusting for annual and semi-annual signals. Right: Map over a one year period (cycles 193 to 230).

3.2.11. Radiometer wet troposphere correction

The percentage of edited measurements due to radiometer wet troposphere correction criterion is represented in figure 13. It is about 0.2%. When removing cycles which experienced problems, percentage of edited measurements drops to about 0.1%. For some cycles the percentage of edited measurements is higher than usual. This is linked to radiometer wet troposphere correction at default value due to AMR unavailability in case of cycle 19, AMR reset in case of cycles 168 and 169, and time lag between altimeter restart and radiometer restart after safe hold modes in case of cycles 174, 175 and 191.

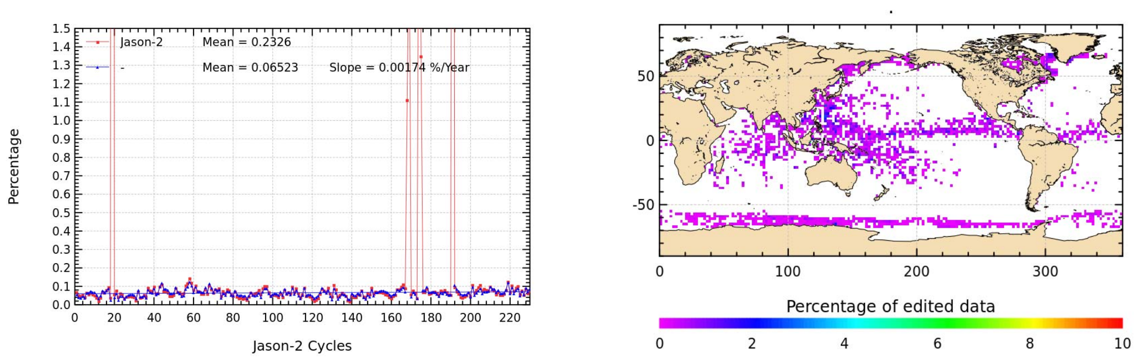

Figure 13: Percentage of edited measurements by radiometer wet troposphere criterion. Left: Cycle per cycle monitoring. The blue curve shows the trend of edited measurements after adjusting for annual and semi-annual signals. Right: Map over a one year period (cycles 193 to 230).

3.2.12. Dual frequency ionosphere correction

The percentage of edited measurements due to dual frequency ionosphere correction criterion is represented in figure 14. It is about 1.2% and shows no drift. The map 14 shows that measurements edited by dual frequency ionosphere correction are mostly found in equatorial regions, but also near sea ice.

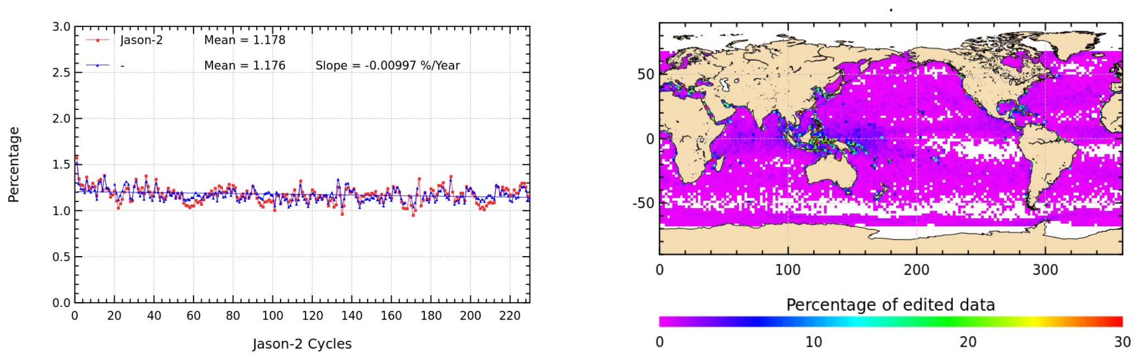

Figure 14: Percentage of edited measurements by dual frequency ionosphere criterion. Left: Cycle per cycle monitoring. The blue curve shows the trend of edited measurements after adjusting for annual and semi-annual signals. Right: Map over a one year period (cycles 193 to 230).

3.2.13. Square off-nadir angle

The percentage of edited measurements due to square off-nadir angle criterion is represented in figure 15. It is about 0.6%. As for other parameters, impact of low signal tracking anomalies is visible in general for the first 16 cycles and especially for cycle 1. The map 15 shows that edited measurements are mostly found in coastal regions and regions with disturbed waveforms.

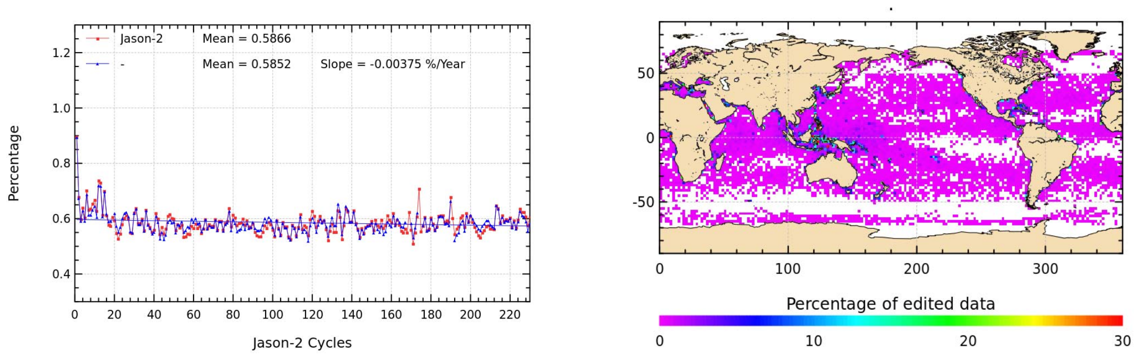

Figure 15: Percentage of edited measurements by square off-nadir angle criterion. Left: Cycle per cycle monitoring. The blue curve shows the trend of edited measurements after adjusting for annual and semi-annual signals. Right: Map over a one year period (cycles 193 to 230).

3.2.14. Sea state bias correction

The percentage of edited measurements due to sea state bias correction criterion is represented in figure 16. The percentage of edited measurements is about 0.6% and shows no drift.
The map 16 shows that edited measurements are mostly found in equatorial regions near coasts.

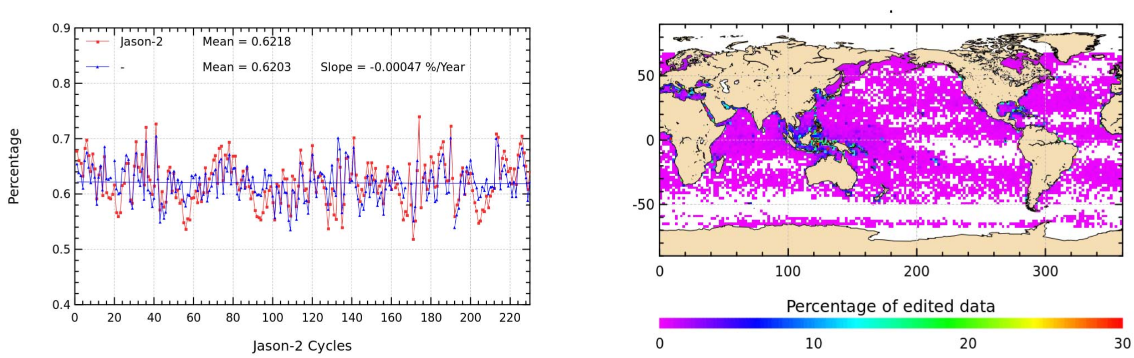

Figure 16: Cycle per cycle percentage of edited measurements by sea state bias criterion (left). The blue curve shows the trend of edited measurements after adjusting for annual and semi-annual signals. Right: Map of percentage of edited measurements by sea state bias criterion over a one year period (cycles 193 to 230).

3.2.15. Altimeter wind speed

The percentage of edited measurements due to altimeter wind speed criterion is represented in figure 17. It is about 1.0%. The measurements are edited, because they have default values. This is the case when sigma0 itself is at default value, or when it shows very high values (higher than 25 dB), which occur during sigma bloom and also over sea ice. Indeed, the wind speed algorithm (which uses backscattering coefficient and significant wave height) can not retrieve values for sigma0 higher than 25 dB.
Wind speed is also edited, when it has negative values, which can occur in GDR products. Nevertheless, sea state bias is available even for negative wind speed values. Therefore, the percentage of edited altimeter wind speed is higher than that of edited sea state bias.

The map 17 showing percentage of measurements edited by altimeter wind speed criterion is correlated with maps 16 and 10.

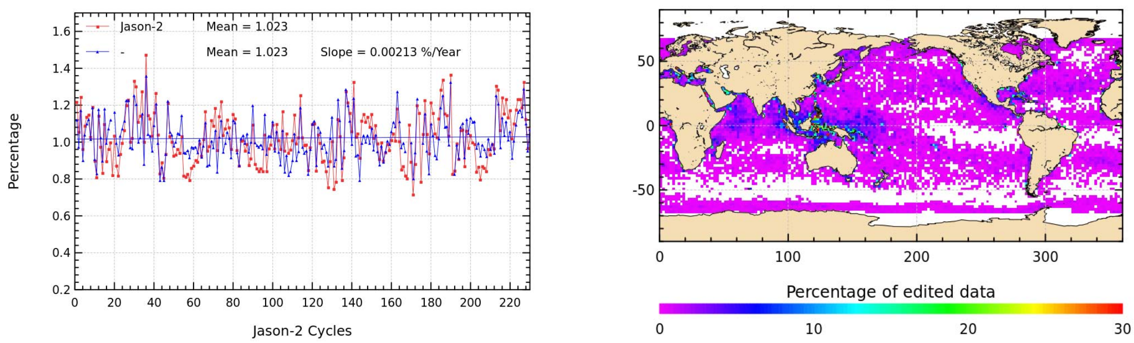

Figure 17: Percentage of edited measurements by altimeter wind speed criterion. Left: Cycle per cycle monitoring.The blue curve shows the trend of edited measurements after adjusting for annual and semi-annual signals. Right: Map over a one year period (cycles 193 to 230).

3.2.16. Ocean tide correction

The percentage of edited measurements due to ocean tide correction criterion is represented in figure 18. It is less than 0.01% and is very stable. The ocean tide correction is a model output, there should therefore be no edited measurements. Indeed there are no measurements edited in open ocean areas, but only very few near coasts (Alaska, Kamchatka, Labrador). These measurements are mostly at default values. The percentage of measurement increases for cycle 174 and 175 (2013 safe hold mode).

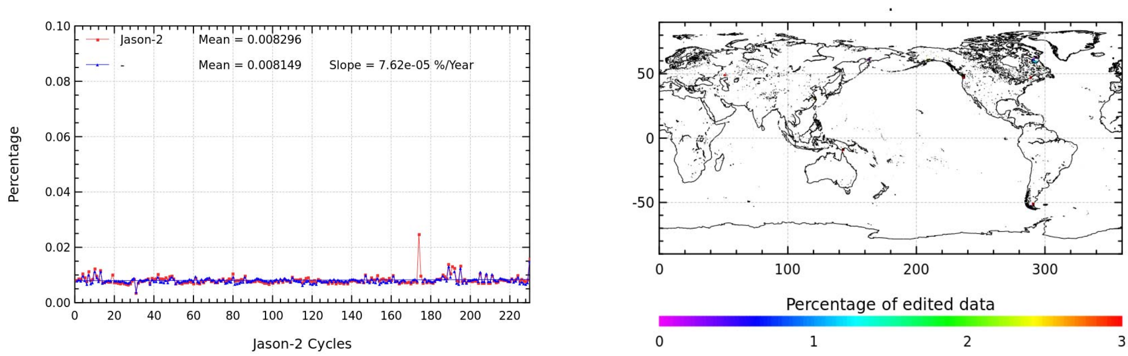

Figure 18: Percentage of edited measurements by ocean tide criterion. Left: Cycle per cycle monitoring. The blue curve shows the trend of edited measurements after adjusting for annual and semi-annual signals. Right: Map over a one year period (cycles 193 to 230).

3.2.17. Sea surface height

The percentage of edited measurements due to sea surface height (orbit - ku-band range) criterion is represented in figure 19. It is about 0.77% and shows no drift. The measurements edited by sea surface height criterion are mostly found near coasts in equatorial regions (see map 19). The majority of the edited measurements has defaulted range values.

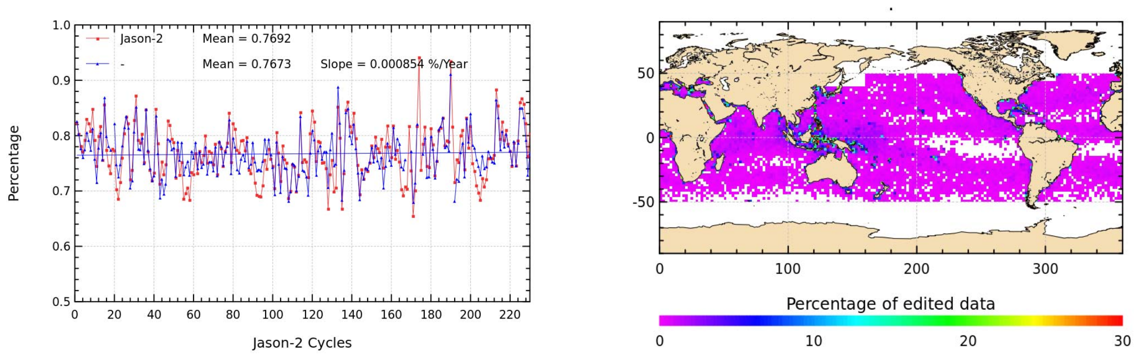

Figure 19: Percentage of edited measurements by sea surface height criterion. Left: Cycle per cycle monitoring. The blue curve shows the trend of edited measurements after adjusting for annual and semi-annual signals. Right: Map over a one year period (cycles 193 to 230).

3.2.18. Sea level anomaly

The percentage of edited measurements due to sea level anomaly criterion is represented in figure 20. It is about 1.0% (0.9% without cycles 19,168,169,174,175,191) and shows no drift. The peaks are related to AMR unavailabilities (see figure 13 (showing the percentage of measurements edited by AMR)), as the SLA clip contains, among other parameters, the radiometer wet troposphere correction.
Whereas the map in figure 20 allows us to plot the measurements edited due to sea level anomaly out of thresholds (after applying all other threshold criteria). There are only very few measurements, principally located in Caspian Sea.

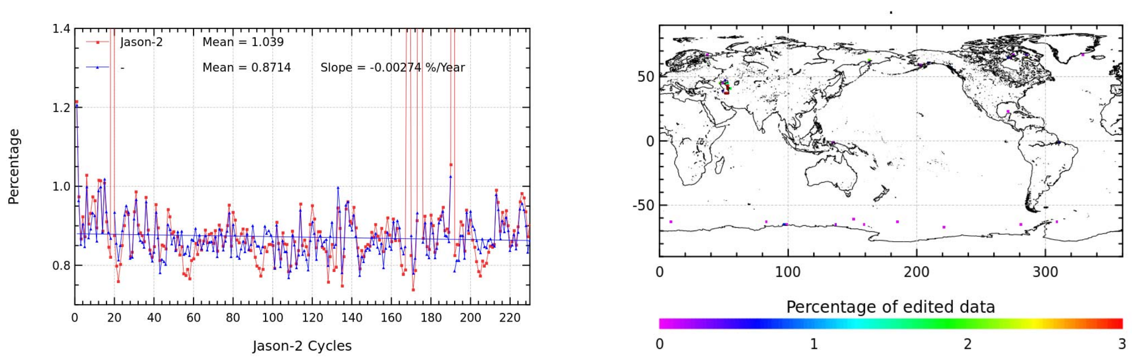

Figure 20: Percentage of edited measurements by sea level anomaly criterion. Left: Cycle per cycle monitoring. The blue curve shows the trend of edited measurements after adjusting for annual and semi-annual signals. Right: Map over a one year period (cycles 193 to 230).

4. Monitoring of altimeter and radiometer parameters

4.1. Methodology

Both mean and standard deviation of the main parameters of Jason-2 (GDR-D) have been monitored since the beginning of the mission. Moreover, a comparison with Jason-1 parameters has been performed: it allows us to monitor the bias between the parameters of the 2 missions. Two different methods have been used to compute the bias:

- Till Jason-2 cycle 20, Jason-2 and Jason-1 are on the same ground track and are spaced out about 1 minute apart. The mean of the Jason-1 - Jason-2 differences can be computed using a point by point repeat track analysis.
- From Jason-2 cycle 21 (Jason-1 cycle 260), a maneuver sequence was conducted (from 26th of January to 14th of February 2009) to move Jason-1 to the new tandem mission orbit. Jason-1 has a repeat ground-track which is interleaved with Jason-2. It is the same ground-track as already used by Topex/Poseidon during its tandem phase with Jason-1, but there is a time shift of 5 days. Geographical variations are then too strong to directly compare Jason-2 and Jason-1 parameters on a point by point basis. Therefore day per day global differences have been carried out to monitor differences between the two missions. A filter over 11 days was applied. Nevertheless the differences are still quite noisy, especially for corrections which vary rapidly in time and space. Therefore occasional small jumps might be covered by the noise of the differences. Nevertheless it should be possible to detect drifts and permanent jumps. Jason-2 and Jason-1 were in this tandem phase from Jason-2 cycles 22 to 135 (Jason-1 cycles 262 to 374).

In February and March of 2012, Jason-1 experienced severals safe holds (anomaly on gyro3, double EDAC error in RAM memory). It was decided to move Jason-1 to a geodetic orbit (more about the Jason-1 geodetic mission can be found in [9]). Science data on the geodetic orbit are available from 7th of May 2012 onwards. Note that the first cycle on the geodetic orbit starts with cycle 500 (this corresponds to end of Jason-2 cycle 141). The last (incomplete) cycle of Jason-1 on the repeat ground-track was cycle 374. As during the tandem phase, day per day global differences of the parameters have been carried out to monitor differences between the two missions.
Finally, after loss of telemetry on 21 June 2013 (during cycle 537), Jason-1 was passivated and decommissioned on 01 July 2013, with the last command sent at 16:37:40 UTC. Note that differences are done over Jason-2 cycles 1 to 183, corresponding to Jason-1 cycles 240 to 537.

4.2. 20 Hz Measurements

The monitoring of the number and standard deviation of 20 Hz elementary range measurements used to derive 1 Hz data is presented here. These two parameters are computed during the altimeter ground processing. For both Jason-1 and Jason-2, before performing a regression to derive the 1 Hz range from 20 Hz data, a MQE (mean quadratic error) criterion is used to select valid 20 Hz measurements. This first step of selection consists in verifying that the 20 Hz waveforms can be approximated by a Brown echo model (Brown, 1977 [32]) (Thibaut et al. 2002 [79]). Then, through an iterative regression process, elementary ranges too far from the regression line are discarded until convergence is reached. Thus, monitoring the number of 20 Hz range measurements and the standard deviation computed among them is likely to reveal changes at instrumental level.

The Jason-1 MQE threshold are not applicable to Jason-2, using those thresholds would edit more measurements than necessary. Therefore, for the first GDR release of Jason-2 (GDR-T), the MQE threshold had been set to default, leading to no editing based on MQE values. Note that for Jason-2 data in version GDR-D, specific Jason-2 MQE thresholds were computed and are applied.

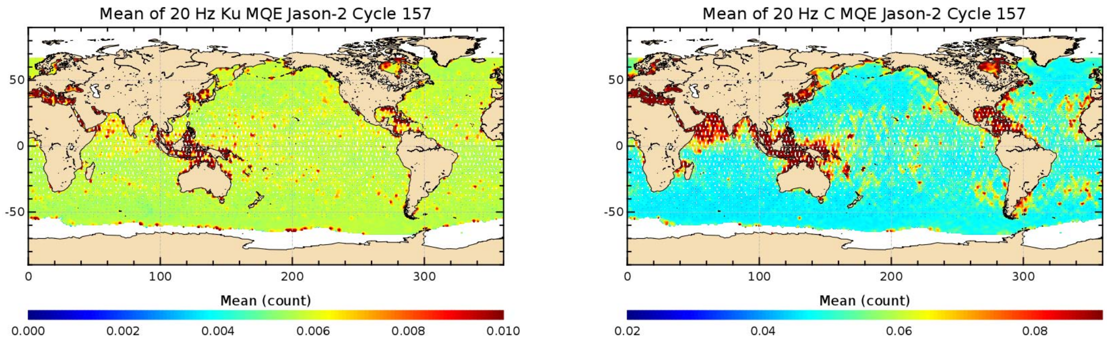

Figure 21: Map of 20 Hz Ku-band (left) and C-band (right) MQE for Jason-2 cycle 157. Note that the color scales are different for the two maps.

4.2.1. 20 Hz measurements number in Ku-Band and C-Band

GDR-D Jason-2 number of elementary 20 Hz range measurements is very similar to Jason-1's (especially for C-band) with an average of 19.61 for Ku-band and 19.25 for C-band as shown on figure 22. For both satellites a slight annual signal is visible (especially for C-band). Figures 23 and 24 show on the left the daily monitoring of the mean and standard deviation of Jason-1 - Jason-2 differences of 20-Hz measurements number in Ku-Band and C-band during the formation flight phase. Besides a slight variation, they are quite stable and do not show any anomaly. Number of 20 Hz Ku-band range measurements is slightly higher for Jason-2 than for Jason-1, since mean of Jason-1 - Jason-2 difference is slightly negative (-0.07 for Ku-band), whereas the difference for C-band is close to zero. The regions where Jason-1 has less elementary Ku-band range measurements are especially located around Indonesia, as shown on map of Jason-1 - Jason-2 differences (right side of figures 23). Indeed in regions of sigma bloom or rain, using a MQE criterion during the regression to derive 1Hz from 20Hz data, discards 20 Hz measurements and therefore reduces the value of number of the 20 Hz measurements used for the 1 Hz data. It is possible that differences in the tuning of the MQE criterion for Jason-1 and Jason-2 Ku-band explain what is observed on the right side of figure 23.

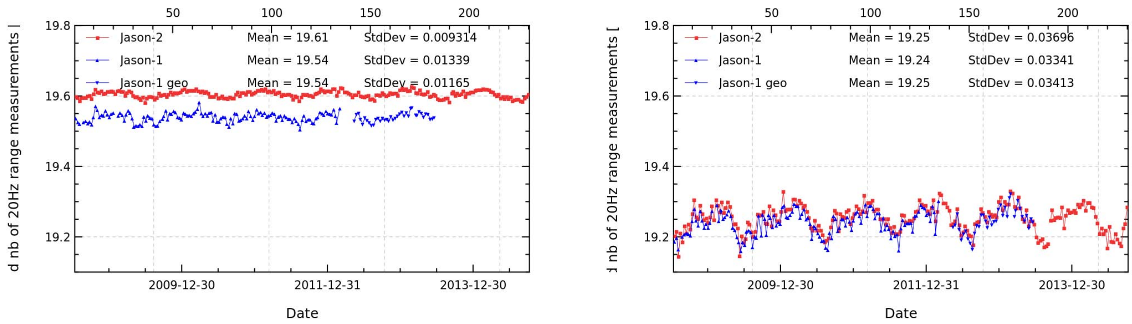

Figure 22: Cyclic monitoring of number of elementary 20 Hz range measurements for Jason-1 and Jason-2 for Ku-band (left) and C-band (right).

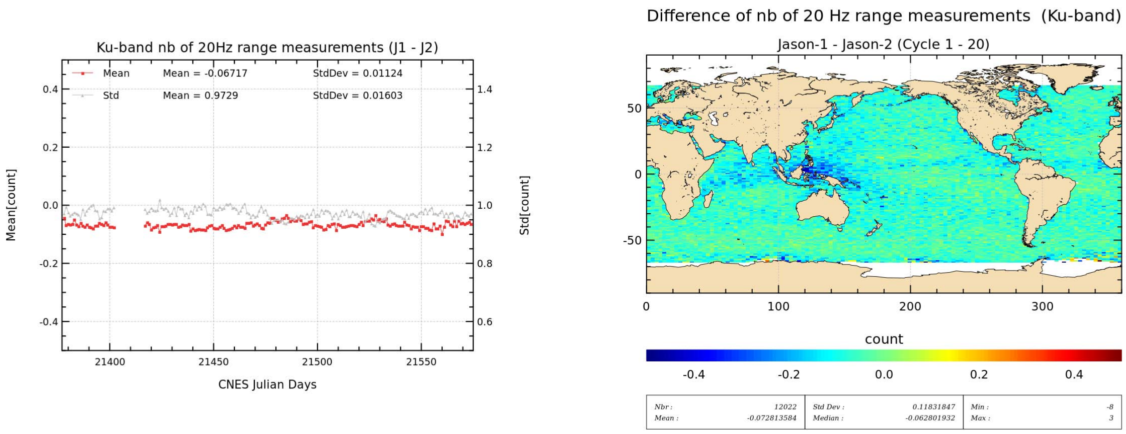

Figure 23: Daily monitoring of mean and standard deviation of Jason-1 - Jason-2 differences for number of elementary 20 Hz Ku-band range measurements (left) and map showing mean of Jason-1 - Jason-2 differences over cycles 1 to 20.

4.2.2. 20 Hz measurements standard deviation in Ku-Band and C-Band

Jason-2 standard deviation of the 20 Hz measurements is 8.0 cm for Ku-Band and 17.3 cm for C-Band (figure 25). It is very similar to Jason-1 data. Figure 26 and 27, showing daily monitoring of Jason-1 - Jason-2 difference of standard deviation of the 20 Hz measurements in Ku-Band and C-Band (on the left), reveal no trend neither anomaly. C-Band standard deviation of the 20 Hz measurements rms is noisier than those of Ku-Band. This is directly linked to the C-band standard deviation which is higher than the Ku, as the onboard averaging is performed over less waveforms (6 Ku for 1 C) leading to an increased noise.

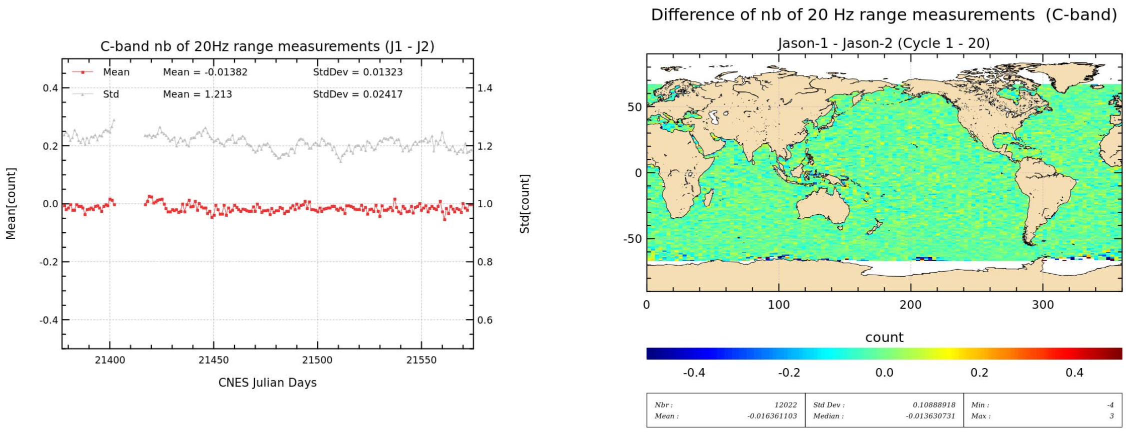

Figure 24: Daily monitoring of mean and standard deviation of Jason-1 - Jason-2 differences for number of elementary 20 Hz C-band range measurements (left) and map showing mean of Jason-1 - Jason-2 differences over cycles 1 to 20.

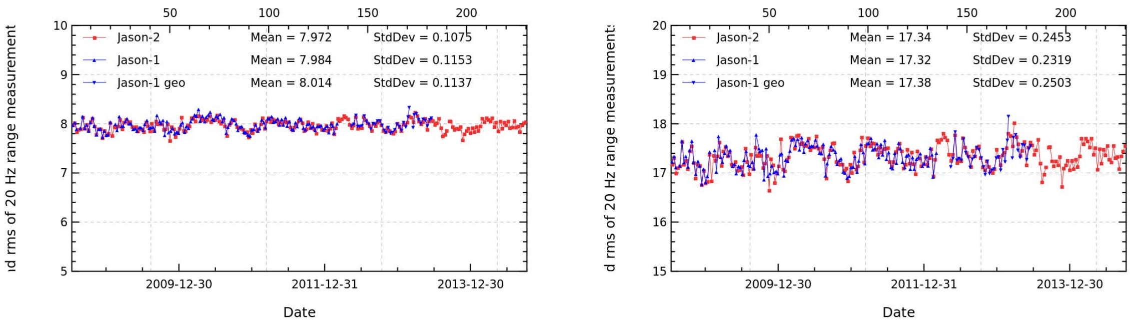

Figure 25: Cyclic monitoring of rms of elementary 20 Hz range measurements for Jason-1 and Jason-2 for Ku-band (left) and C-band (right).

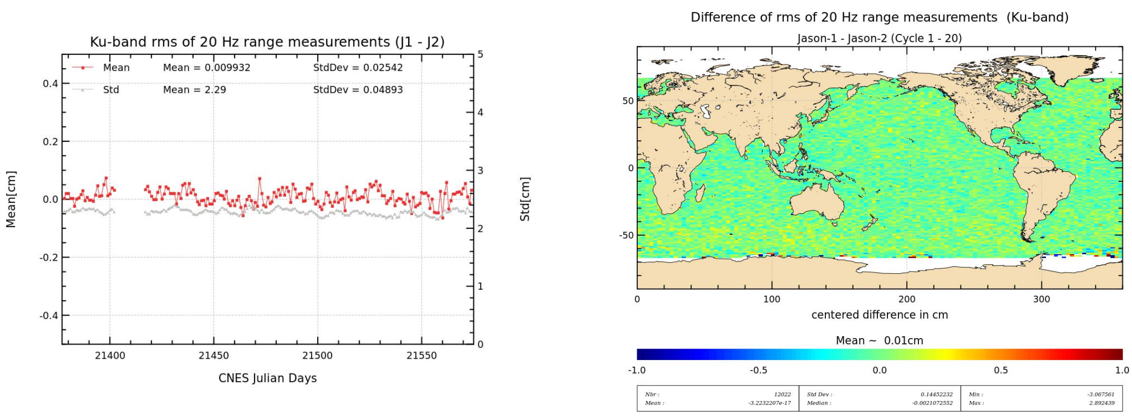

Figure 26: Daily monitoring of mean and standard deviation of Jason-1 - Jason-2 differences for the rms of elementary 20 Hz Ku-band range measurements (left) and map showing mean of Jason-1 - Jason-2 differences over cycles 1 to 20 (right).

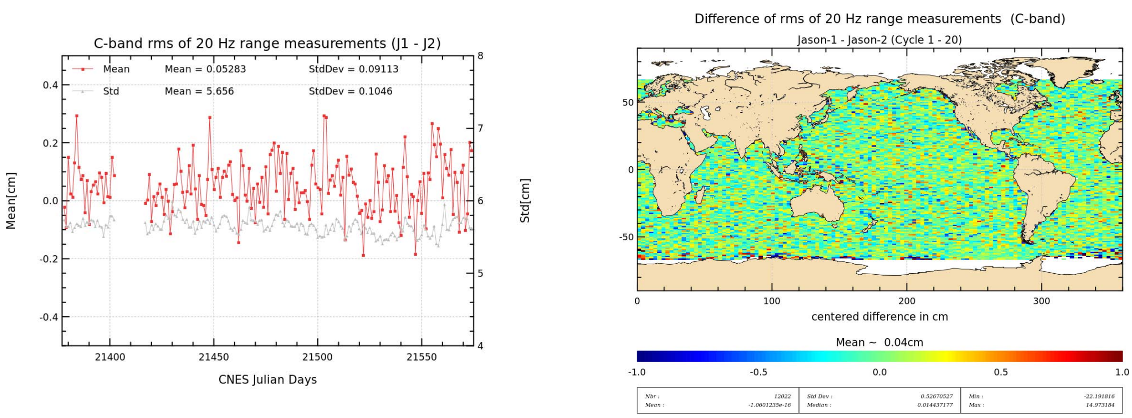

Figure 27: Daily monitoring of mean and standard deviation of Jason-1 - Jason-2 differences for rms of elementary 20 Hz C-band range measurements (left) and map showing mean of Jason-1 - Jason-2 differences over cycles 1 to 20 (right).

4.3. Off-Nadir Angle from waveforms

The off-nadir angle is estimated from the waveform shape during the altimeter processing. The square of the off-nadir angle, averaged on a daily basis, has been plotted for Jason-1 and Jason-2 on the left side of figure 28, whereas the right side shows the histograms over one cycle. For GDR-D Jason-2 the mispointing is very stable and very close to zero (though very slightly negative). Whereas Jason-1 may show higher values (related to the reduced tracking performance of both star trackers, especially during fixed-yaw). Jason-1 experienced especially during 2010 very high mispointing values, for more information see Jason-1 validation report [11]. Jason-1 mispointing situation has been highly improved since end of 2010.
Jason-2 GDR-T mispointing was slightly positive (see also reprocessing report ([16])), which was related to the antenna aperture values used for data processing (1.26° for GDR-T, 1.29° for GDR-D). Indeed [81] shows, that retracking with different values of antenna aperture, changes the mean value of Jason-2 mispointing (see figure 29). Note that for Jason-1 1.28° is used for the antenna aperture.

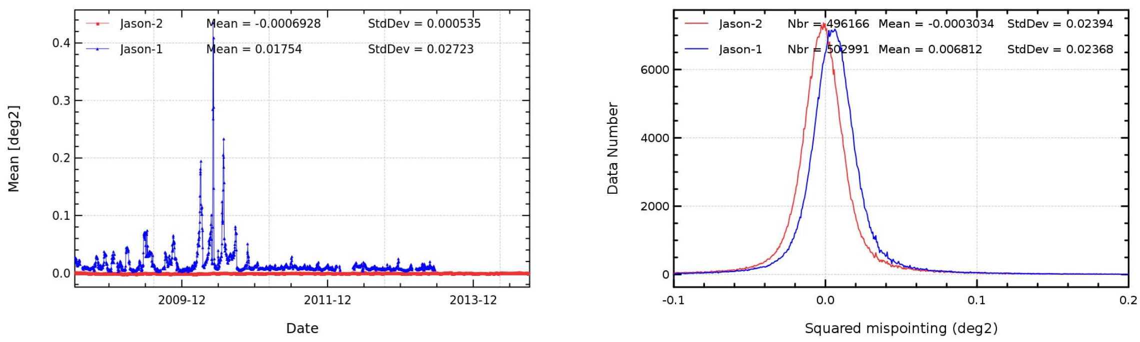

Figure 28: Square of the off-nadir angle deduced from waveforms (deg^2) for Jason-1 and Jason-2: Daily monitoring (left), histograms for Jason-2 cycle 157 (Jason-1 cycle 513/514).

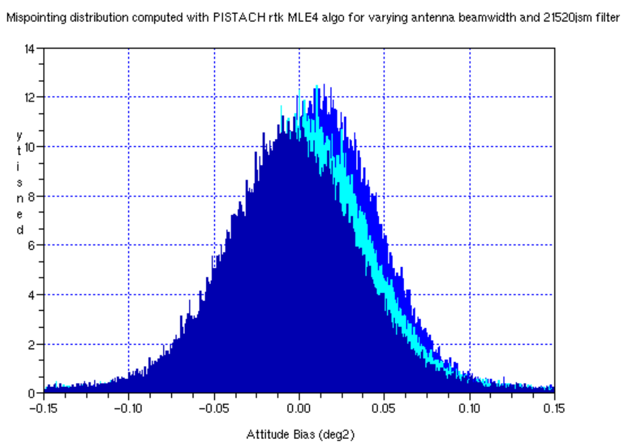

Figure 29: Histograms of Jason-2 mispointing after retracking with different antenna beamwidth (from [81]): 1.26° (blue), 1.28° (light blue), 1.30° (dark blue).

4.4. Backscatter coefficient

The Jason-2 Ku-band and C-band backscattering coefficient shows good agreement with Jason-1 as visible for cyclic monitoring in figure 30 (top left and right). Left sides of figures 31 and 32 show daily monitoring of mean differences during the formation flight phase. For Ku-band, a bias close to 0.3 dB is detected, it varies slightly (+/- 0.05 dB). This slight variation ($\pm$ 0.05 dB) is related to Jason-1 backscattering coefficient which is slightly impacted by the higher off-nadir angles (due to low star tracker availability). Note that backscattering coefficients include instrumental corrections, which include also atmospheric attenuation which comes from the radiometer. Therefore differences between backscattering coefficients can also be partly due to differences between the atmospheric attenuation algorithms of Jason-1 and Jason-2. The main reasons for the differences (between Jason-1 and Jason-2 backscattering coefficients) are related to the antenna calibrations and to the internal calibrations of the altimeters (steps of numerical gain control).
The average standard deviation of both Sigma0 differences (measurement by measurement) is also very low around 0.15 dB rms. C-Band sigma0 differences indicate a small bias close to 0.16 dB. In the meantime, the map of mean differences (right side of figures 31 and 32) highlights very small differences. During the tandem phase (from Jason-2 cycle 21 onwards), mean differences continue to be calculated but comparing only the global day per day statistics (see bottom of figure 30). Although the statistic is calculated less accurately, a similar bias is observed as during the formation flight phase. After the last safe hold mode of Jason-1 (March 2013), a small jump is visible in the Jason-1 minus Jason-2 Sigma0 difference, investigations are ongoing.

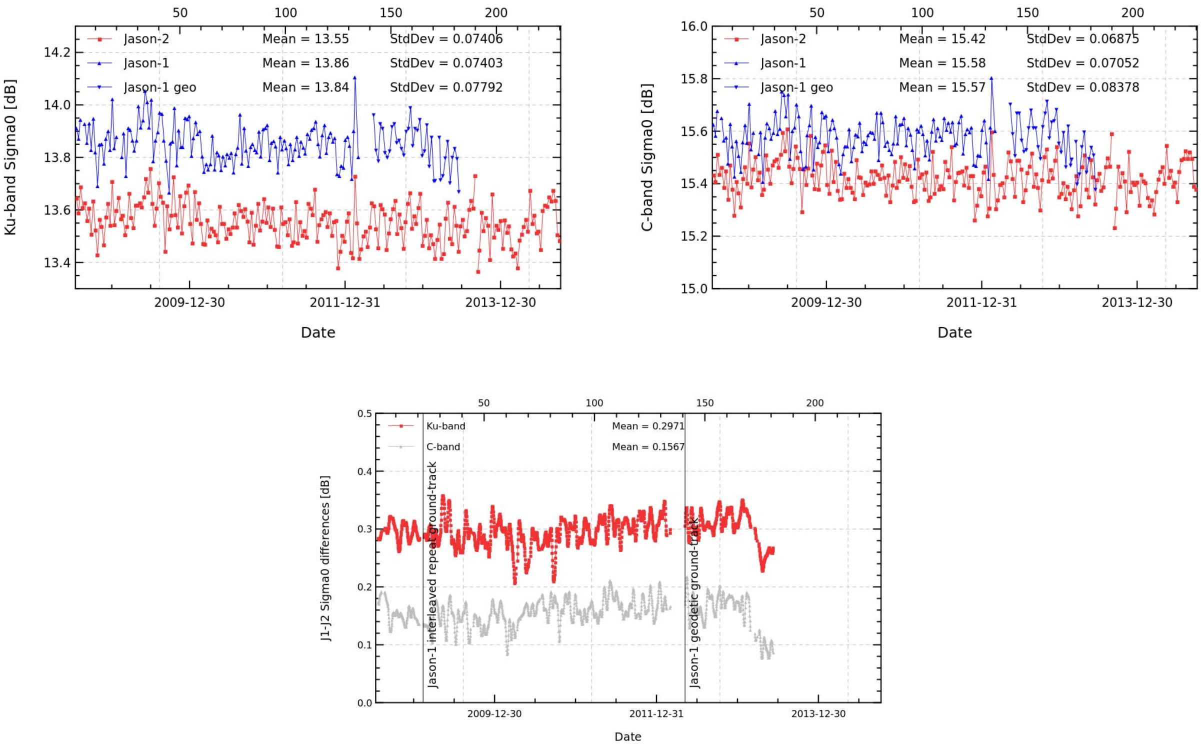

Figure 30: Cyclic monitoring of Sigma0 for Jason-1 and Jason-2 for Ku-band (left) and C-band (right). Daily monitoring of Jason-1 - Jason-2 differences (bottom), a 10 day filter is applied.

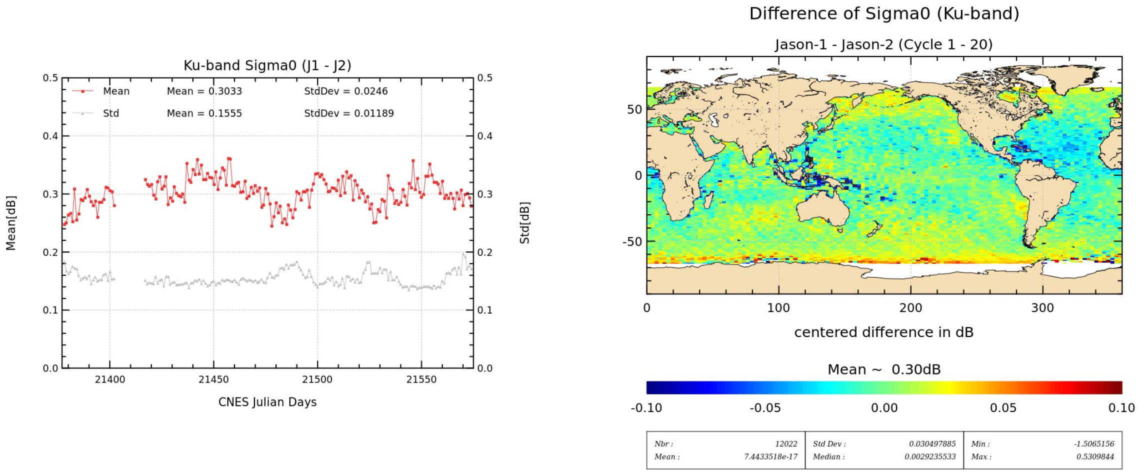

Figure 31: Daily monitoring of mean and standard deviation of Jason-1 - Jason-2 differences for Ku-band Sigma0 (left) and map showing mean of Jason-1 - Jason-2 differences over cycles 1 to 20.

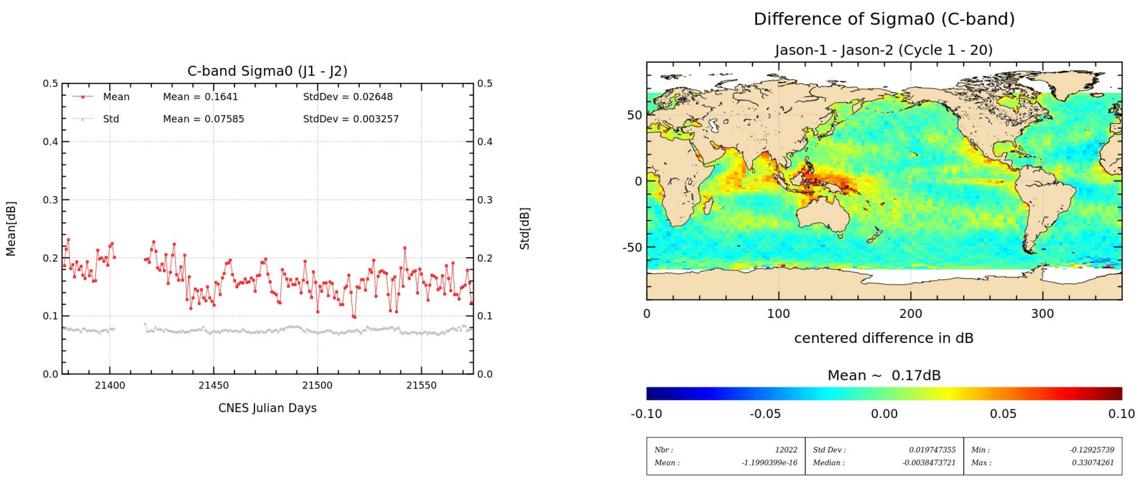

Figure 32: Daily monitoring of mean and standard deviation of Jason-1 - Jason-2 differences for C-band Sigma0 (left) and map showing mean of Jason-1 - Jason-2 differences over cycles 1 to 20.

4.5. Significant wave height

As for Sigma0 parameter, a very good consistency between both significant wave height is shown (see top left and right of figure 33). A small bias close to around -1.3 cm is calculated over the formation flight phase. It is close to -1.7 cm in C-band (see left side of figures 34 and 35). It is stable in time and space (see map of differences in right side of figures 34 and 35). These differences are too weak to impact scientific applications. They are probably due to ground processing differences between both missions. Differences are noisier for C-band. As previously, extending the monitoring of SWH bias during the tandem phase (bottom of figure 33) highlights larger variations since both satellites do not measure the same SWH. However bias is still stable and no drift is detected.

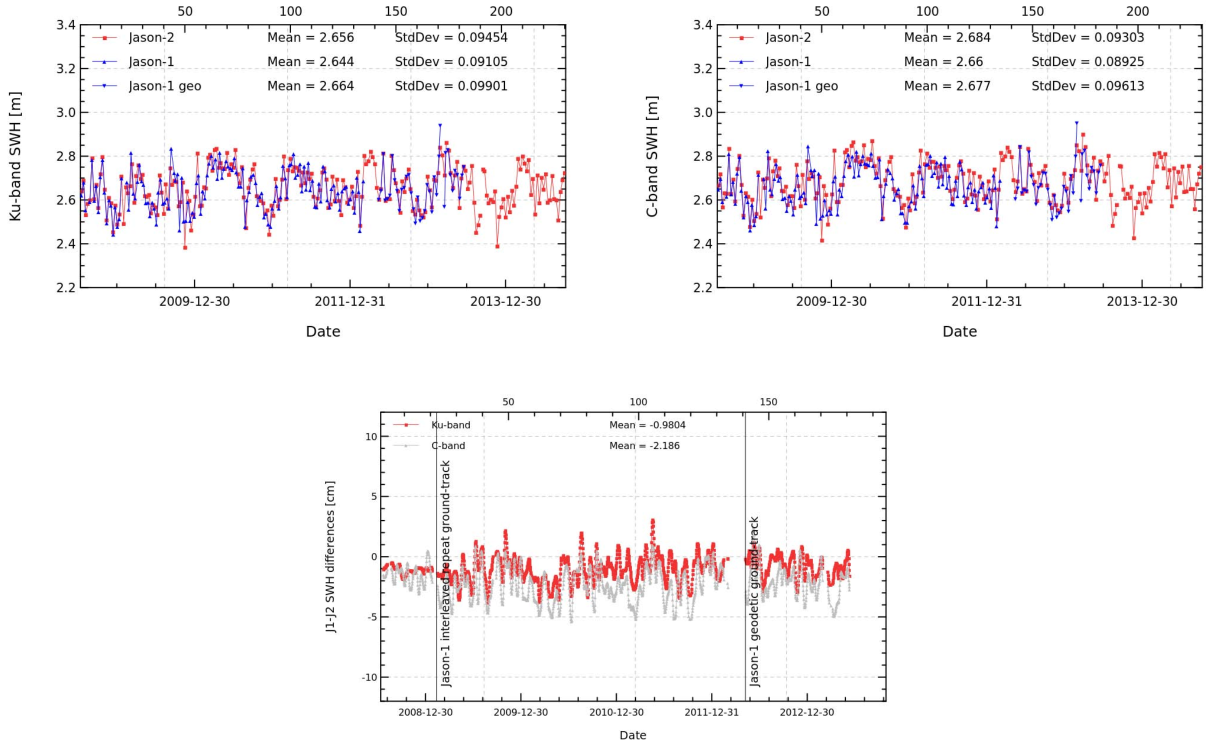

Figure 33: Cyclic monitoring of SWH for Jason-1 and Jason-2 for Ku-band (left) and C-band (right). Daily monitoring of Jason-1 - Jason-2 differences (bottom), a 10 day filter is applied.

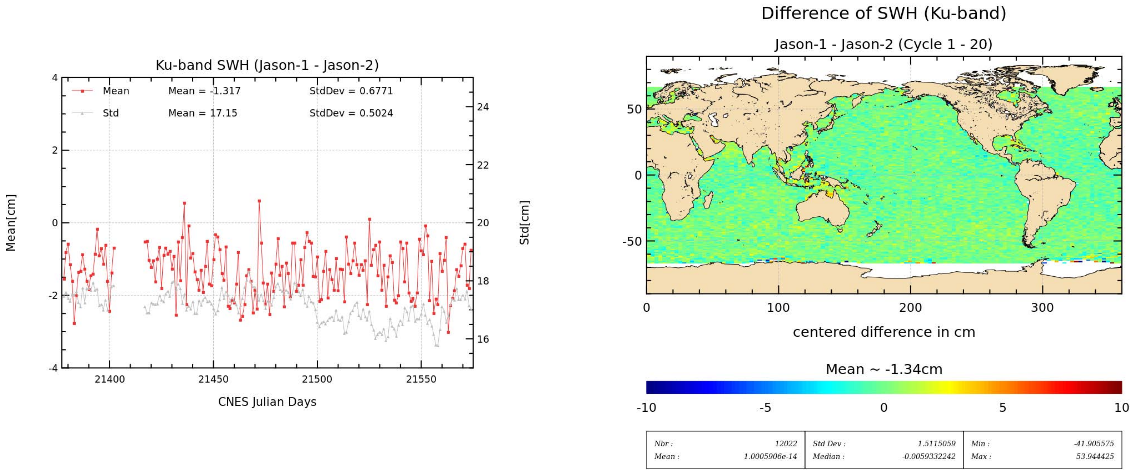

Figure 34: Daily monitoring of mean and standard deviation of Jason-1 - Jason-2 differences for Ku-band SWH (left) and map showing mean of Jason-1 - Jason-2 differences over cycles 1 to 20.

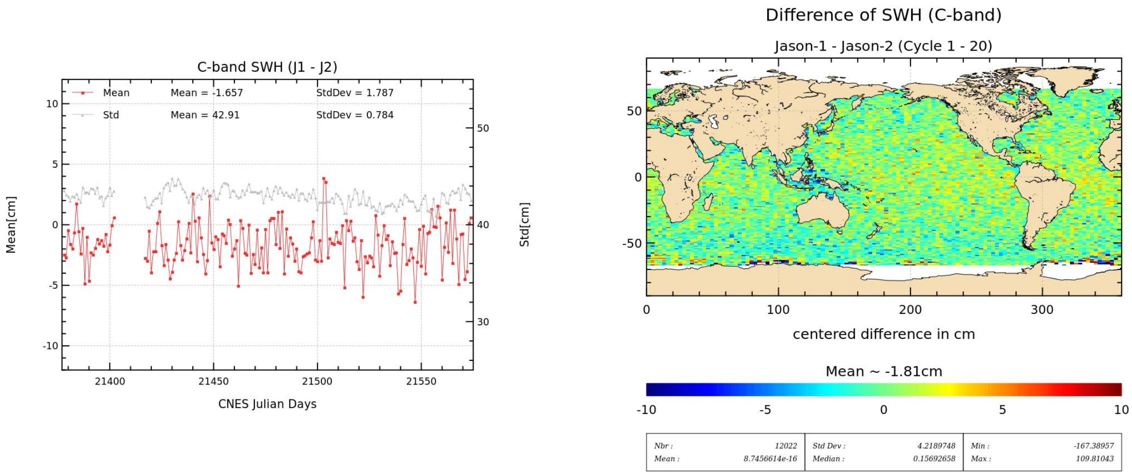

Figure 35: Daily monitoring of mean and standard deviation of Jason-1 - Jason-2 differences for C-band SWH (left) and map showing mean of Jason-1 - Jason-2 differences over cycles 1 to 20.

4.6. Dual-frequency ionosphere correction

The dual frequency ionosphere corrections derived from the Jason-2 and Jason-1 altimeters show a mean difference of about -0.3 cm (figure 36 (left)), with cycle to cycle variations lower than 1 mm. This bias is due to the relative Ku-band (-7.0 cm) and C-band (-2.2 cm) range difference between Jason-1 and Jason-2, as well as the relative Ku-band (-2.8 cm) and C-band (-6.0 cm) sea state difference between Jason-1 and Jason-2. As the dual-frequency ionosphere correction is derived from a combination of Ku and C band ranges (corrected for the corresponding sea state bias), a bias of -3 mm between Jason-1 and Jason-2 ionospheric corrections results. Apart from this bias, the two corrections are very similar and vary according to the solar activity. The map of local differences (figure 36 right) shows small regional differences.

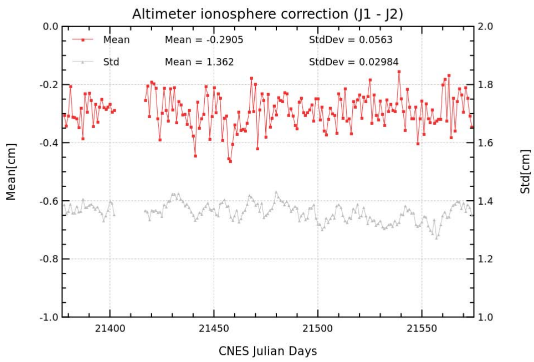

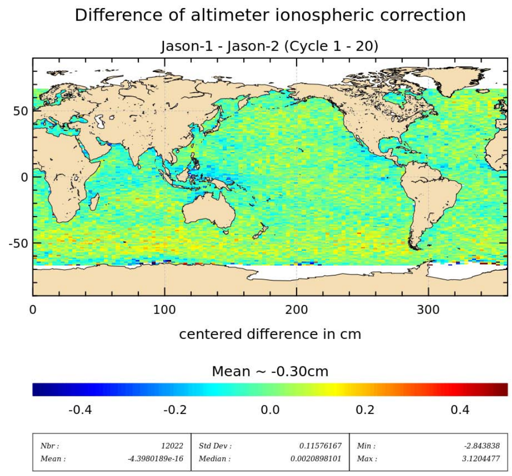

Figure 36: Daily monitoring of mean and standard deviation of Jason-1 - Jason-2 differences for dual-frequency ionospheric correction (left) and map showing mean of Jason-1 - Jason-2 differences over cycles 1 to 20.

Notice that, as for TOPEX and Jason-1 (Le Traon et al. 1994 [59], Imel 1994 [55], Zlotnicky 1994 [88]), it is recommended to filter the Jason-2 dual frequency ionosphere correction before using it as a SSH geophysical correction (Chambers et al. 2002 [38]). A low-pass filter has thus been used to remove the noise of the correction in all SSH results presented in the following sections. Plotting difference of non-filtered ionospheric correction between Jason-1 and Jason-2 versus Jason-2 ionospheric correction shows an apparent scale error, which disappears when using filtered data (see figure 37). As in the beginning of the Jason-2 mission, ionosphere correction was very low, the ionosphere noise is of the same order of magnitude as the ionosphere correction itself. Therefore plotting the difference of non-filtered dual-frequency ionospheric correction versus dual-frequency ionospheric correction induces an apparent scale error.

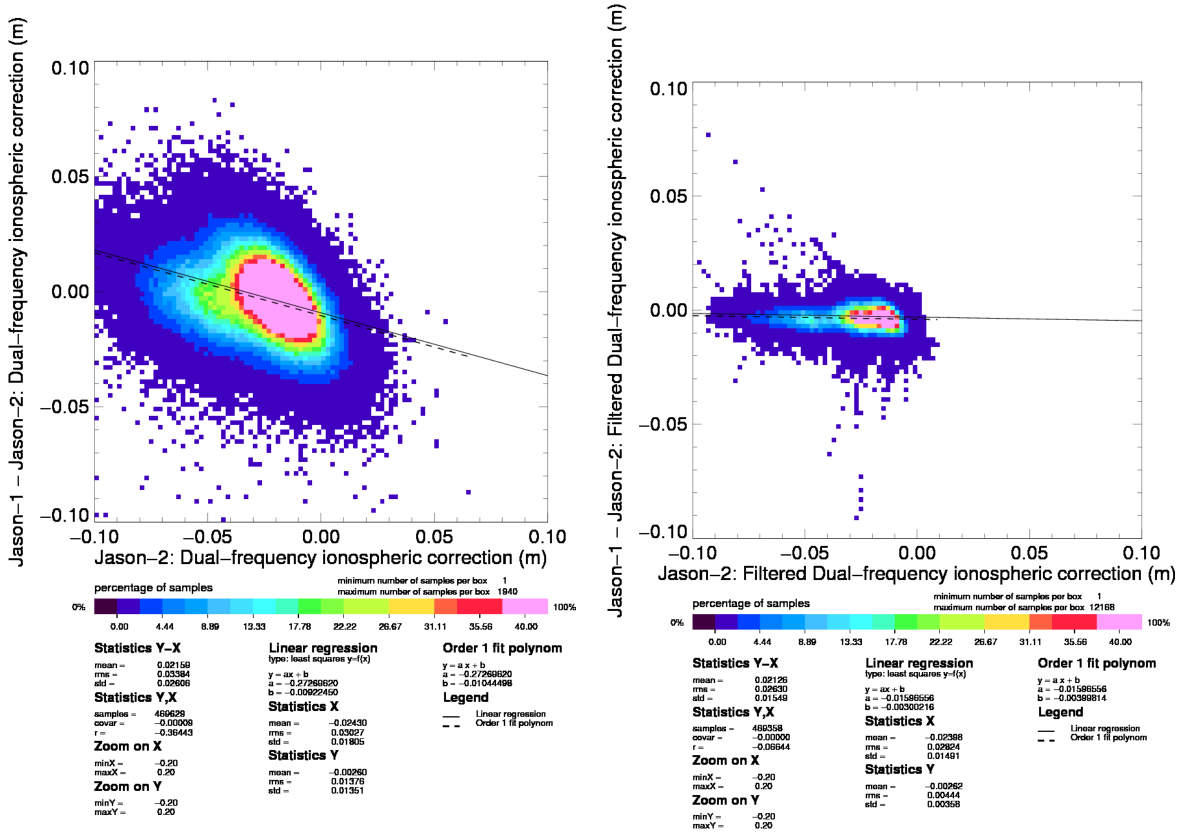

Figure 37: Diagram of dispersion of Jason-1 - Jason-2 versus Jason-2 dual-frequency ionosphere correction for Jason-2 cycle 15. Left: non-filtered, right: filtered.

During 2011, as at the end of 2013 and the beginning of 2014 solar activity has increased and therefore also the absolute value of ionosphere correction (right part of figure 38).

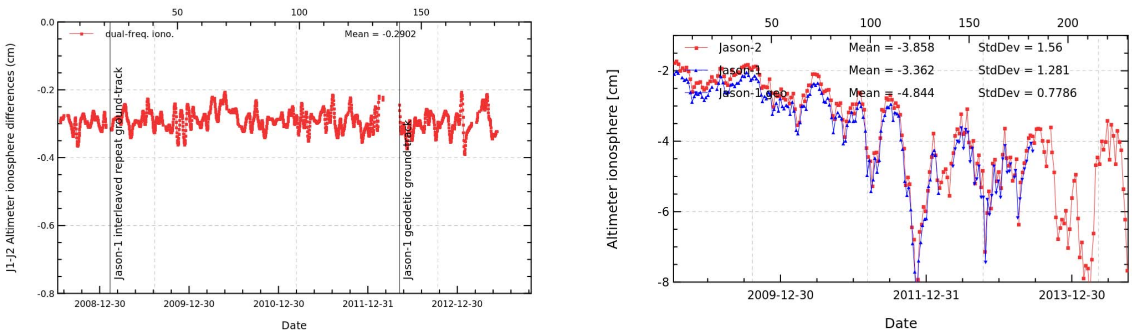

Figure 38: Cyclic monitoring of dual-frequency ionosphere for Jason-1 and Jason-2 (right). Daily monitoring of Jason-1 - Jason-2 differences (left), a 10 day filter is applied.

When comparing altimeter ionosphere correction to GIM correction (figure 39), mean as well as standard deviation of this difference increases since 2011. This concerns both Jason missions.

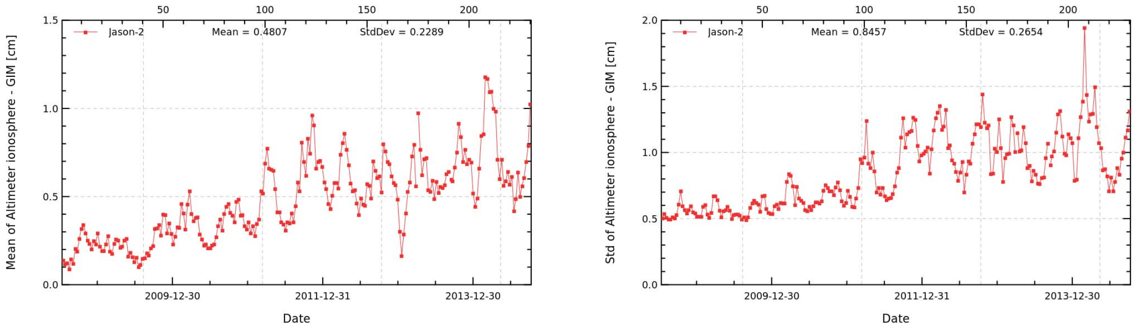

Figure 39: Cycle per cycle monitoring of filtered altimeter ionosphere correction minus GIM ionosphere correction for Jason-1 and Jason-2. Left: Mean, right: standard deviation.

Figure 40 shows the mean difference between altimeter ionosphere and GIM correction after a one-year smooth for slots of local hours. Ionosphere differences between altimeter and GIM are higher for day time measurements than for night time measurements.

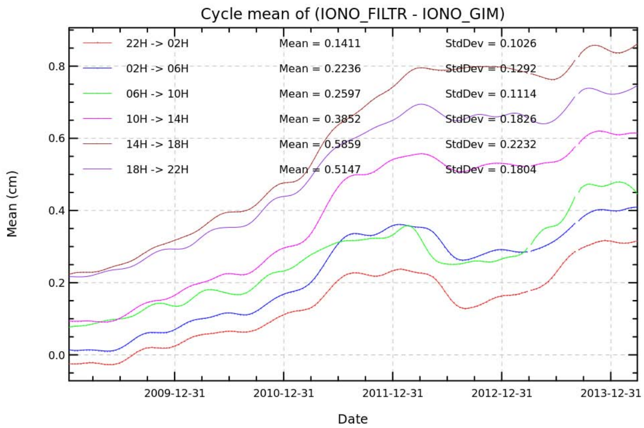

Figure 40: Cycle per cycle monitoring of filtered altimeter ionosphere minus GIM correction computed per local hour time intervals. A one-year smooth is applied.

4.7. AMR Wet troposphere correction

4.7.1. Overview

The Jason-2 radiometer wet troposphere correction available contains an improved retrieval algorithm near coasts ([35]). Note that the product AMR radiometer wet troposphere correction has (according to S. Brown) several level of calibration:

- Cycles 1-113 - Climate data record quality calibration Cycles
- 114-140 - Intermediate quality calibration (somewhere between climate quality and operational(ARCS) quality)
- Cycle 141 onward - Operational(ARCS) quality calibration

Figure 41 shows on the left side the daily monitoring of the difference of radiometer wet troposphere correction between the two missions (JMR - AMR) during the formation flight phase. Note that for Jason-1 the JMR replacement product (which was available for cycles 228 to 259) was used. This corrects for stability problems of JMR which occurred after the safehold in August 2008. For the other cycles the correction available in Jason-1 GDR-C is used. AMR is globally slightly dryer than JMR (-0.09 cm). But locally, especially near coasts (right side of figure 41), AMR is wetter than JMR. This is related to the fact that the Jason-2 correction uses improved retrieval algorithm in coastal areas, whereas this is not the case for Jason-1. The daily monitoring is very stable, except for julian day 21556 (2009-01-07), where the difference between the two radiometers shows a drop of 3 mm. This is related to the JMR replacement, which is for this day about 3 mm wetter than usually.

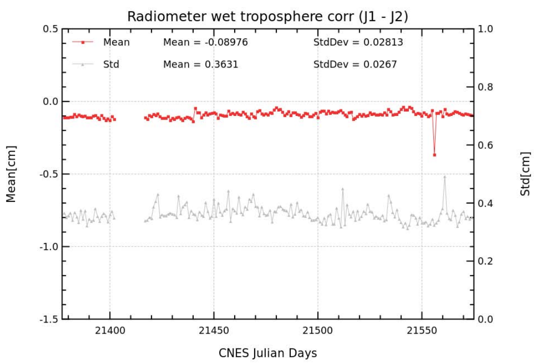

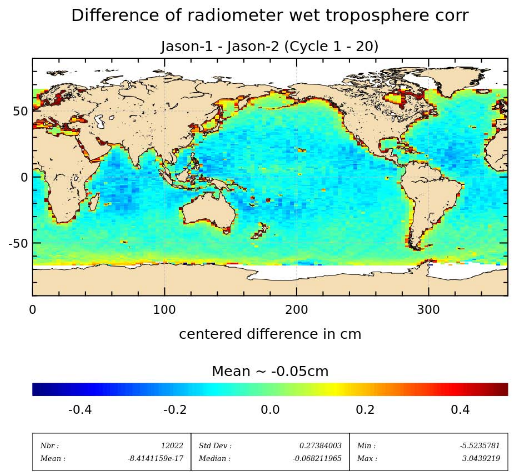

Figure 41: Daily monitoring of mean and standard deviation (left) of Jason-1 - Jason-2 radiometer wet troposphere correction. Map showing mean of Jason-1 - Jason-2 differences over cycles 1 to 20.

4.7.2. Comparison with the ECMWF model

The ECMWF wet troposphere correction has been used to check the Jason-1 and Jason-2 radiometer corrections. Daily differences are calculated and plotted in figure 43. It clearly appears (on left side of figure 43) that Jason-2 radiometer correction (AMR) from GDR products is much more stable than for Jason-1 (JMR), especially at the beginning of Jason-2 period where large oscillations (up to 7mm) are observed between JMR (from GDR-C product) and model. Indeed after the safehold mode of Jason-1 in August 2008 (corresponding to Jason-2 cycle 4), JMR experienced some thermal instability. In addition, small differences linked to yaw-dependent effects (as also observed on TOPEX radiometer (Dorandeu et al., 2004, [46])) are visible (yaw maneuvers are indicated as gray lines on left side of figure 43). In order to take into account these effects, new JMR calibration coefficients are provided and updated at each Jason-1 GDR reprocessing campaign. Using the JMR replacement product (available for Jason-1 cycles 228 to 259) corrects for the instabilities during August 2008 (Brown et al. 2009, [34]). Now, thanks to the new ARCS (Autonomous Radiometer Calibration System) (Brown et al. 2009, [34]) calibration system set up for Jason-2, AMR radiometer correction is calibrated at each GDR cycle and the calibration coefficients are modified if necessary. On right side of figure 43 the black lines indicate, each time a modification of the calibration coefficients were necessary. The lines are only drawn from cycle 114 onwards.
During 2011, the frequency of application of new calibration coefficients has increased, especially during summer 2011. The AMR wet troposphere correction shows jumps and drifts in the IGDRs. The calibrations applied for the GDRs correct most of these anomalies, nevertheless small jumps persist. There can also be small drifts visible within a cycle, as the ARCS corrections apply a constant value over a whole cycle. Furthermore, the AMR comparison with model highlights also long-term signals with Jason-2 not clearly observed with Jason-1 (figure 43 (left side)). Finally, the cross-comparison between all radiometers and models available is necessary to analyze the stability of each wet troposphere correction. An overview of the wet troposphere correction importance for mean sea level is given in Obligis et al. [63].

Figure 42 shows mean and standard deviation for cycle per cycle differences between Jason-2 radiometer and ECMWF model wet troposphere corrections for several data types. Over year 2014, OGDR, IGDR and GDR radiometer data were less subject to drifts and jumps. The mean of IGDR and GDR radiometer minus ECMWF model wet troposphere differences are only different just after cycle 198 and cycle 205 as there the change of radiometer calibration coefficient happened for GDR production (as there is a roughly 1 to 2 month delay between GDR and IGDR production, IGDR production was already a couple of cycles ahead). The standard deviation of OGDR and IGDR wet troposphere differences is higher for OGDR than for IGDR, as OGDR contain predicted model fields instead of analyzed model field (for IGDR and GDR products).

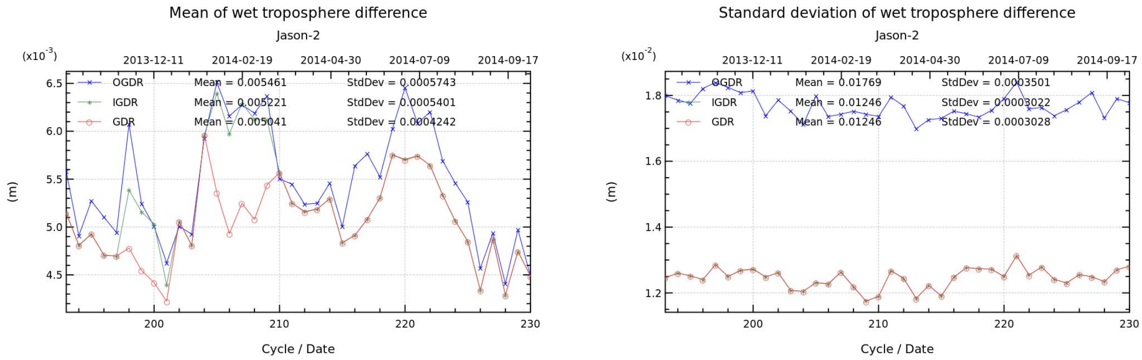

Figure 42: Cycle per cycle monitoring of mean (left) and standard deviation (right) of radiometer minus ECMWF model wet troposphere correction over 2013 (until cycle 195) for Jason-2 O/I/GDR.

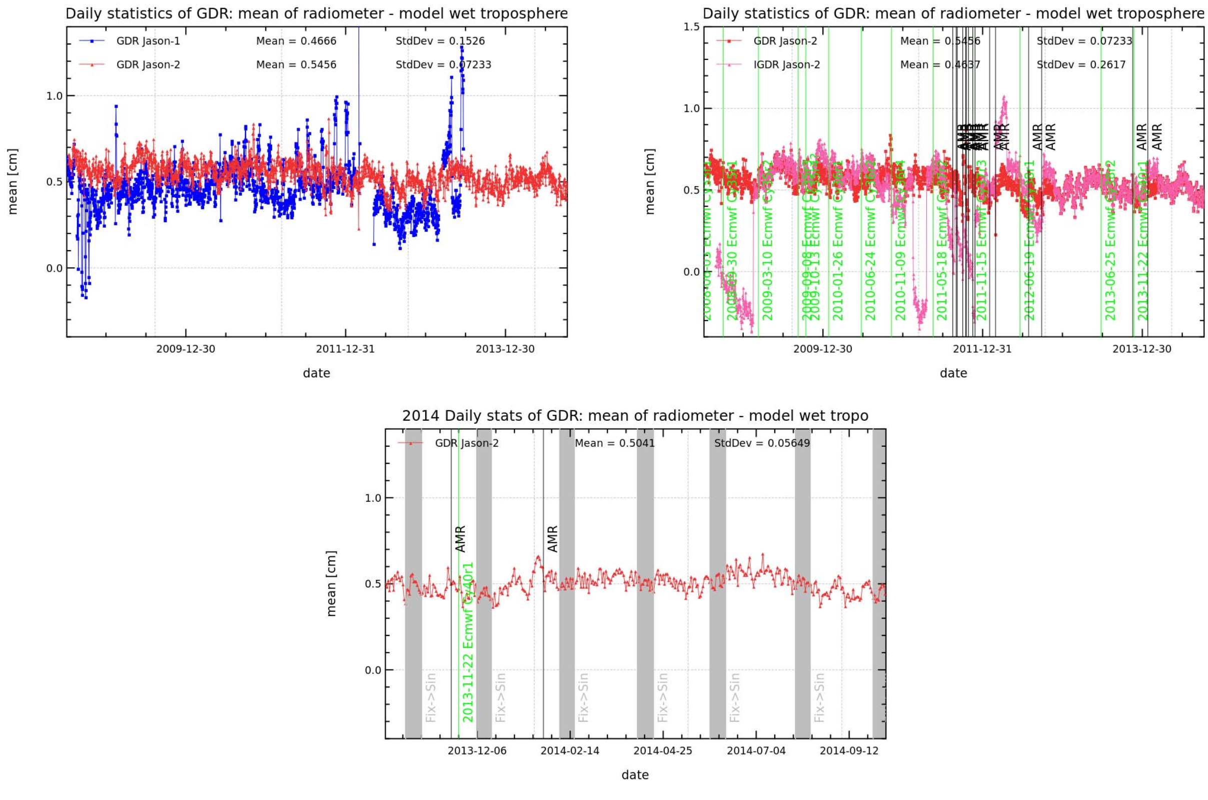

Figure 43: Left: Daily monitoring of radiometer and ECMWF model wet troposphere correction differences for Jason-1 (blue) and Jason-2 (red). Right: daily monitoring for Jason-2 GDRs (red) and IGDRs (pink). Vertical green lines correspond to ECMWF model version changes, black lines correspond to AMR calibration coefficients changes on GDR products also impacting IGDR product (but later). Bottom: Daily monitoring for Jason-2 GDRs (red) for 2014. Vertical green lines correspond to ECMWF model version changes, black lines correspond to AMR calibration coefficients changes on GDR products. They impact also IGDR products (but later). Vertical gray bands correspond to yaw maneuvers on Jason-2.

4.8. Altimeter wind speed

Figure 44 shows on the left side the daily monitoring of the difference of altimeter wind speed between the two missions. Before the Jason-2 reprocessing, there was a difference of about -0.4 m/s between Jason-1 and Jason-2. Note that the histograms of Jason-2 GDR-T and Jason-1 had different shapes. Using GDR-D data, the mean difference between Jason-1 and Jason-2 altimeter wind speed is reduced to 0.06 m/s, and the shapes of the histograms (figure 45) are also much more closer. Finally the regional differences are also reduced. Locally (right side of figure 44), altimeter wind speed from Jason-1 is higher than from Jason-2. The signal visible on daily monitoring, is anti-correlated to the signal visible on daily monitoring of backscattering coefficient (see figure 31), as wind speed computation uses principally backscattering coefficient. This signal is related to events of high mispointing of Jason-1.

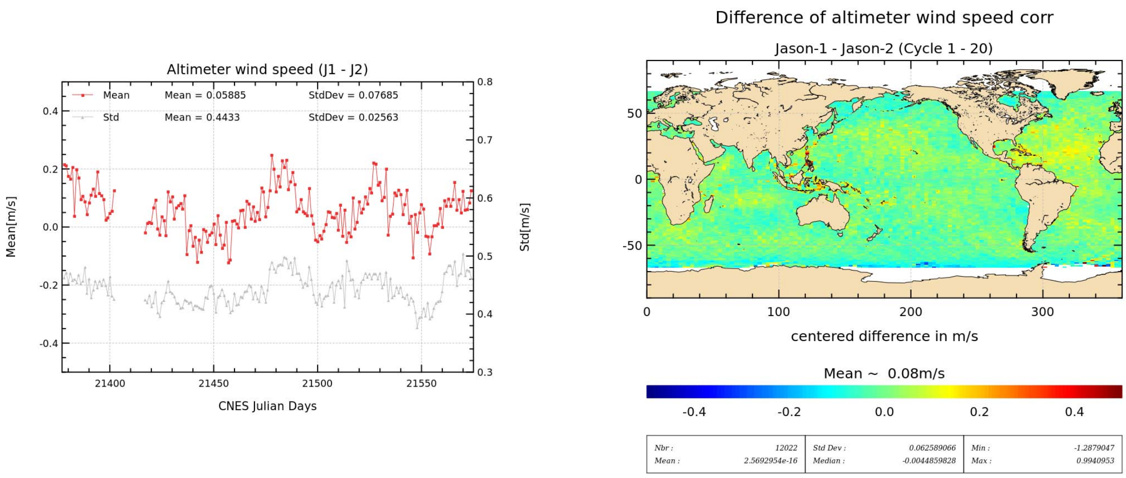

Figure 44: Daily monitoring of mean and standard deviation (left) of Jason-1 - Jason-2 altimeter wind speed. Map showing mean of Jason-1 - Jason-2 differences over cycles 1 to 20.

For Jason-1 Gdr-C release, the wind speed is calculated with an algorithm based on ([51]), fitted on Jason-1 Sigma0 (Collard algorithm). It is the same algorithm applied for Jason-2 now. As there is a bias between Jason-1 and Jason-2 Ku-band backscattering coefficients, prior to the altimeter wind speed computation of GDR-D, a calibration bias of 0.32 dB has been added to the Ku-band backscattering coefficient.
Thanks to the altimetry standard improvements since Jason-1 launch ([72], [40]), the error budget of SSH calculation has been reduced. Through the sea state bias correction, the Sigma0 bias uncertainty has thus become not inconsiderable as shown in recent study ([83], [3]). Indeed an error of 0.1 dB on the backscattering coefficient has an impact of about 0.5 m/s on the altimeter wind speed, which in turn has an impact of about 1.6 mm on the sea state bias correction.

Figure 46 shows mean and standard deviation for cycle per cycle altimeter wind speed for several data types of Jason-2. The altimeter wind speed of the different data types is coherent.

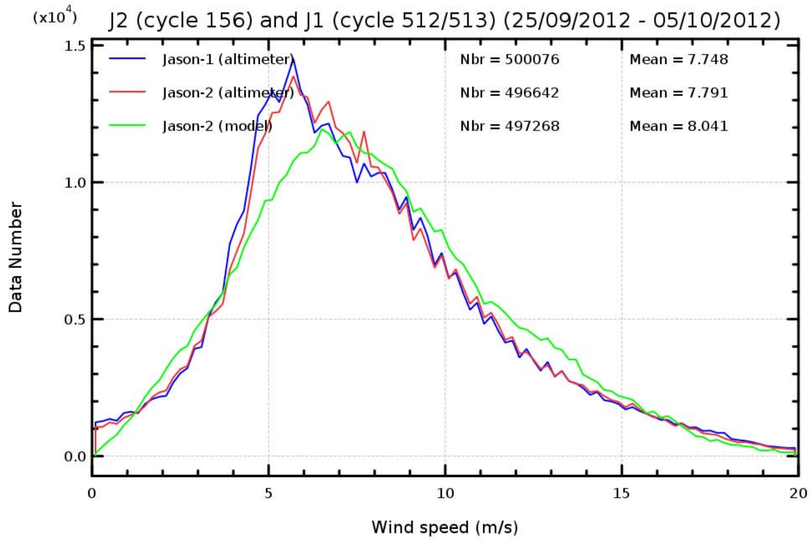

Figure 45: Histogram of altimeter (Jason-1 in blue, Jason-2 in red) and model wind speed (green) for a 10 day period.

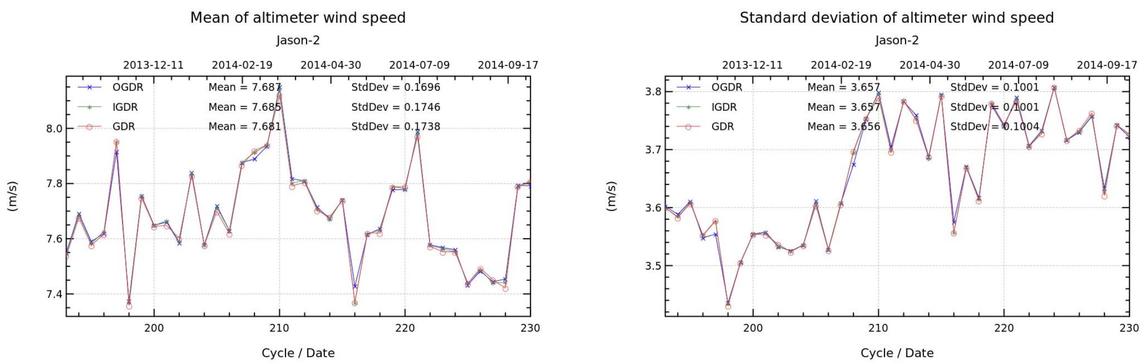

Figure 46: Cycle per cycle monitoring of mean (left) and standard deviation (right) of altimeter wind speed over 2014 (until cycle 230) for Jason-2 O/I/GDR.

4.9. Sea state bias

The sea state bias look-up table used for GDR-D was computed using Jason-2 data from internal reprocessing which were as close as possible to the GDR-D standards. Differences between Jason-1 and Jason-2 are about -3 cm (left of figure 47).

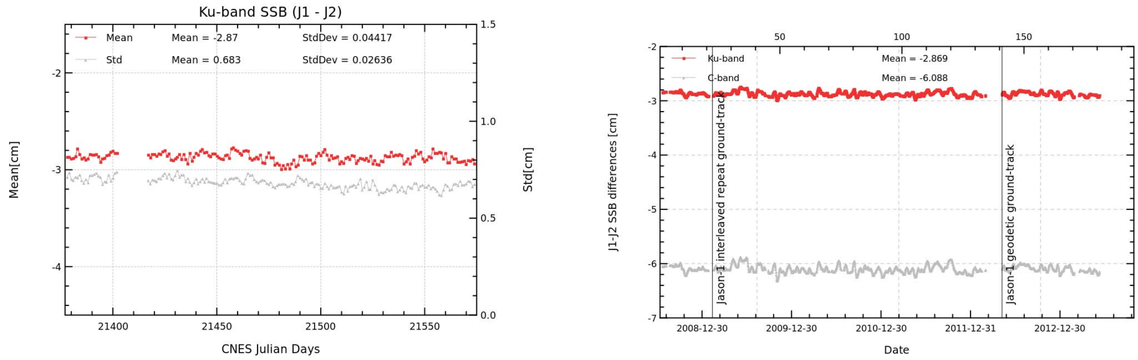

Figure 47: Daily monitoring of mean and standard deviation (left) of Jason-1 - Jason-2 sea state bias over cycles 1 to 20. Daily monitoring of Jason-1 - Jason-2 differences (right), a 10 day filter is applied.

This difference is not a bias, as can be seen from the maps of the Jason-1 - Jason-2 sea state bias difference (figure 48). Differences between Jason-1 and Jason-2 sea state bias increase using Jason-2 GdrD (top of figure 48), as the methods (as well as data) used for the SSB model computation are different.

In the case of top left side of figure 48, the method for Jason-1 and Jason-2 are different (the new method used in case of Jason-2 is explained in (see [83]) and the input values (wind, wave) for Jason-2 are those of standard D version. Indeed, GDR-D sea state model is calculated with a different approach of low sea states. In these areas, the editing method has changed so that differences are mainly observed here.

On the top right, the Tran 2012 sea state bias model is used for Jason-2. At OSTST 2012 meeting, Tran et al. [85] presented a new SSB model computed using one year of GDR-D data. This model seems better than the SSB model used for the GDR-D product. Though the SSB model used for the GDR-D products was computed on Jason-2 data from an internal reprocessing which was as close as possible to the GDR-D standard, there were nevertheless some differences with the GDR-D data. Indeed, the wind speed (necessary for SSB computation) from the internal reprocessing was tuned with a preliminary bias on sigma0, whereas the wind speed of the GDR-D product uses a fine-tuned bias (takes additionally into account a correction from LTM and corrected atmospheric correction from S. Brown in sigma0).

When using the updated sea state bias proposed by Tran et al. [85] for both missions, the Jason-1 minus Jason-2 differences are much more homogeneous (see bottom of figure 48). Note that this homogenization is mainly due to the updated Jason-2 SSB and to a lesser extent due to the updated Jason-1 SSB.

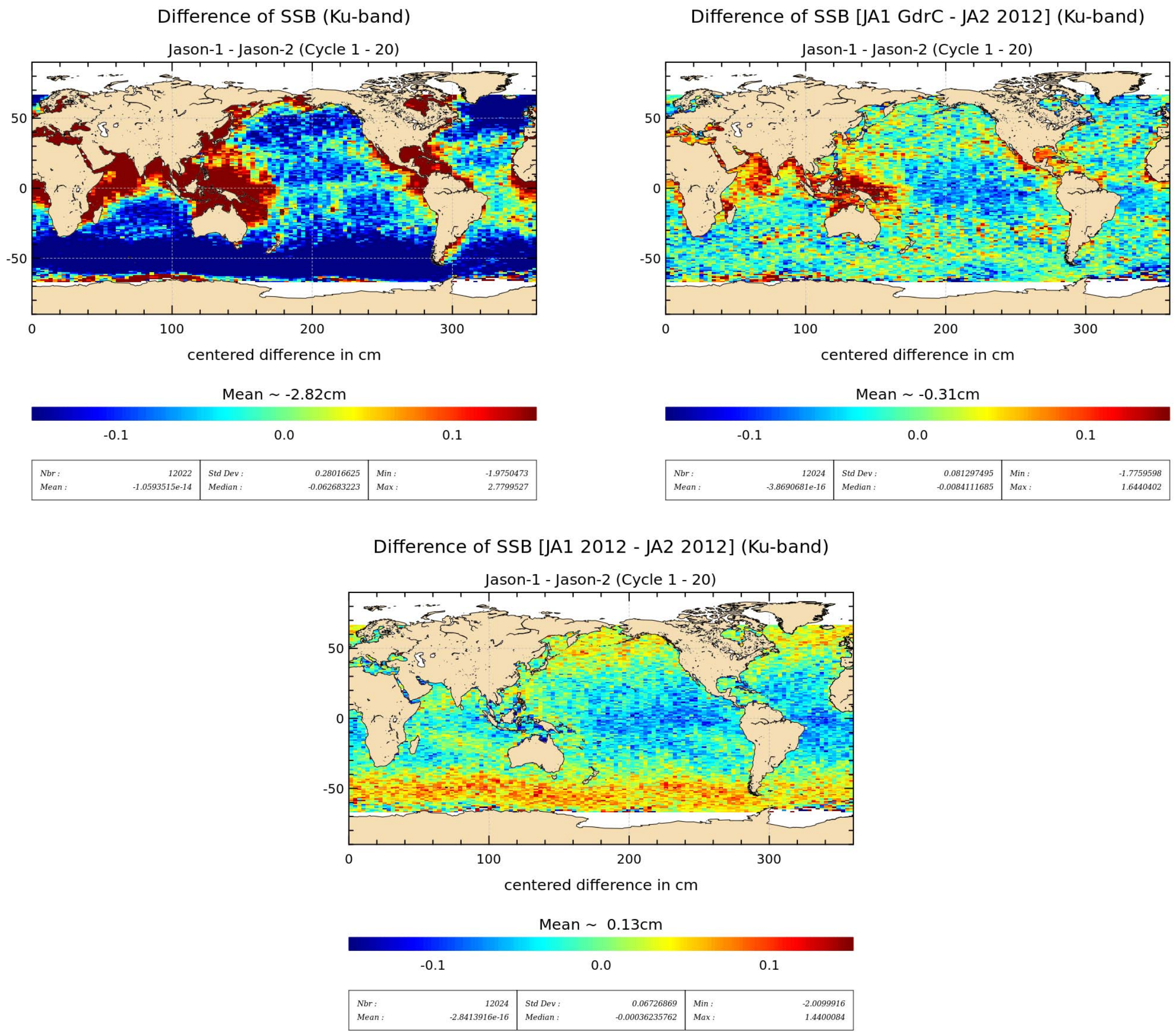

Figure 48: Map showing mean of Jason-1 - Jason-2 sea state bias differences over cycles 1 to 20. ***Top left:*** *using SSB from Jason-1 GDR-C and Jason-2 GDR-D (map centered around -2.82 cm).* ***Top right:*** *using SSB from Jason-1 GDR-C and updated (2012) SSB for Jason-2 (map centered around -0.31 cm).* ***Bottom:*** *using updated (2012) SSB for both Jason-1 and Jason-2 (map centered around 0.13 cm).*

5. SSH crossover analysis

5.1. Overview

SSH crossover differences are the main tool to analyze the whole altimetry system performances. They allow us to analyze the SSH consistency between ascending and descending passes. However in order to reduce the impact of oceanic variability, we select crossovers with a maximum time lag of 10 days. Mean and standard deviation of SSH crossover differences are computed from the valid data set to perform maps or a cycle by cycle monitoring over all the altimeter period. In order to monitor the performances over stable surfaces, additional editing is applied to remove shallow waters (bathymetry above -1000m), areas of high ocean variability (variability above 20 cm rms) and high latitudes ($> |50| deg$). SSH performances are then always estimated with equivalent conditions. The main SSH calculation for Jason-2 and Jason-1 are defined below.

$$SSH = Orbit - Altimeter\ Range - \sum_{i=1}^{n} Correction_i$$

with $Jason-1/Jason-2\ Orbit = CNES\ orbit$ for GDR products, and

$$\begin{aligned}
\sum_{i=1}^{n} Correction_i &= Dry\ troposphere\ correction \\
&+ Dynamical\ atmospheric\ correction \\
&+ Radiometer\ wet\ troposphere\ correction \\
&+ Dual\ frequency\ ionospheric\ correction\ (filter\ 250\ km) \\
&+ Non\ parametric\ sea\ state\ bias\ correction \\
&+ Ocean\ tide\ correction\ (including\ loading\ tide) \\
&+ Earth\ tide\ height \\
&+ Pole\ tide\ height
\end{aligned}$$

In order to allow better comparisons between Jason-1 and Jason-2, some standards of Jason-1 GDR-C were updated. *Note that from 7th of May 2012 (Jason-1 cycle 500, which corresponds to end of Jason-2 cycle 141) and until the end of the Jason-1 mission (21st of June 2013, during Jason-2 cycle 183), Jason-1 was on a geodetic ground-track. The Jason-1 GDR-C product contains from cycle 500 onwards already the POE-D solution and the MSS CNES_CLS_2011.*

Parameter	Jason-1 GDR-C	Jason-1 GDR-C with updates
Orbit	CNES POE-C	CNES POE-D
radiometer wet troposphere correction	JMR	JMR replacement product for period which corresponds to Jason-2 cycles 001 to 020
		.../...

Parameter	Jason-1 GDR-C	Jason-1 GDR-C with updates
Global ocean tide	GOT00V2	GOT 4.8
Mean Sea Surface	CLS_2001	CNES_CLS_2011

Table 8: updated standards of Jason-1 for comparison with Jason-2

5.2. Mean of SSH crossover differences

The cycle by cycle mean of SSH differences is plotted in figure 49 for Jason-2 and Jason-1 (using standards from Jason-1 GDR-C products and updated standards). The curves are very similar and do not highlight any anomaly. However, a small 120 day signal is visible for Jason-2 data. It is increased for updated Jason-1 products (compared to Jason-1 GDR-C products). SSH differences of OGDR products (using Doris/Diode navigator orbit) show slightly stronger variations (right of figure 49) till early 2014.
Mean of SSH differences at crossovers for Jason-2 IGDR products (using MOE orbits) has noticeable negative values in average (-0.71cm over the last year versus -0.20cm in case of GDR), as can be seen on figure 49. In addition, the IGDR data monitoring shows a 120 day signal that is reduced in case of GDR. This difference of behaviour for IGDR and GDR is now explained by the way the solar radiation pressure is taken into account in orbit solution computation (different for MOE and POE). For the future orbit standard E, an identical modeling of solar radiation pressure is planned for MOE and POE, which will reduce the 120 day signal on IGDR. In addition, even the remaining 120 day signal on GDR will be reduced with POE-E (see POE-E on figure 50).

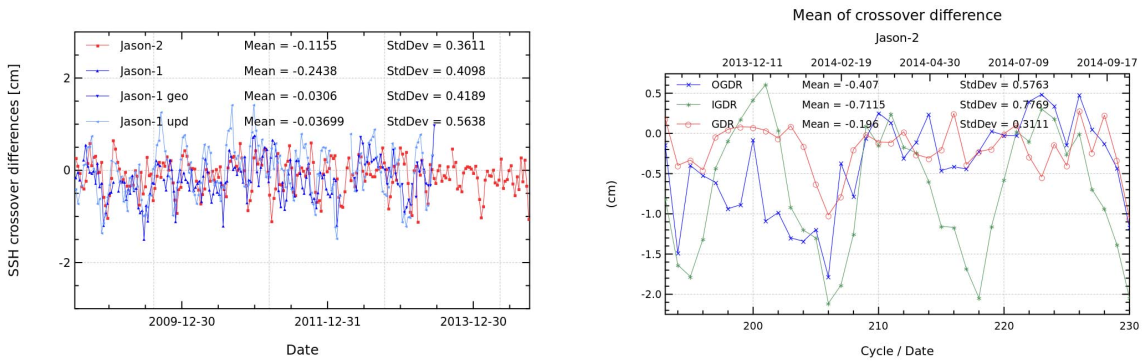

Figure 49: Left: Monitoring of mean of SSH crossover differences for Jason-2 and Jason-1 using Jason-2 (red), Jason-1 GdrC (blue), Jason-1 GdrC Upd with GOT4.8 + POE-D + JMR replacement (light blue). right: Monitoring over 2014 of mean of SSH crossover differences for different data types of Jason-2: OGDR (blue), IGDR (green), GDR (red).

The map of mean SSH crossover differences plotted in left side of figure 50 was calculated using Jason-2 GDR products, no strong geographically correlated patterns are detected. Nevertheless, there is a slight geographically correlated pattern on the map with POE-D orbit solution. This pattern disappears (right of figure 50) using the preliminary POE-E solution (see details about POE-E here 8.1.). This pattern seems related to the 120 day signal, as it disappears in the same time as the 120 day signal is reduced in the periodogram of the preliminary POE-E solution.

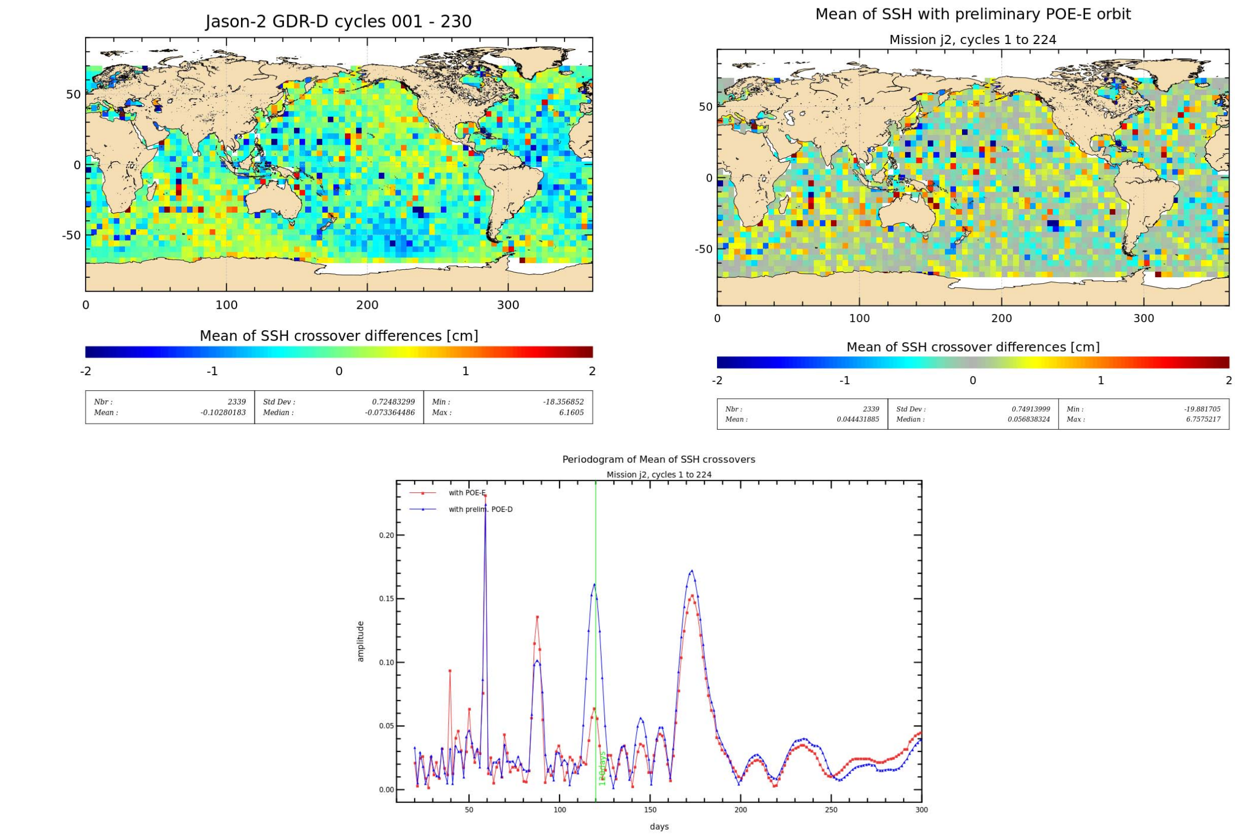

Figure 50: Left: Map of mean of SSH crossovers differences for Jason-2 cycle 1 to 230. Right: Map of mean of SSH crossovers differences for Jason-2 cycle 1 to 224 using preliminary POE-E orbit solution. Bottom: periodogram of mean of SSH crossovers differences for Jason-2 cycle 1 to 224, with POE-D or preliminary POE-E.

Dual-mission crossover performances are computed between Jason-2 and Jason-1, as well as Jason-2 and Envisat. Jason-1 GDR-C data were used with updated standards (see table 8). Mean SSH differences at Jason-2/Jason-1 crossovers (shown on left side of figure 51) have a bias of about 10 cm (JA1-JA2). This bias is mostly due to the range differences between the two satellites, but also due to different sea state bias models. The map shows small regional structures of about ±1 cm, especially in southern Pacific, but also around Indonesia and in the Mediterranean Sea. These structures are stronger than those observed between Jason-2 GDR-T and Jason-1 GDR-C (see Jason-2 annual report 2011 [[13]]). This difference comes mainly from the different sea state biases used for Jason-1 GDR-C and Jason-2 GDR-D (see also chapter 4.9.). Using updated sea state bias (presented at 2012 OSTST by Tran et al. [[85]]) for both Jason-2 and Jason-1 data, reduces most of the geographical pattern (right of figure 51). A small pattern remains. This structure was also seen during the flight formation phase, when differences without applying geophysical corrections were possible. It is dependent on orbit solutions, as it is strongly reduced when using GSFC orbit solutions for both missions ([6], see also bottom of figure 58).

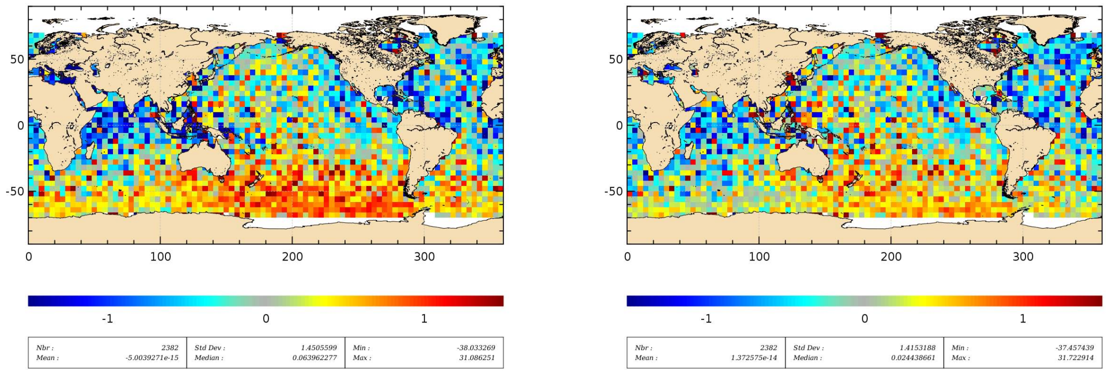

Figure 51: Map of mean of SSH crossovers differences between Jason-2 and Jason-1 (JA1-JA2) for 2011 using POE-D orbit (left). The map is centered around the mean (10.06 cm). Right: same as left, but using 2012 sea state bias for both satellites. The map is centered around the mean (7.09 cm).

For comparisons with Envisat, reprocessed V2.1 Envisat data were used, in addition GOT4.8 global ocean tide was updated. Though Jason-2 GDR-T and Envisat V2.1 are using CNES produced POE (POE-C standard), a large east/west bias is observed on the left side of figure 52, see also [45]. This is also seen on Jason-1/Envisat crossovers, especially since 2007 (see [48]). This behavior is related to the gravity field used during orbit computation. When using Jason-2 GDR-D, as well as POE-D for Envisat (POE-D is based on EIGEN-GRGS_RL02bis_MEAN-FIELD gravity fields), this east/west biased disappears, as shown on right side of figure 52 (see also annual report of Envisat 2011 [66]). The remaining structure is partly due to the different SSB models, especially in South Pacific and Mediterranean Sea, as these differences are decreased using OSTST 2012 sea state model for both satellites (as shown on bottom of figure 52). The remaining differences could be due to the ionosphere correction (as the dual-frequency ionosphere correction is no longer available for this period on Envisat) or other differences. Note that comparison between Jason-2 and AltiKa are detailed in [22].

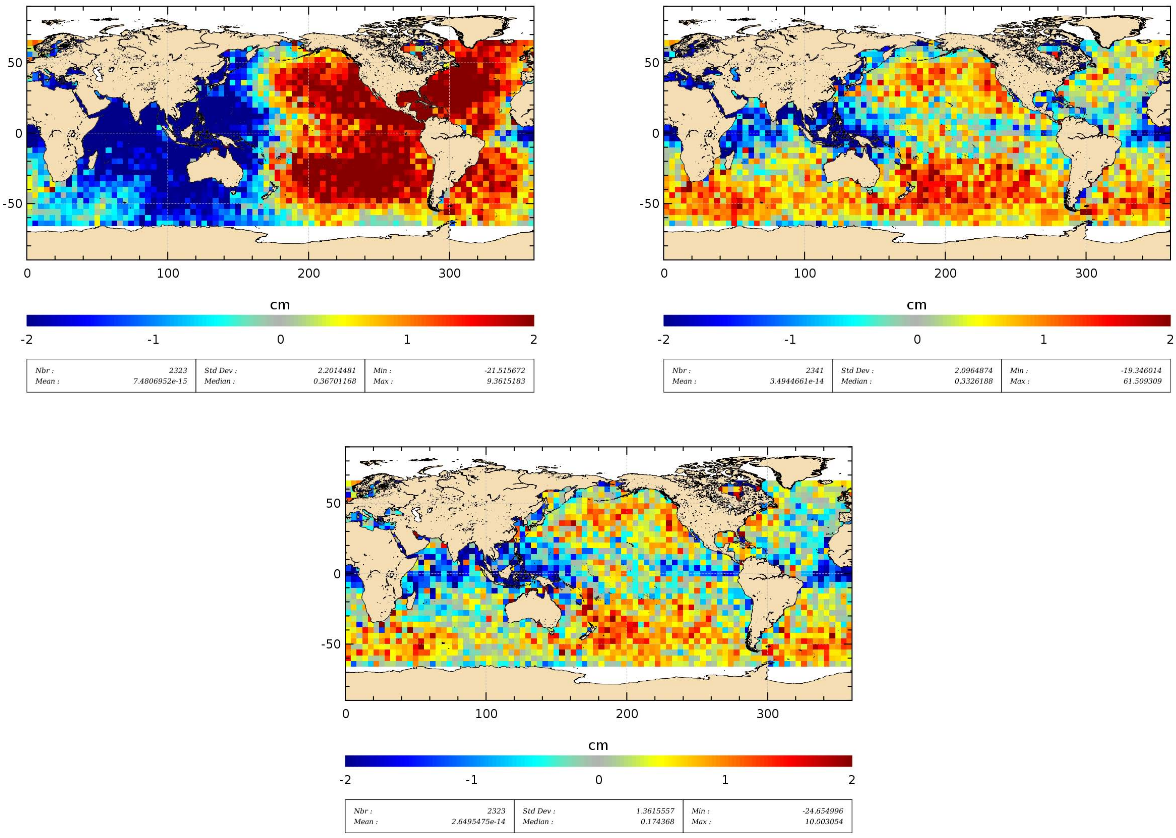

Figure 52: Map of mean of SSH crossovers differences between Jason-2 and Envisat (EN-JA2) for 2011 using model wet troposphere correction. Left: Jason-2 GdrT (POE-C already included) and Envisat V2.1 data (POE-C already included). The map is centered around the mean of 28.64 cm. Right: Jason-2 GdrD (POE-D already included) and Envisat V2.1 data + POE-D standard. The map is centered around the mean of 46.18 cm. Bottom: Jason-2 GdrD and Envisat V2.1 data + POE-D standard + OSTST 2012 sea state bias (for both missions). The map is centered around 44.74 cm.

5.3. Standard deviation of SSH crossover differences

The cycle by cycle standard deviation of SSH crossovers differences are plotted for Jason-2 and Jason-1 in figure 53 after applying geographical criteria (bathymetry, latitude, oceanic variability) as defined previously (chapter 5.1.). Both missions show very good performances, very similar and stable in time. No anomaly is detected (the value above 6 cm for Jason-1 is related to degraded orbit quality due to several inclination maneuvers during Jason-1 cycle 315). The average figure is 5.1 cm rms for Jason-1, 5.0 for updated Jason-1, and 4.9 cm rms for Jason-2 data. Keeping in mind that during the Jason-1/TOPEX formation flight phase in 2002, the same statistic using Jason-1 GDR-A products was close to 6.15 cm (see [46]). This illustrates the improvements performed in the altimetry ground processing since the Jason-1 launch especially thanks to new retracking algorithms, new geophysical corrections (oceanic tidal, dynamic atmospheric correction, ...) and new orbit calculations implemented first in GDR-B and later in GDR-C release (see [72] concerning impact of GDR-B/GDR-A, [40] concerning impact of GDR-C/GDR-B). The reprocessing of Jason-

2 in GDR-D also improved the performance at crossover points. The variance of SSH crossover differences was reduced by 1.7 cm2 when switching from GDR-T to GDR-D standards, as shown on [14]. The main contributors to this improvement are the POE-D orbit standard and the GOT4.8 global ocean tide. Though Jason-1 and Jason-2 show very good performances and are within the mission specifications, their standard deviation of SSH differences at crossovers is sometimes higher than usual.

When comparing the performances of the different Jason-2 data types (OGDR, IGDR, GDR) over 2014 (right of figure 53), OGDR have the highest standard deviation with 6.2 cm, though this value is already extremely good considering that OGDR have a latency of about 3h, recalling that Jason-1 GDR-A products had a standard deviation of 6.15 cm. IGDR data have a standard deviation of 5.1 cm over 2014.

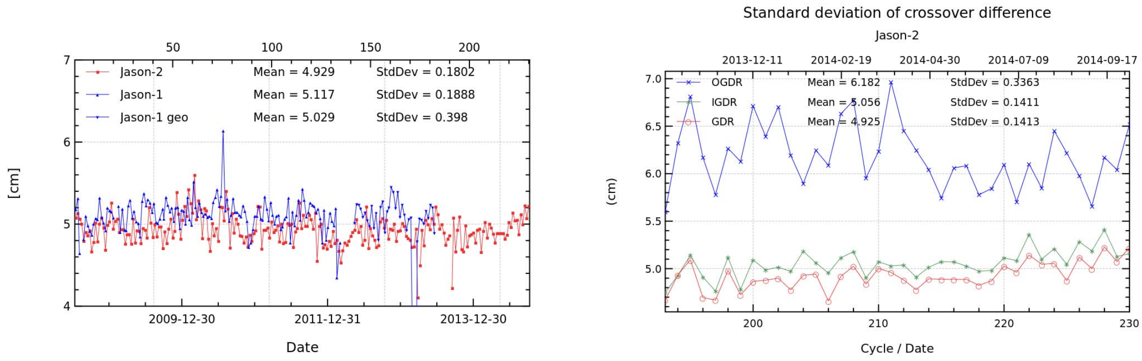

Figure 53: Cycle by cycle standard deviation of SSH crossover differences for Jason-2 and Jason-1. Only data with abs(latitude) < 50°, bathymetry < -1000m and low oceanic variability were selected.

5.4. Estimation of pseudo time-tag bias

The pseudo time tag bias (α) is found by computing at SSH crossovers a regression between SSH and orbital altitude rate ($\dot{H}$), also called satellite radial speed:

$$SSH = \alpha\dot{H}$$

This empirical method allows us to estimate the potential real time tag bias but it can also absorb other errors correlated with $\dot{H}$. Therefore it is called “pseudo” time tag bias. The monitoring of this coefficient estimated at each cycle is performed for Jason-1 and Jason-2 in figure 54. Both curves are very similar highlighting an almost 59-day signal with almost no bias (close to 0.01 ms for Jason-1 and -0.02 ms for Jason-2).
Before the Jason-2 reprocessing the GDR-T showed a bias of -0.29 ms. The origin of constant part of the pseudo time tag bias was found by CNES [31] and so corrected in the GDR-D product (see also the Jason-2 handbook [52]), nevertheless the 59 day-signal is still unexplained. For Jason-1 GDR-C products ([5], an empirical correction containing $\alpha\dot{H}$ has been already added to improve the Jason-1 SSH calculation.

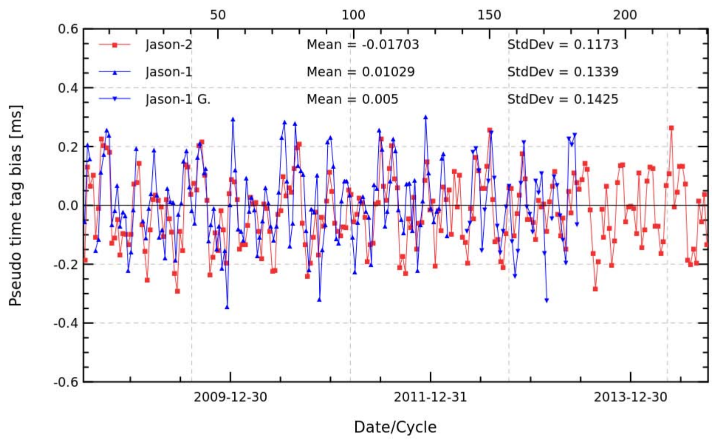

Figure 54: Monitoring of pseudo time-tag bias estimated cycle by cycle from GDR products for Jason-2 and Jason-1

In 2014, comparisons have been done in order to analyze the impact of the ocean tide solution on this signal (see figure 55), some signals are consequently reduced using a FES2012 solution instead of a GOT4.8 solution: the 59days signal is reduced of about 74%, a 174days signal is reduced of 65%, in addition the 118days signal is reduced of about 35% from GOT solution to FES solution.

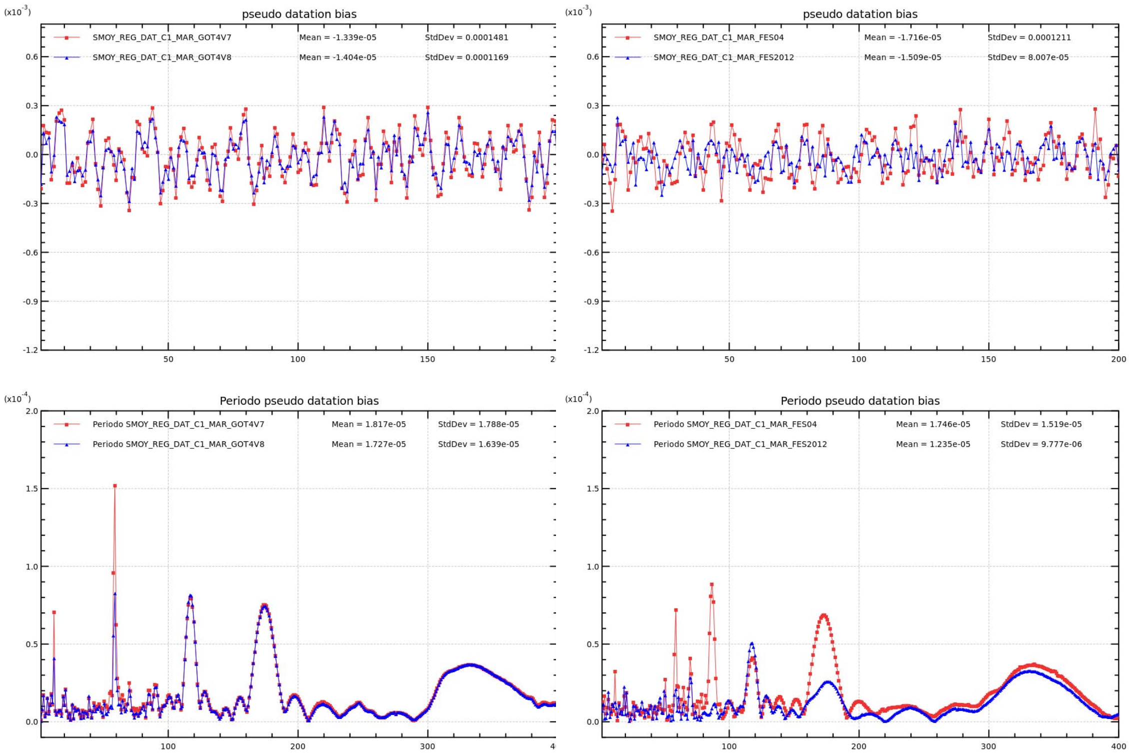

Figure 55: ***Top:*** *Monitoring of pseudo time-tag bias estimated cycle by cycle from GDR products for Jason-2 for different ocean tide solutions.* ***Bottom:*** *Periodogram on pseudo time tag bias signals.* ***Left:*** *GOT solutions.* ***Right:*** *FES solutions.*

6. Sea Level Anomalies (SLA) Along-track analysis

6.1. Overview

The Sea Level Anomalies (SLA) are computed along track from the SSH minus the mean sea surface with the SSH calculated as defined in previous section 5.1. :

$$SLA = SSH - MSS(CNES/CLS2011)$$

Note that Jason-2 GDR-D products contain MSS_CNES_CLS_2011. For better comparison with Jason-1, in this study MSS 2011 was also updated on Jason-1 data (in addition to the other updates: POE-D, GOT4.8, JMR replacement product).

SLA analysis is a complementary indicator to estimate the altimetry system performances. It allows us to study the evolution of SLA mean (detection of jump, abnormal trend or geographical correlated biases), and also the evolution of the SLA variance highlighting the long-term stability of the altimetry system performances. In order to take advantage of the Jason-2/Jason-1 formation flight phase (cycles 1 to 20), we performed direct SLA comparisons between both missions during this period.

Corrections applied in SSH calculation are theoretically the same for Jason-1 and Jason-2 since both satellites measure the same ocean. Thus, it is possible to not apply them in order to obtain directly information on the altimeter range and the orbit calculation differences. However, as the stability of both ground passes is not exact (the ground track is maintained within a window of ± 1 km across-track distance from the theoretical ground track), SLA measurements have to be projected and interpolated over the Jason/TOPEX theoretical ground pass after applying the MSS in order to take into account cross-track effects on SSH.

$$\Delta SLA_{J1-J2} = [(Range_{Ku} - Orbite - MSS)_{J1}]_{\bar{T}} - [(Range_{Ku} - Orbite - MSS)_{J2}]_{\bar{T}}$$

This allows us also to select the intersection of both datasets and compare exactly the same data. After Jason-1 ground track change to its interleaved ground track, direct SLA comparisons are no more possible. Thus, global statistics computed cycle by cycle are just basically compared.

6.2. Mean of SLA differences between Jason-2 and updated Jason-1

The cycle by cycle monitoring of mean SLA differences between updated Jason-1 data and Jason-2 is plotted in figure 56 over all the Jason-2 period. During the formation flight phase, the SSH bias is computed with and without the SSH corrections. During this period, both types of curves are very similar and stable in time with variations close to 1 mm rms, except that they are spaced out by a 3.3 cm bias (3.2 cm when using ECMWF model wet troposphere correction). This bias results from differences between Jason-1 and Jason-2 sea state bias model used, and to a small amount due to ionosphere correction differences. The global average SSH bias is close to 10.3 cm using SSH corrections (10.2 cm when using ECMWF instead of radiometer wet troposphere correction) and 7.1 cm without. The differences between Jason-1 and Jason-2 are related to a small bias due to troncated altimeter PRF (-0.316 cm) before the geodetic ground track, the characterization file (-11.7 cm) and the antenna reference point (+18.09 cm), which sums up to a difference of 6.1 cm

(see [74]). This is quite close to the currently observed value of 7.1 cm. These biases are present in Jason-1 data only as they were corrected in Jason-2 GDR-D data thanks to the 2012 reprocessing (see [16]), the correction will be applied to Jason-1 data during the 2015 reprocessing. However, the more crucial point for scientific applications is to insure that there is no drift between both missions, since the global bias can be corrected a fortiori. The extension of the monitoring of the SSH bias after the Jason-1 ground track change is precisely a good way to check the long-term Jason-1 and Jason-2 stability. It is plotted over all Jason-1 cycles in figure 56.
When Jason-1 was moved to a geodetic ground track, a jump is visible, it is slightly smaller when using ECMWF model wet troposphere correction (around 6.2mm) than when using radiometer wet troposphere correction (6.6mm). Indeed from Jason-1 cycle 500 (geodetic ground-track) to cycle 527, a different JMR calibration file was used, accounting for a bias of 1 to 2 mm (a new JMR calibration file was also used after Jason-1 safe hold mode, from Jason-1 cycle 528 to 537, which can explain another smaller jump in March 2013). Furthermore, since the geodetic ground-track, Jason-1 PRF is no longer truncated (as it was previously). This accounts for a bias of 3.16 mm. Nevertheless a small part of the jump remains unexplained.

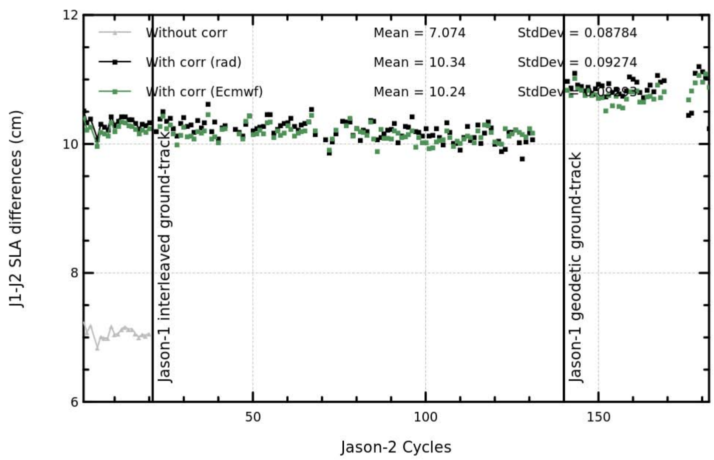

Figure 56: Cycle by cycle monitoring of SSH bias between Jason-1 and Jason-2 before and after Jason-1 ground-track change (black curve and dots) and SSH bias without applying corrections in SSH calculation for both missions only during the formation flight phase (gray curve). Mean and standard deviation are calculated only over the formation flight phase.

Figure 57 shows the mean differences between Jason-1 and Jason-2 during formation flight phase (cycles 1 to 20).

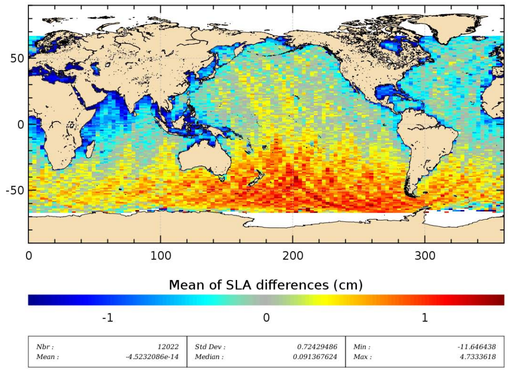

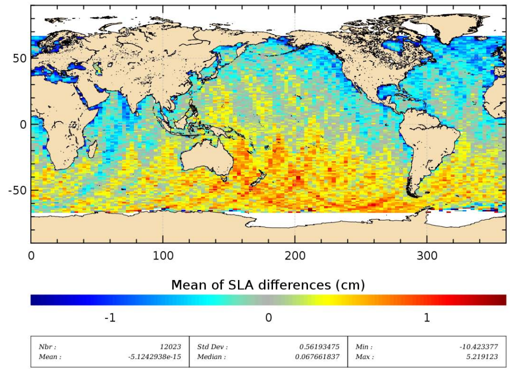

Figure 57: Maps of SLA (orbit - range - geophysical corrections - MSS2011) mean differences between Jason-1 and Jason-2 during formation flight phase (cycles 1 to 20). Top left: using Jason-2 GDR-D and Jason-1 updated GDR-C (the map is centered around the mean of 10.24 cm). Top right: same as left, but in addition using for both satellites OSTST 2012 sea state bias (the map is centered around the mean of 7.26 cm).

There are geographically correlated structures of up to ± 1.5 cm amplitude between Jason-2 GDR-D and updated Jason-1 GDR-C data (see left of figure 57). This is particularly the case for regions with low, but also high significant wave height. Most of this difference comes from the still different sea state bias models used on both satellites (see also chapter 4.9.). Updating both satellites with the OSTST 2012 sea state bias strongly reduces the differences, as shown on right side of figure 57. The remaining differences are due to orbit differences (though for both POE-D orbit standard was used), as shown on figure 58.

In order to obtain directly information on the altimeter range and the orbit calculation differences, spatial uncorrected SLA (orbit - range - MSS) differences (only during the Jason-1/Jason-2 formation flight phase) between both missions is plotted in left side of figure 58. It shows a weak hemispheric bias lower than 1 cm. In addition, positive differences are stronger in South Pacific and negative differences are stronger in North Atlantic. These differences are in relationship with orbit calculation differences. Though for both satellites POE-D was used, there are some differences between Jason-1 POE-D and Jason-2 POE-D, for Jason-1 orbit computation the GPS data are no longer available, whereas they are used for the Jason-2 POE computation. Jason-2 POE-D is therefore based on three orbit determination techniques (Doris, GPS, Laser), whereas Jason-1 POE (over the Jason-2 period) is only based on two orbit determination techniques (Doris and Laser). On the right of figure 58 the difference between Jason-1 and Jason-2 uncorrected SLA is shown using for Jason-2 also a Doris/Laser orbit (instead of an Doris/GPS/Laser orbit, see also part *"Towards a new Jason-1 orbit solution for climate studies"* in [12]). The hemispheric differences seems to be more homogeneous, but are still present. When using GSFC std 0905 orbits for both satellites (bottom of figure 58) the hemispheric bias disappears (the same result has been found using GSFC std 1204 orbit solution, but it is not shown here).

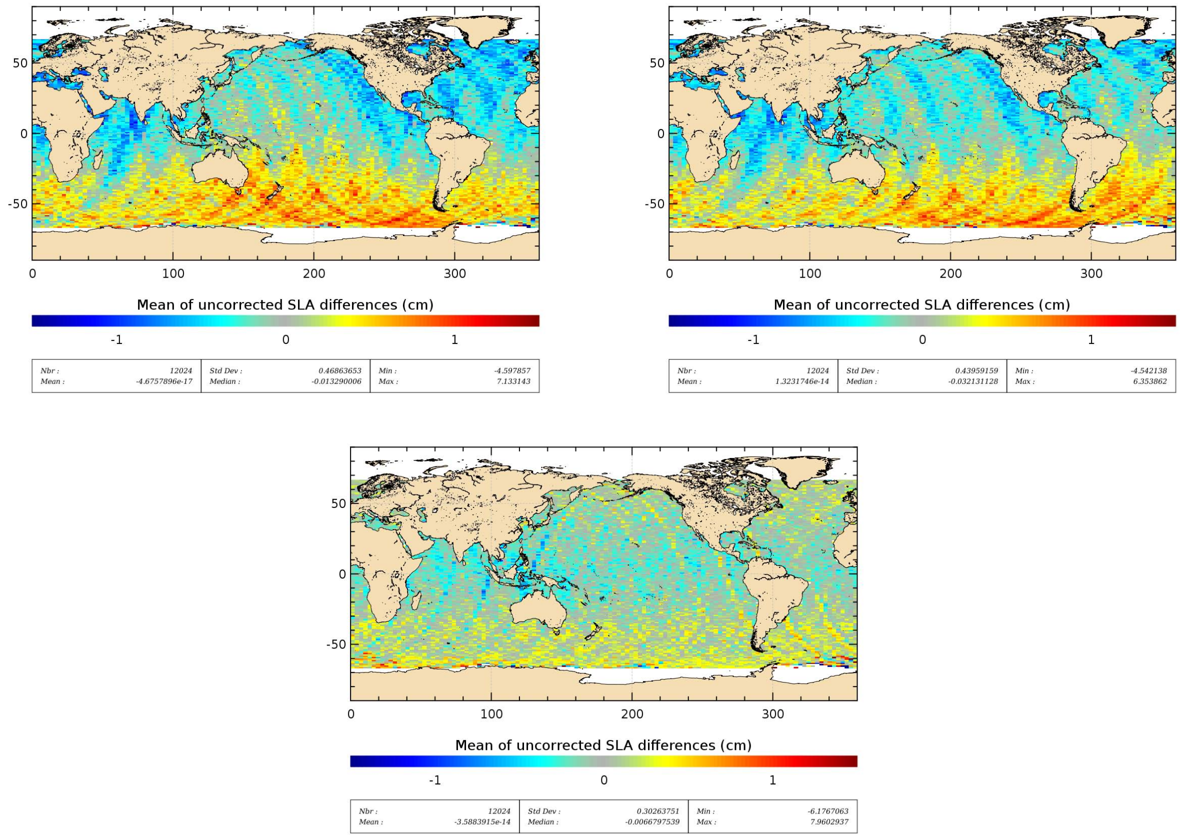

Figure 58: Maps of SLA (orbit - range - MSS2011) mean differences between Jason-1 and Jason-2 during formation flight phase (cycles 1 to 20). Top left: using POE-D orbits. Top right: using POE-D orbit for Jason-1 and Doris/Laser POE-D orbit for Jason-2. Bottom: using GSFC09 orbits.

6.3. Standard deviation of SLA differences between Jason-2 and Jason-1

The monitoring of SLA standard deviation has been computed for both missions, as well as updated Jason-1 standards over the whole data set (plotted in figure 59). As concerned Jason-1, the blue curves are drawn using the standards that are in the GDR products. The curves are very well correlated during the formation flight phase, as well as after Jason-1 moved to the geodetic ground-track, but during the Jason-1 interleaved repetitive ground-track (from Jason-2 cycle 21 to 134), Jason-1 standard deviation increases by 3 mm rms in average (11.0 cm rms for Jason-1 instead of 10.7 cm rms for Jason-2). Similar feature was observed comparing Jason-1 and TOPEX performances after T/P satellite was moved on its new ground track in August 2002 ([46]).

For the geodetic ground-track Jason-1 GDR-C contain the MSS CNES/CLS 2011 which is improved compared to the 2001 MSS ([53]) especially for ground-tracks outside the historical T/P-Jason ground track, so that the blue (JA1) and red (JA2) curves are very well correlated during this period.

The new MSS CNES/CLS 2011 ([76]), using all the satellite tracks including the interleaved

T/P and Jason-1 ground tracks - which was computed in the frame of the SLOOP project ([47]) - improves the SLA calculation also for the interleaved ground tracks. When updating Jason-1 data (green curve), Jason-1 and Jason-2 curves are very well correlated. Cartography of standard deviation of spatial Jason-1 minus Jason-2 SLA differences (not shown here) does not show any anomaly. It varies indeed in function of noise on measurements, which is dependent on significant wave height. Therefore, standard deviation of SLA differences is higher in regions with important significant wave heights.
In addition to these results, a special investigation on SLA with 500km filtering is detailed in the investigation part about SLA in [17].

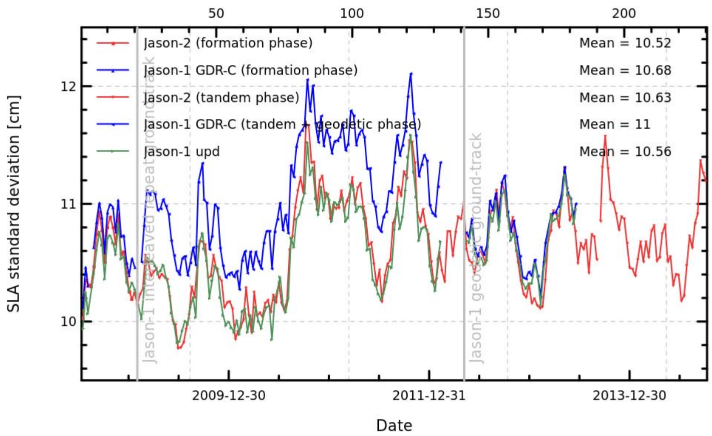

Figure 59: Cycle by cycle monitoring of SLA standard deviation for Jason-1 and Jason-2.

7. Mean Sea Level (MSL) calculation

7.1. Altimeter Mean Sea Level evolution

7.1.1. Mean sea level (MSL) calculation of reference time serie

The global mean level of the oceans is one of the most important indicators of climate change. Precise monitoring of changes in the mean level of the oceans, particularly through the use of altimetry satellites, is vitally important, for understanding not just the climate but also the socioeconomic consequences of any rise in sea level. Thanks to the T/P, Jason-1 and now Jason-2 altimetry missions, the global MSL has been calculated on a continual basis since January 1993 (figure 60) highlighting a trend of 3.27 mm/yr (see http://www.aviso.oceanobs.com/msl). We connect Topex/Poseidon and Jason-1 at Jason-1's cycle 11 (May 2002) by subtracting a bias of 5.46 cm to Jason-1's MSL. We replaced Jason-1 by Jason-2 in the MSL time data series at Jason-2 cycle 11 (October 2008) by subtracting a bias of -7.34 cm to Jason-2's MSL as calculated previously (in addition to the bias between Jason-1 and Topex/Poseidon). The altimeter standards used are described on Aviso website (http://www.aviso.oceanobs.com/en/news/ocean-indicators/mean-sea-level/processing-corrections.html). Note that Jason-2 GDR-D data (updated for MSS 2011 referenced to 20 years period and Sea State bias) and Jason-1 GDR-C data (updated for GOT4.8, JMR replacement product (cycles 228 to 259), MSS 2011 referenced to 20 years period, Sea State Bias and POE-D orbit) were used. To calculate a precise MSL rate, it is essential to link accurately time data series together. A study ([1]) showed the uncertainty on the global MSL trend resulting from the impact of MSL bias uncertainties between TOPEX-A and TOPEX-B (due to altimeter change in February 1999) and between TOPEX-B and Jason-1 (in May 2002) is close to 0.2 mm/yr from 1993 onwards. As we showed just previously, the SSH consistency between Jason-1 and Jason-2 is very good in space and stable in time during the formation flight phase, the SSH bias uncertainty is consequently very weak and close to 0.5 mm. It is lower than between T/P and Jason-1 (estimated close to 1 mm ([1])). Its impact on global MSL trend error budget is thus very weak: lower than 0.05 mm/yr. Zawadzki et al ([89]) computed a confidence envelop of global MSL time-series deduced from Jason-1 and Jason-2 data, by tuning identified parameters (standards, data selection, average mesh grids, mission linking). The resulting envelop allowed to verify that AVISO and CU (University of Colorado) MSL stay within the confidence interval.
Notice, that MSL decreased in 2010/2011, similar, but much stronger to what was already observed in 2007. According to Boening et al. ([29] and [30]) the global mean sea level drop of 5 mm between beginning 2010 and mid-2011 is due to a decline of ocean mass coinciding with an equivalent increase in terrestrial water storage (primary over Australia, northern South America and Southeast Asia). The authors write, that this temporally shift of water from ocean to land is closely related to the transition from El Niño conditions in 2009/2010 to a strong 2010/2011 La Niña which affected precipitation patterns world wide. As these terrestrial water mass are not all directly linked to the ocean (thanks to rivers for example), they can only return to ocean thanks to evaporation. This process is long, which could explain the rise in GMSL in 2012.

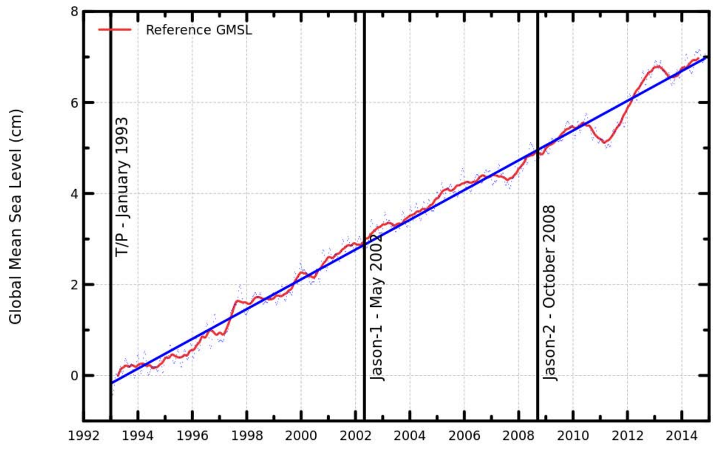

Figure 60: MSL evolution calculated from T/P, Jason-1 and using Jason-2 data from October 2008 onwards. GIA (-0.3 mm/yr, [71]) is applied.

7.1.2. Regional and global mean sea level trend for Jason-2

Although, 6 years of Jason-2 is still a short time period for MSL trend calculation, it is possible to compute a MSL trend. Nevertheless, slope values are to be taken with caution and are rather used to compare between several standards. Due to the relatively short period, slope values change much when passing from one period to another period. Using radiometer wet troposphere correction increases for Jason-2 data the slope by around 0.3 mm/yr (left side of figure 61). Separating in ascending and descending passes, shows very similar slopes thanks to the POE-D standard (see right of figure 61). The amplitude of the MSL curve computed from descending passes is higher than for ascending passes. The difference of MSL slopes (MSL ascending passes - MSL descending passes) for Jason-2 is 0.1mm/yr. The difference between ascending and descending passes shows a signal of a period around 120 days (see also chapter 5.2.), that disappears when using POE-E preliminary orbit solution.

The regional MSL trends over the Jason-2 period (figure 62) show a small increase in western tropical pacific and a small decrease in eastern tropical pacific. This is probably influenced by the La Niña or neutral conditions which occurred before mid-2009 and after mid-2010 ([86],[87]).

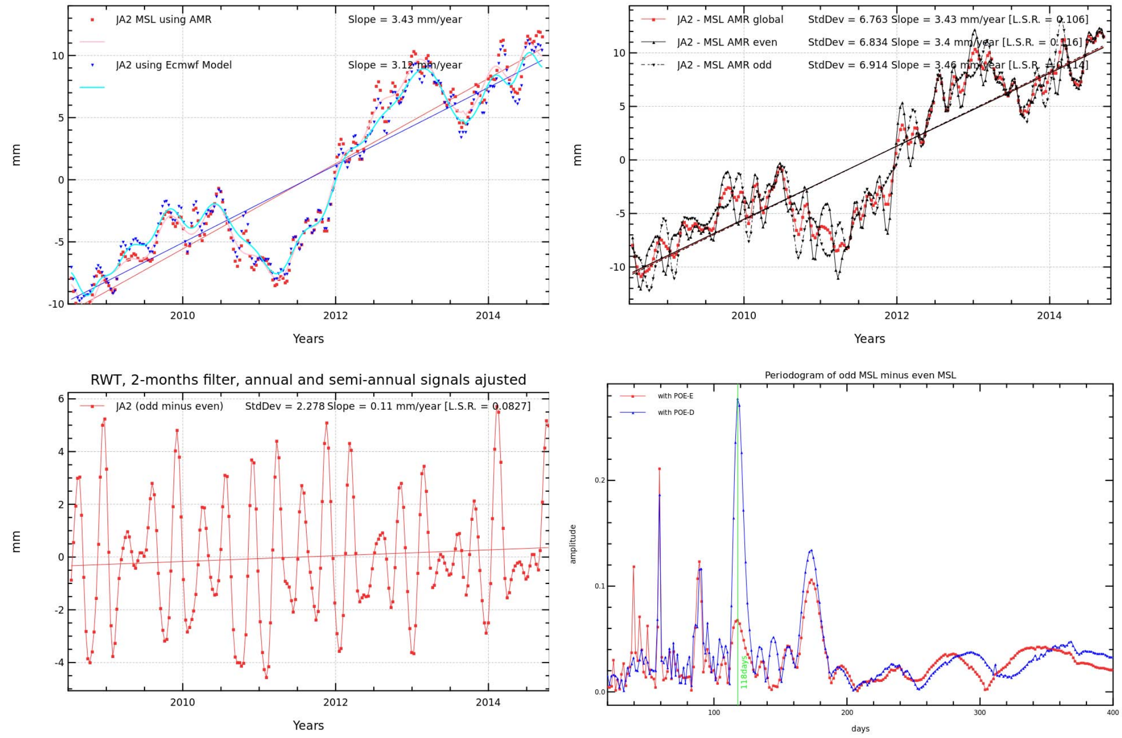

Figure 61: Global MSL trend evolution calculated for Jason-2 (top left). MSL trend evolution when separating in ascending and descending passes (top right) , Seasonal signal (annual and semi-annual) is adjusted for top figures. Bottom: Difference of MSL slopes (MSL ascending passes - MSL descending passes) for Jason-2. Slopes are computed for 2 month filtered data. GIA correction is not applied. Bottom right: periodogram of MSL difference (MSL ascending passes - MSL descending passes)

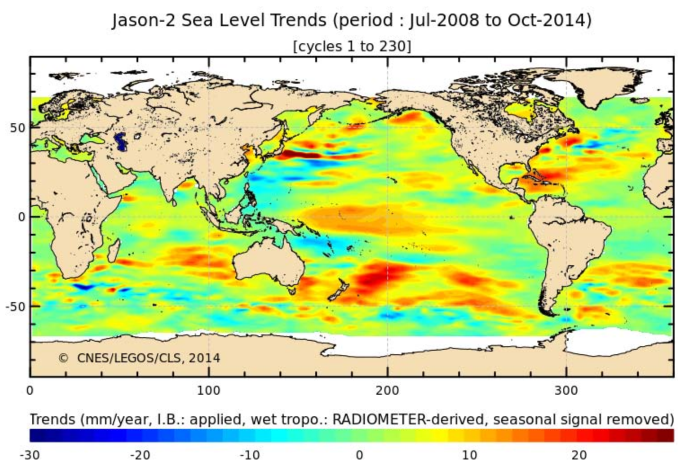

Figure 62: Maps of regional MSL slopes for Jason-2 cycles 1 to 230, seasonal signal removed.

7.1.3. Comparison to Jason-1

Global Mean Sea Level computed over common period of Jason-1 and Jason-2 (this study has been computed over about 4.5 years from July 2008 to February 2013) shows differences of about 0.7 mm/yr with radiometer wet troposphere correction (the bias between JA1 repetitive and JA1 geodetic has been corrected as described in [12] (Jason-1 updates= homogeneous POE-D orbit, GOT4.8 tide, and MSS 2011)).

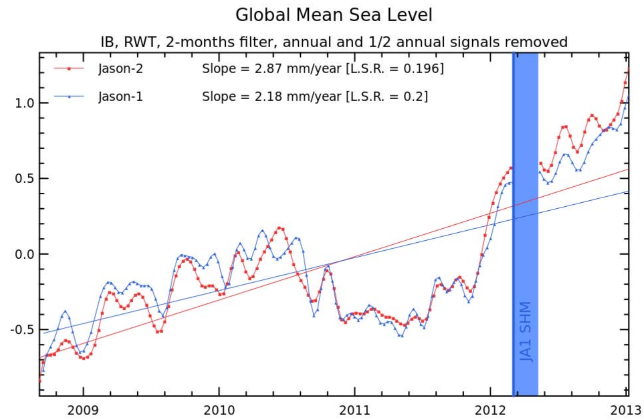

Figure 63: Global Mean Sea Level using Jason-1 or Jason-2 data (with 2-months filter, with adjustment of the annual and semi-annual signals, no GIA applied)

Updating Jason-1 data to Jason-2 standards allows to reduce the difference in GMSL trends between Jason-1 and Jason-2 (reduction of the difference of about 0.1mm/yr, see top right of figure 64). The radiometer drift between JMR and AMR explains 0.4mm/yr in the difference that remains (a difference of about 0.2 mm/yr is still unexplained between the two monomission GMSL when using a model wet troposphere correction, see bottom of figure 64).

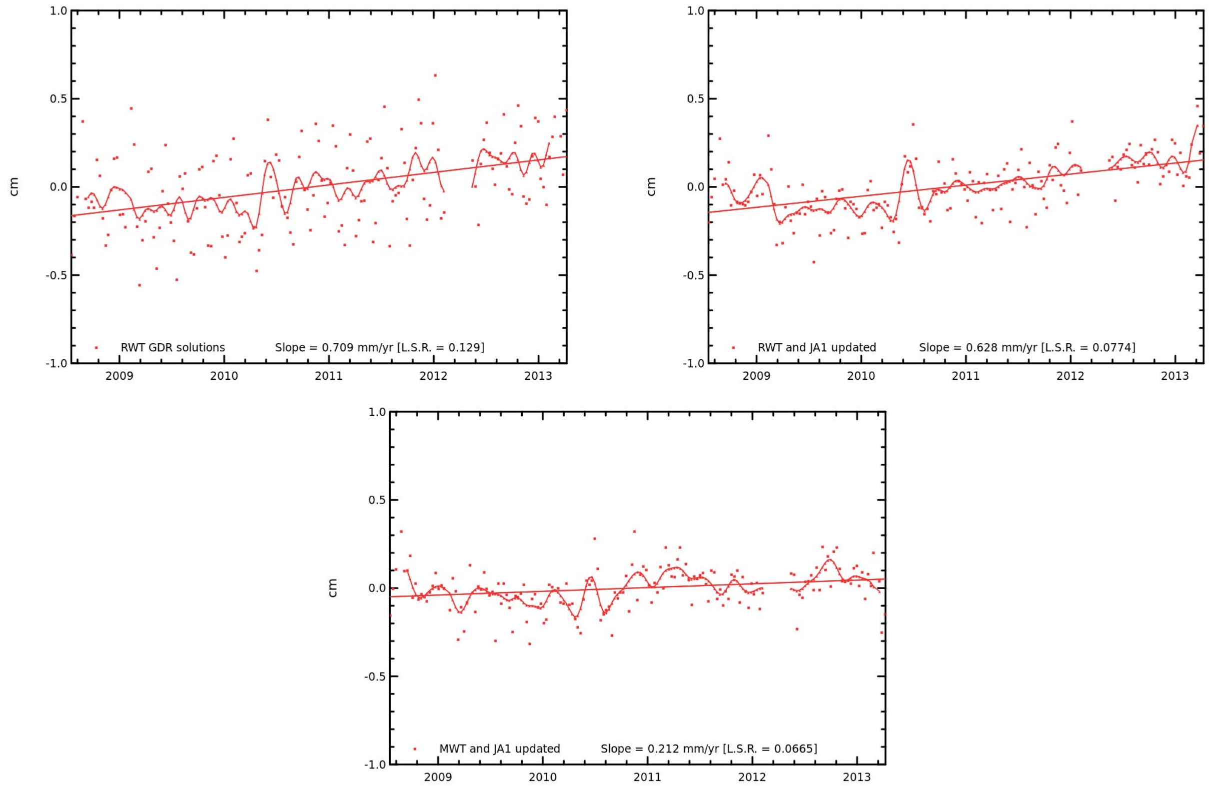

Figure 64: Difference of Jason-2 GMSL – Jason-1 GMSL computed over Jason-2 cycles. Top left: with radiometer wet troposphere. Top right: with radiometer wet troposphere and Jason-1 updates. Bottom:with model wet troposphere and Jason-1 updates. (Jason-1 updates= homogeneous POE-D orbit, GOT4.8 tide, and MSS 2011)

7.2. External data comparisons

In order to assess the global MSL trend, comparisons to independent in-situ datasets are of great interest. Two methods have been developed in the frame of in-situ Calval studies and thoroughly described in annual reports ([27] and [28]).

7.2.1. Comparison with tide gauges

The cycle by cycle monitoring of global average differences between altimetry and in-situ sea surface height measurements provides a way to assess the satellite data quality and to detect jumps an drifts affecting sea level records.
Jason-2 altimeter data is compared with tide gauge measurements thanks to a dedicated method which aims at detecting potential drifts in sea surface heights (SSH). For more information on the method and more detailed results, please refer to the 2014 report of comparison between altimeter data and tide gauges ([27]).
Moreover, note that the time series presented in this section have been corrected for GIA effects on satellite altimetry data using a uniform $-0.3\,mm.yr^{-1}$ trend correction. The details of this GIA correction can be found in the 2013 annual report for the altimetry/tide gauges global comparisons [25].
Figure 65 displays the time series of global average differences between Jason-2 and tide gauges, either keeping (65a) or removing (65b) the seasonal cycle. Considering both curves, the comparison with tide gauges measurements shows no long-term trend differences (0.2 mm/year with the seasonal cycle, 0.02 mm/yr without). The formal adjustment error is low, close to 0.1 mm/yr, but we estimate that the total error of the method is larger, around 0.7 mm.yr.

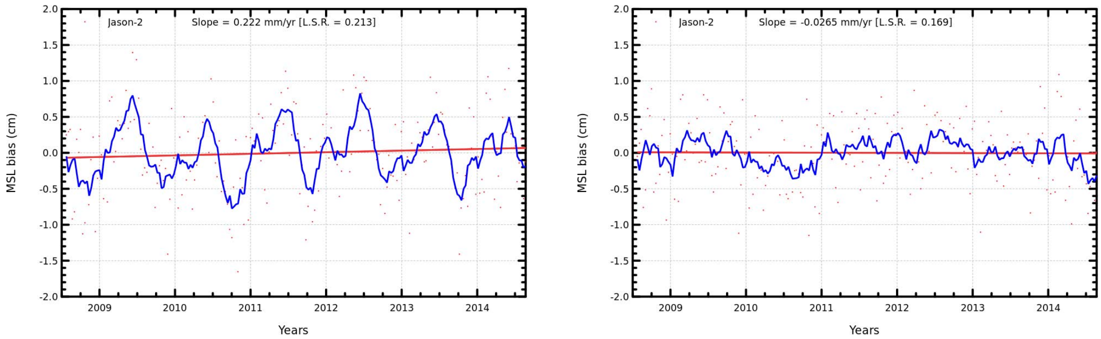

(a) with seasonnal signal *(b) seasonnal signal removed*

Figure 65: time series of global average differences between Jason-2 and tide gauges, with (65a) and without the annual cycle (65b). The red points represent the raw data while the blue curve is obtained after applying a two months running mean filter

Figure 65 confirms the excellent stability of the Jason-2 mission with respect to tide gauges.

7.2.2. Inter annual evolution of the altimeter residuals compared with Argo T/S profiles

Argo DHA (Dynamic Height Anomaly) can be used for the quality assessment of altimeter sea level measurements as an independent reference. This concerns the analysis of the relative mean sea level, including the detection of global and regional MSL drift and anomalies and the detection of the impact of new altimeter standards or products. This method constitutes an essential approach for the quality assessment of the altimeter measurements. In order to improve the method, a large part of the analyses performed in 2014 have focused on the analyses on the sensitivity of the altimeter / in-situ sea level comparisons to the processing method of these data sets (see the 2014 annual report [28]).

The estimation of the absolute altimeter mean sea level drift requires the additional information related to the mass contribution to the sea level that can be derived from GRACE satellite measurements. Several GRACE datasets are available with different processing of the satellite measurements. Together with the steric in-situ dynamic heights from Argo, these GRACE datasets provide sea level estimations with the same physical content as the altimeter measurements. The conducted studies have shown that there is a strong sensitivity to these GRACE data, which affect the analysis of the altimeter mean sea level closure budget and the inter-annual variability.

The sensitivity of the altimetry / Argo comparisons to the Argo dataset and the associated data processing have been performed. The global and regional coverage of the ocean by Argo floats are impacted by the choice of the reference level of integration of the Argo T/S profiles for the computation of the steric dynamic heights. In terms of sea level closure budget, the drift between altimeter and Argo T/S profiles is significantly affected by this choice (see figure 66 for Jason-1 and Jason-2). The future evolution of the Argo network such as the deployment of deep Argo floats (4000m) should contribute to the improvement of the results.

Some additional studies (which have not focused only on Jason-2 data) have contributed to better characterize the uncertainty of the method and improve the confidence in the results. This work is performed in an operational framework which is essential to make this activity durable. Major part of the results would not have been obtained with the same confidence without comparison with the results derived from global altimeter internal analyses and from the comparison with tide gauges. The synergy between these approaches is a key element to provide more and more reliable and accurate results, globally as well as regionally. And as suggested by preliminary comparisons of Jason-2 and SARAL/AltiKa measurements with Argo data, this approach will also be an asset for the quality assessment of new altimeter missions such as Sentinel-3, Jason-3 and SWOT.

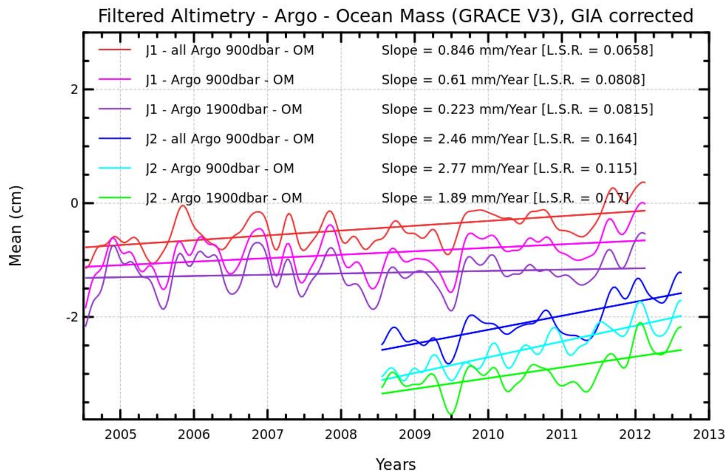

Figure 66: Temporal evolution of the mean differences between altimeter SLA, Argo DHA and GRACE ocean mass contribution. Time series are filtered and GIA corrected

8. Investigations

8.1. Assessment of orbit quality through the SSH calculation towards POE-E standards

The POE-E (precise orbit ephemeris) available in future altimetry products are getting prepared. The details of the result are available in [67].
There are several improvements on the orbit modeling :

- The new gravity field EIGEN-GRGS.RL03.MEAN-FIELD has annual and semi annual fit, and in addition to the previous one, trend estimated per year
- Harmonic 31 is relaxed : geopotential coefficients are adjusted during the orbit determination process
- The modeling of the center-of-mass of the total Earth system position is upgraded
- The solar radiation pressure (SRP) model-tuning is calibrated on a semi-empirical solar radiation pressure model on the solar panels
- The stochastic solution is improved by the introduction of reduce dynamic and minor evolutions

Two major impacts are particularly noticeable : first, relaxing the new gravity field and the harmonic 31 has a large scale significant impact on Regional Mean Sea Level trend and interannual signature (see figure 67 on left); secondly, changing the SRP and introducing a reduced dynamic approach to the solution enables to reduce significantly the variance at crossovers by about 0.35 cm2 (see figure 67 on right). The other effects are weak and especially have an impact at crossovers. The quality of the orbits are keeping improving : points that were previously considered as negligible are now observable. Last upgrade from POE-C to POE-D had been the introduction of a drift in the time gravity field with a large impact in a regional Mean Sea Level trend. Today, the change from POE-D to POE-E is dominated by the impact of the interannual variability on the regional MSL and a variance reduction at crossovers due to a better SLR modeling and/or stochastic model improvement. The impact must now also be studied for other missions than Jason-1 and Jason-2. This will enable to make a more complete assessment using multimission comparisons. Following these studies and if no regression is noticed, the full POE-E standards will be computed, including the latest ITRF (currently under preparation).

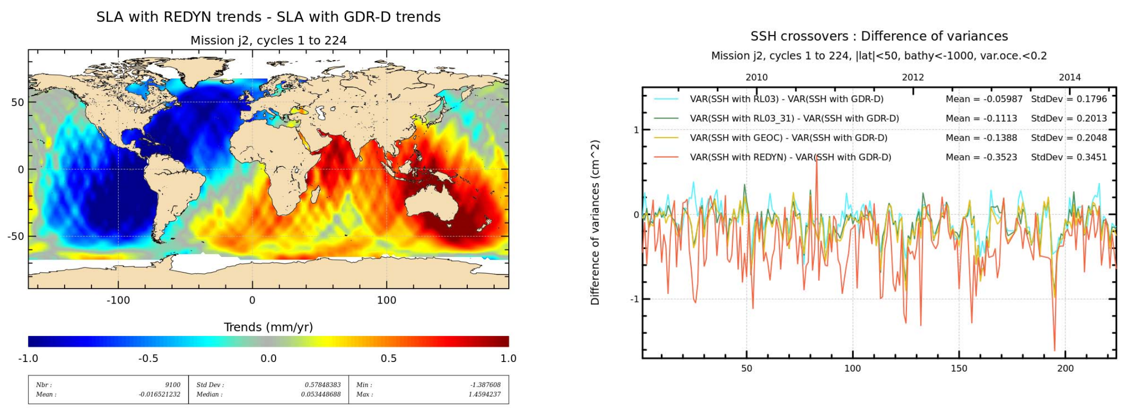

Figure 67: On left : Map of the differences of SLA using preliminary POE-E - SLA using POE-D. On right : Difference of variance monitoring through the new orbit model step by step.

8.2. Comparison of the latest GSFC SLR/DORIS std1204 orbits with current orbits for TP, J1 and J2

8.2.1. Introduction

The main goal of this section is to compare the latest GSFC SLR/DORIS std1204 orbits with current orbits for TP, J1 and J2 (either available in the GDR products or used for AVISO mean sea level computation).
GSFC std1204 (see [56] for more information on GSFC orbits) incorporates several significant changes especially in modeling time varying gravity (TVG) and represent an improvement over the previous GSFC standards and orbits. They are summarized in table 9. The different corrections used for all satellites are indicated in table 11.

We will consider several points :

- The differences of orbits (radial component);
- The impact on the performances at crossover;
- The consistency between missions during the formation flight phases (J1/TP and J2/J1);
- The impact on global and regional mean sea level trend.

Note that here after, figures are only shown for Jason1 and Jason2, but results for Topex are available in [50].

8.2.2. Difference between orbits

8.2.2.1. Temporal evolution of differences

Figures 68 and 69 represent the evolution throughout time of mean and standard deviation of differences between orbit solutions for Jason1 and Jason2 respectively.
Concerning Jason1, we notice a significant slope (0.13mm/yr) in mean throughout time, and it is close to zero at the end of the period. Nevertheless, we notice 3 different phases delimited by two major events : the switch from Doris #2 (Backup) to Doris #1 (Nominal) on June 28th 2004 and the reduced availability of GPS tracking starting from August 2006. During the first phase, the differences are around half a millimeter in mean and around 1cm in standard deviation. After the switch to Doris #1, the differences decrease in mean and standard deviation. During the third phase, the differences in mean are very close to zero because the type of the orbit Jason1 POE-D becomes Doris+Laser, just as GSFC. The standard deviation of differences is more stable but a little higher during this last phase.
Concerning Jason2, the difference of orbits is constant throughout time around 0.03cm for the mean, which means that there is a very small constant bias between orbits. Notice that the mean throughout time is very close to the one for Jason1 (0.03cm) which seems quite logical given the current orbits for both satellites are CNES POE-D standards. In terms of standard deviation, the mean throughout time is close between both missions, it is quite stable in both cases, with a slight increase for Jason2 throughout time.

		Current orbit standards used for Aviso MSL computation			Test orbit standards
Standard		J1	J2	TP	TP,J1,J2
Orbit	name	CNES POE-D		GSFC08	GSFCstd1204
	Type	Doris, GPS (until 2006) and Laser	Doris, GPS and Laser	Doris and Laser	Doris and Laser
	ITRF	Extended ITRF2008 (SLRF/ITRF2008, DPOD2008,IGS08)		SLRF2005 + LPOD2005 (v10) DPOD2005	ITRF2008 (SLRF2008) ITRF2008 (DPOD2008)
	Gravity model	EIGENGRGS RL02bis MEANFIELD (2011) Non-tidal TVG : Annual, Semi-annual, and drifts up to deg/ord 50		Static geopotential: EIGEN_GL04S TVG : Linear C20-dot, C21-dot, S21-dot (IERS2003) + 20x20 annual terms from GRACE	Static geopotential: GOCO2S_fit2; GOCO2S (from 5x5) SLR+DORIS 11 satellites (4x4) TVG : selected linear, annual, semi-annual fit to 4x4 weekly SLR+DORIS 19-year weekly solution time series + 20x20 annual terms from GRACE

Table 9: Differences between current and GSFC SLR/DORIS std1204 orbits.

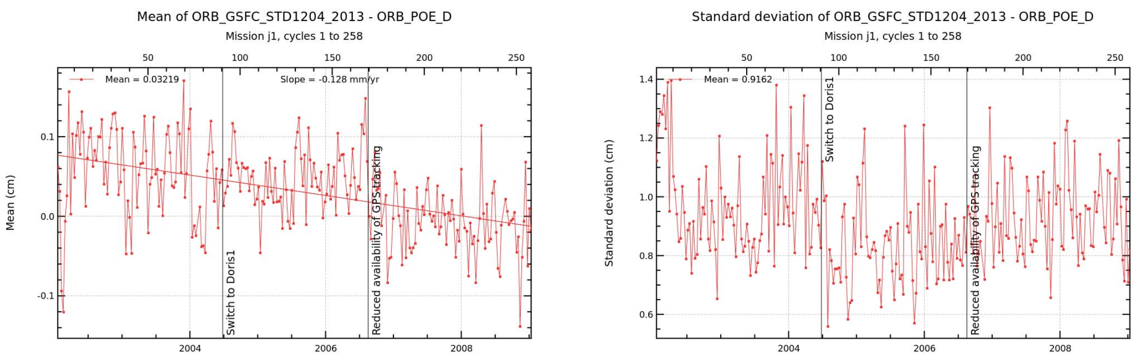

Figure 68: Temporal mean and standard deviation of differences of orbit for J1.

	Satellites		
Correction	J1	J2	TP
Mean Sea Surface	MSS_CNES_2011 (20 years reference)		
Dry troposphere	ECMWF model computed from gaussian grids		ERA-Interim model
Wet troposphere (composite)	JMR for cycles <228 JMR Replacement Product for cycles 228 to 259	AMR	TMR with drift correction [77] and empirical correction of yaw maneuvers [2]
Ionosphere	Filtered (iterative method)		
Sea State Bias	Non parametric 2012 [85]		Non parametric 2010 [83]
Ocean tide	GOT 4.8		

Table 10: Corrections used for SLA computation. Data are for Jason-1 GDR-C, Jason-2 GDR-D and Topex MGDR, but some standards are updated.

Table 11: Corrections used for SLA computation. Data are for Jason-1 GDR-C, Jason-2 GDR-D and Topex MGDR, but some standards are updated.

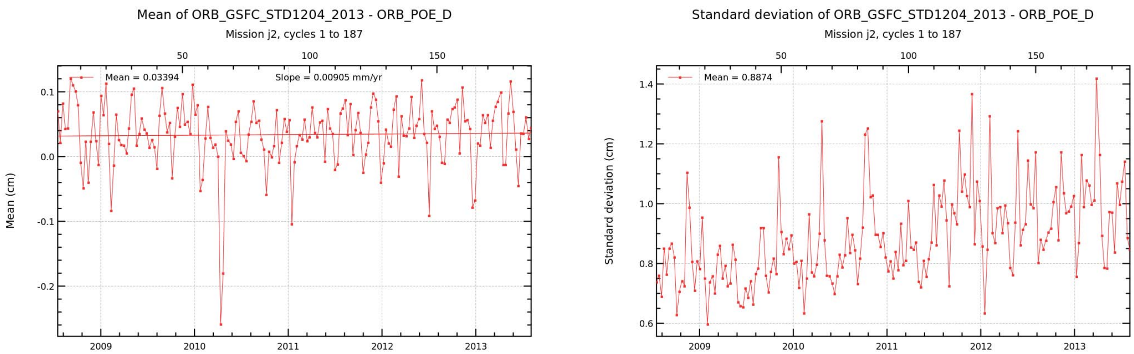

Figure 69: Temporal mean and standard deviation of differences of orbit for J2.

8.2.2.2. Spatial evolution of differences

Figures 70 and 71 represent the map of mean and standard deviation of differences between orbit solutions for Jason1 and Jason2 over the entire period studied.
Concerning Jason1, there is an important bias between the northern and southern hemispheres in the mean. The differences are more important for Jason2, but this time the bias is more between East and West.

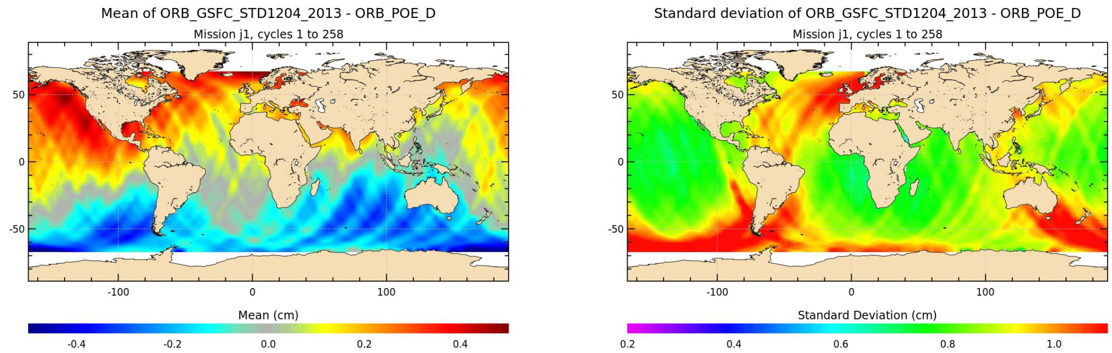

Figure 70: Spatial mean and standard deviation of differences of orbit for J1.

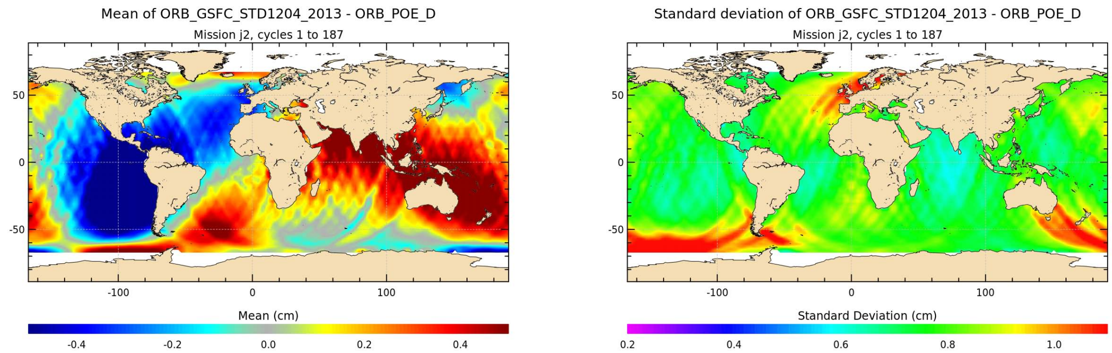

Figure 71: Spatial mean and standard deviation of differences of orbit for J2.

We now represent the same diagnosis but for every year (in mean only, Figures 72, 73), which allows to assess if the geographical differences are stable throughout time. Concerning Jason1, the maps from 2002 to 2006 are quite similar in amplitude with a northern/southern bias. Starting from 2007, the spatial distribution changes since the bias becomes an eastern/western bias, and the differences are more intense. This change in behavior corresponds to the reduced availability of GPS tracking starting from August 2006. The POE-D solution becomes therefore from this moment a Doris/Laser solution (instead of Doris/Laser/GPS). We noticed in section 8.2.2.1. that throughout time the difference between orbits decreases in mean, which suggests that even though the values of differences are higher in each hemisphere starting from 2007, they cancel out each other in order to have a smaller difference over the globe. Concerning Jason2, the eastern/western biais can be noticed every year and seems to increase in amplitude over time.

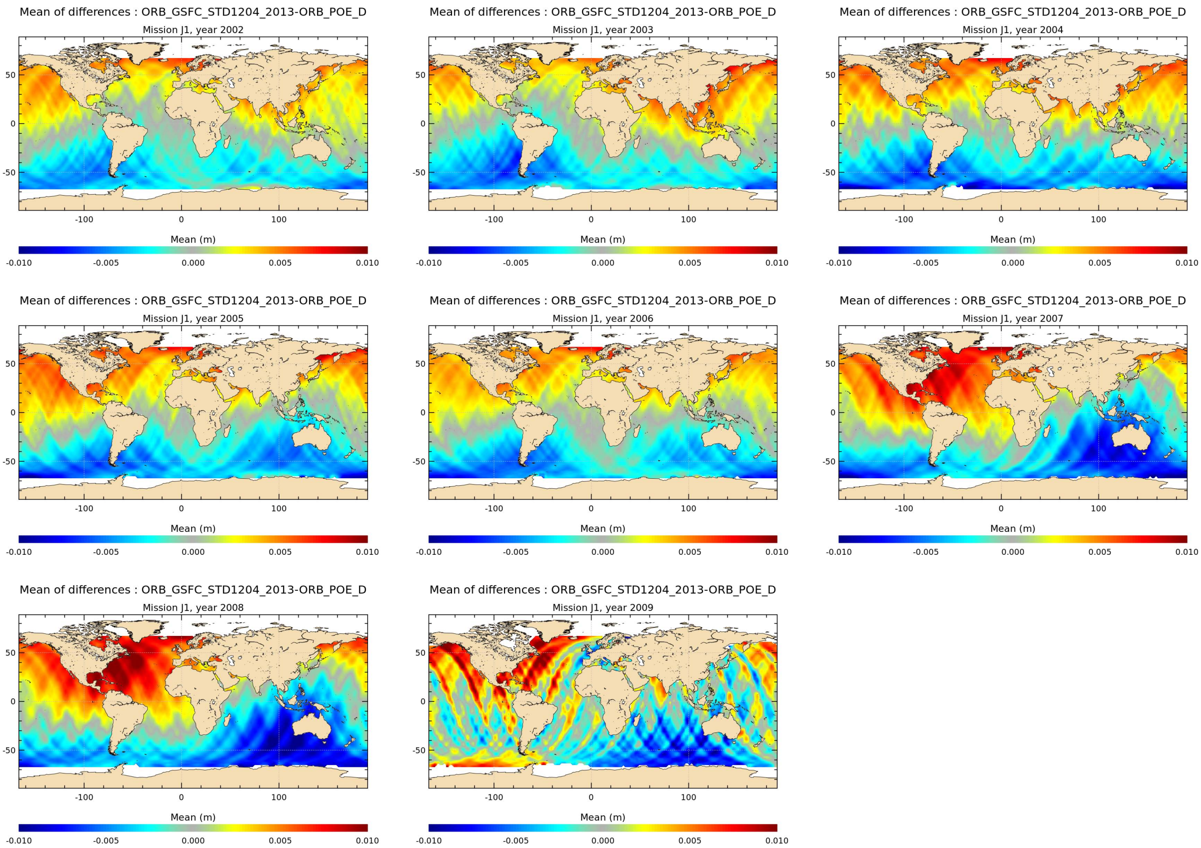

Figure 72: Spatial mean of differences of orbit by year for J1.

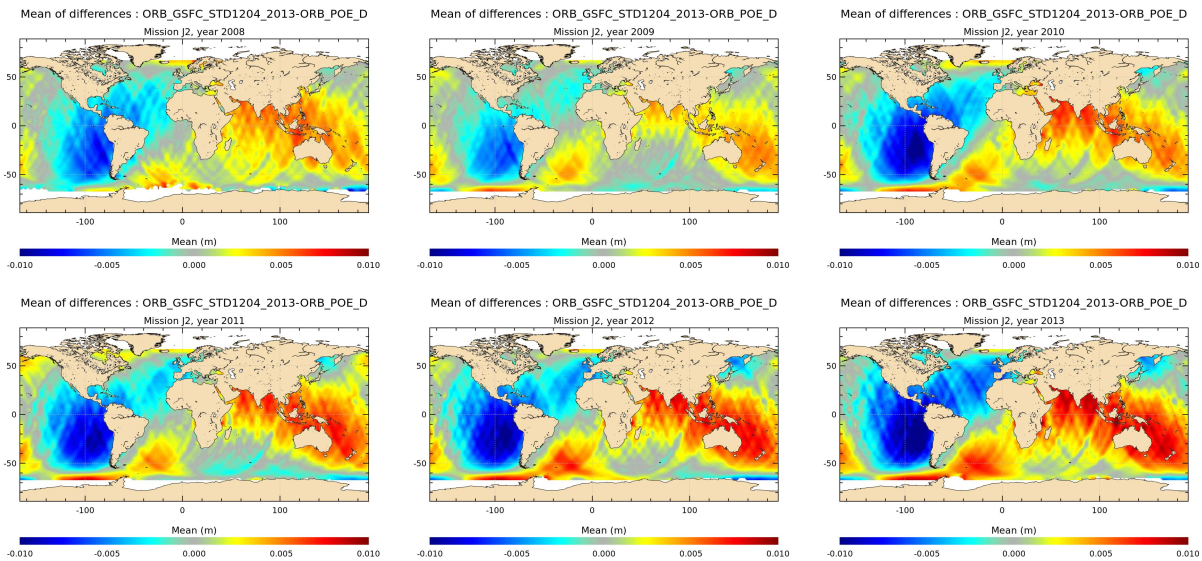

Figure 73: Spatial mean of differences of orbit by year for J2.

8.2.3. Impact on SSH crossover

8.2.3.1. Temporal evolution of SSH crossover

The temporal evolutions of SSH crossover in terms of mean (left of figures 74 and75) and standard deviation are very close between the two different orbits. We expect better performance at crossover for GDR_D since it uses a tri-technic orbit, in comparison to GSFC which uses a bi-technic orbit.
The only significative difference concerning the mean of SSH differences at crossover can be noticed for J2, the mean throughout time is for this satellite closer to 0 for the orbit GDR_D than for GSFC.

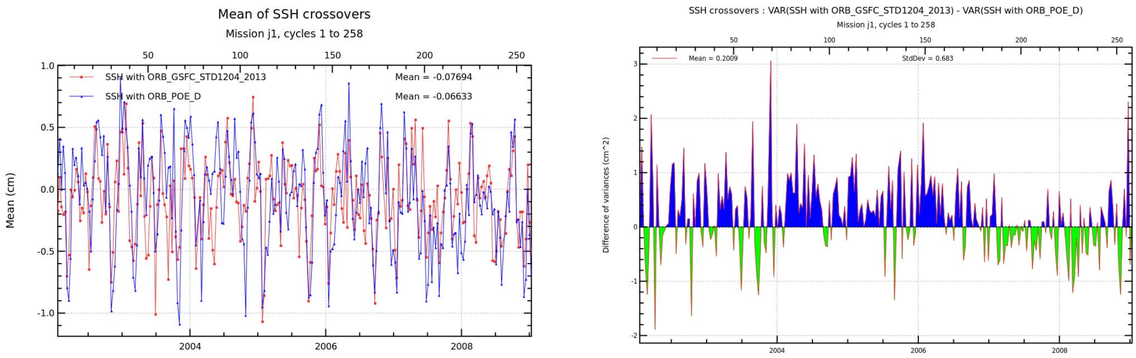

Figure 74: Mean and difference ov variances of SSH crossover for J1.

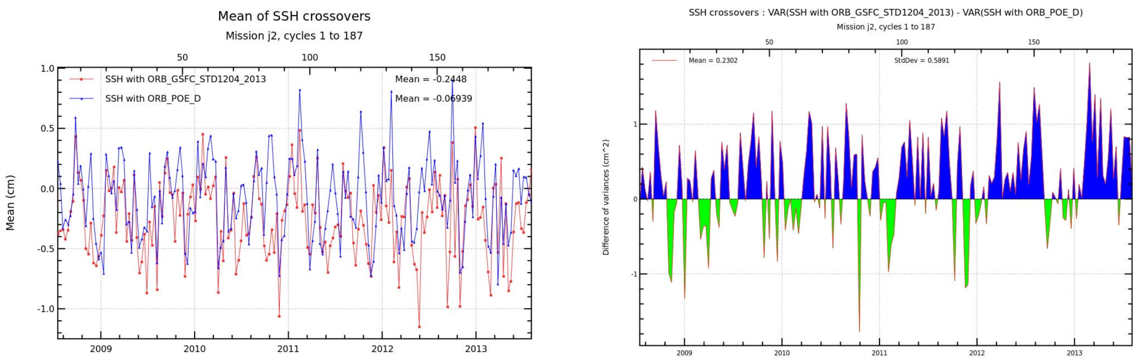

Figure 75: Mean and difference of variances of SSH crossover for J2.

Looking at the difference of variances of SSH at crossover for Jason1 (right of figure 74), we again notice a change in tendency in 2006-2007. Before that, the difference of variances is positive, indicating that the orbit POE-D is better than GSFC, whereas after 2006-2007, GSFC becomes slightly better. These results are in accordance with the previous results at crossover. The difference of variance for Jason2 (right of figure 75) is rather positive, indicating better performance for the orbit POE-D as expected.

In conclusion, set aside the very small improvement for Jason1 following the reduced availability of GPS tracking in August 2006, GSFC is globally not as good as the tri-technic orbit CNES POE-D in terms of performances at crossover. Nevertheless, the use of the GSFC orbit improves slightly the performances at crossovers for Topex/Poseidon (see [50])

8.2.4. Multi-mission comparisons

The goal of this section is to check if using the orbit GSFC 1204 leads to more consistency between satellites than CNES POE-D. We thus compute residuals between J2 and J1 during their "formation flight phase". This is a period of time during which both satellites are in the same ground track, with a 55-second interval for J1/J2. During this period that lasts 20 cycles, both satellites measure the same ocean with a very small temporal interval, which allows to perform "point to point" comparisons. We represent in Figures 76 the difference of residuals between J2 and J1 respectively, with the current orbits in one case and the tested orbit GSFC in the other case.
Concerning the difference between Jason1 and Jason2, there is an important northern/southern bias using POE-D orbits, which disappears using GSFC orbits and represents an improvement. The differences between both satellites are smaller, which means that the satellites "see" the ocean in a more similar way using GSFC orbits. The stronger differences between Jason1 and Jason2 using POE-D orbits is partly due to the different method used : GPS, Doris and Laser for Jason2 and only Doris and Laser for Jason1 (no GPS data in 2008). But mostly the differences come for the downweighting strategy of Doris beacons in South Atlantic Anomaly for Jason1 (see [68]). The downweighting strategy for Jason1 differs for CNES and GSFC orbits. Note that the downweigthing strategy will be changed for Jason1 POE-E orbits (see [67]).

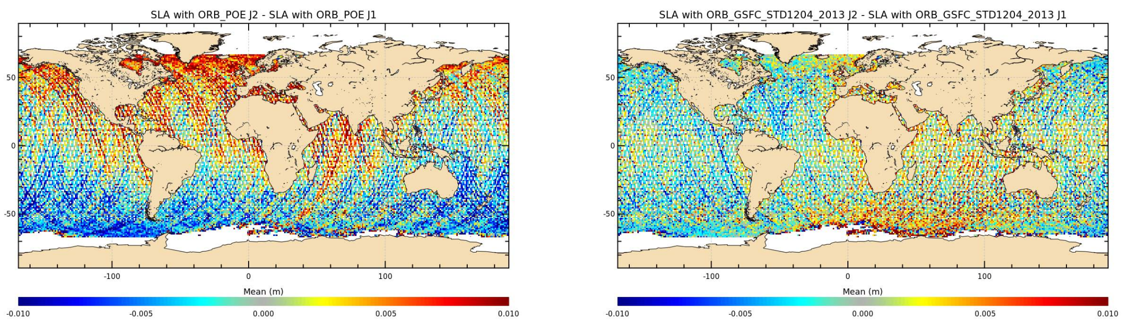

Figure 76: Mean of differences of residuals for J2 and J1 (current orbits left, new GSFC_STD1204 orbits right).

8.2.5. Impact on Mean Sea Level

8.2.5.1. Impact on Global Mean Sea Level

Figure 77 the global mean sea levels calculated by AVISO (therefore with the current standards presented in Table 1), and calculated using GSFC_STD1204 orbits and Figure 78 represents the difference between both. The method used to compute MSL is detailed in [61]. The difference of mean sea levels is very close to 0 until 2002, which corresponds to the period when Topex/Poseidon is used to determine this diagnosis. There is thus very little difference between the 2 GSFC orbits in terms of mean sea level. Starting from 2002, the differences increase and there is a jump of around 0.5mm to 1mm during 2006. Figure 79 where the red line represents the difference of global mean sea level of orbits POE-D and GSFC for Jason1 helps us understand this phenomenon. The amplitude of the difference is stronger at the beginning of the period, with an important oscillation. The latter decreases after the switch to Doris1 with an equivalent amplitude. Starting from 2006-2007, following the loss of GPS, the difference is closer to zero, because POE-D and GSFC are both bi-technic for this period. Looking at the difference between POE-D and Doris alone (blue curve), a small jump is also detectable in the middle of 2006 when for Jason1 POE-D computation the GPS is no longer used. This seems to support the explanation that the small jump in the MSL difference between Aviso and data with GSFC orbits is originated in the loss of GPS data. There are less differences between mean sea levels for Jason2 (Figure 80), the slopes being very close even though there is a small bias between lines. There is still an important difference with AVISO at the end of the period when Jason2 is the satellite considered for the calculation of MSL in Figure 78 because Jason2's level is linked to Jason1's level during the verification phase.

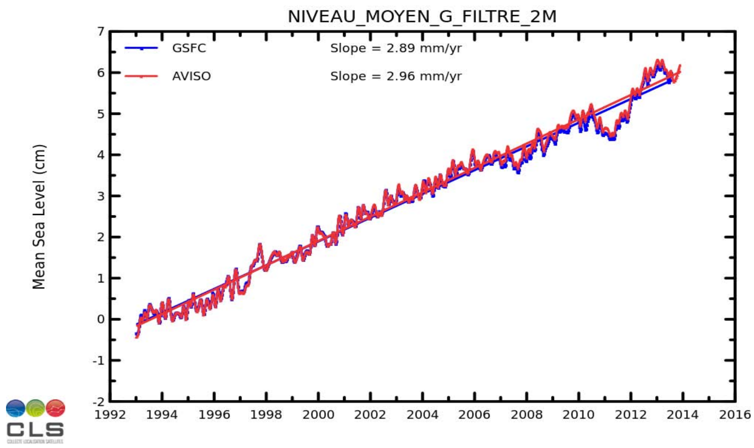

Figure 77: Mean Sea Level for AVISO and using GSFC orbits.

8.2.5.2. Impact on Regional Mean Sea Level

We now represent the difference of regional trends for each mission (Figure 81).
They are consistent for Jason2 with the differences of orbits by year in Figures 73. In fact, for

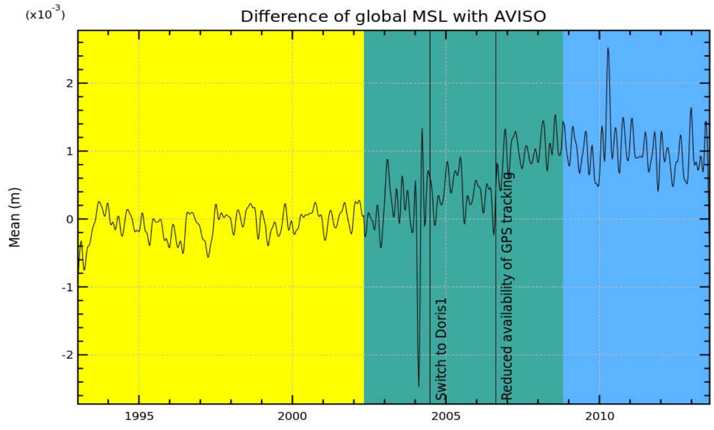

Figure 78: Difference of Mean Sea Level between AVISO and using GSFC orbits. The different colors indicate on which mission is based the global mean sea level : TP : yellow, J1 : green and J2 : blue.

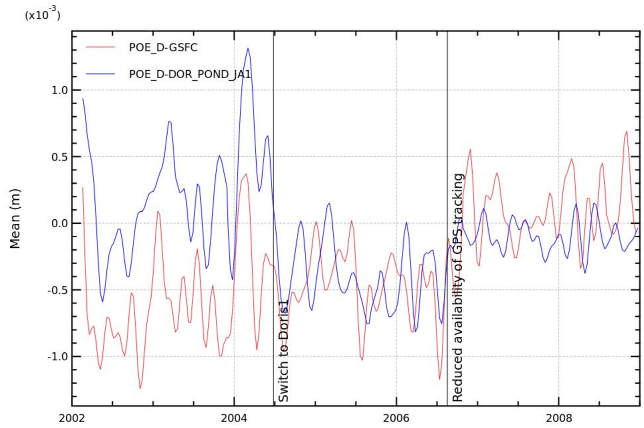

Figure 79: Difference of mean Sea Level for J1 between POE-D and GSFC and between POE-D and Doris alone.

Jason2, the eastern/western bias that becomes stronger at the end of the period is clear in the difference of trends. It is difficult to link the maps of each year to the difference of trends for Jason1 since there is a change in tendency following the loss of GPS in 2006.

In conclusion, the differences with AVISO in global mean sea level are mainly influenced by the differences for Jason1, and in particular, the loss of GPS tracking in 2006 triggers a jump of around 0.5mm on GMSL for this satellite. Regionally (over the whole duration of a mission), the differences are around $\pm 2mm$ for Jason1 and Jason2.

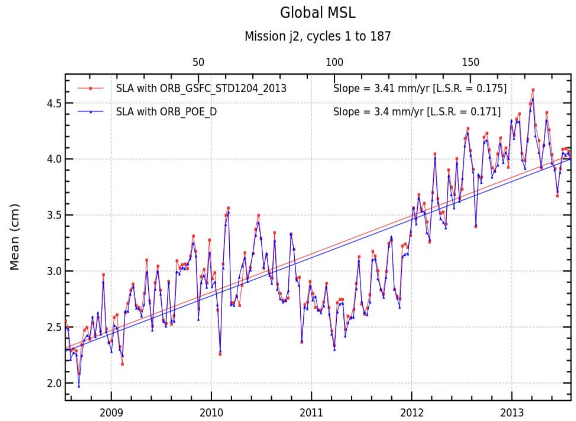

Figure 80: Mean Sea Level for J2 for both orbits.

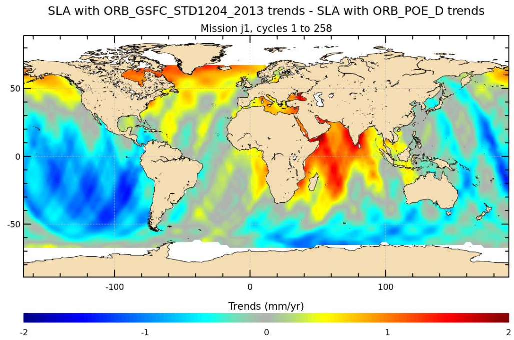

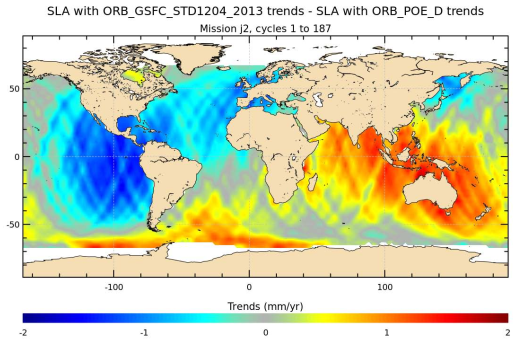

Figure 81: Difference of trends for J1 (left) and J2 (right).

8.2.6. Conclusions

The goal of this study was to compare the orbit GSFC 1204 solution to the current orbits used for Topex/ Poseidon (GSFC standards of 2008), Jason1 and Jason2 (CNES POE-D) for AVISO MSL computation. The differences between orbits for Topex/Poseidon are small but significant, and the performances at crossover are better with the new standards. Regionally, the differences of trends are around 1mm. Considering all of that, we can conclude that the new standards of GSFC can be considered as an improvement for Topex/Poseidon. For Jason1, the differences are bigger, first throughout time where a slope appears while comparing both orbits, as well as spatially since we observe a northern/southern bias while looking at differences of orbits. The orbit CNES POE-D however has slightly better performances in terms of mean and standard deviation of SSH at crossover. The differences are a little higher for Jason2 than Jason1, with a constant bias on temporal evolution, and with an eastern/western spatial bias. Again, the orbit CNES POE-D is slightly better in terms of statistics at crossover. The MSL calculated with GSFC orbit and by AVISO are close until 2006, and after the loss of GPS for Jason1 during the summer 2006, more significant differences appear until the end of the period, even for Jason2 since its MSL is linked to Jason1 MSL during the verification phase. Finally, when looking at the differences between Jason1 and Jason2 during this period, a clear northern/southern bias is noticed, whereas it disappears using GSFC orbits, which represents an improvement (especially when linking two reference time series for MSL computation).
Note, that end of 2014 a new GSFC orbit solution (std1404) (see [58]) was released and CNES is working on POE-E (see [62]).

8.3. Error budget of the Jason-2 mission

8.3.1. Introduction

The objective of this part is to provide an estimation of the global error budget of Jason-2 altimeter level 2 products: OGDR, IGDR, GDR (the naming convention of these products is JA2_(O/I/G)PN). Please note that the results presented here have been obtained using GDR data version D. The main goal is to provide a synthetic table with all the global errors estimated versus each level-2 products. The global errors have been estimated for several instrumental parameters but also geophysical corrections. In order to clarify and explain how each error has been calculated, dedicated sections have been performed with illustrations for all the errors described in the table, these dedicated sections are presented in [17]. It is also very important to mention that the errors described here do not take into account long-term errors impacting climate implications as long-term drift, periodic signals (annual, semi-annual or 60-day signals) and isolated jumps for instance. We also do not describe the spatial repartition of errors but only the mean error at global scale. For most of the parameters presented in Table 82, the errors have been averaged spatially and temporally over a short period (∼10 days).

8.3.2. Description of the error content

Several types of errors can be defined in order to describe the error of altimetry measurements. These errors are depending on time and spatial scales. For time scales, the following errors are defined:

- White noise: this error is uncorrelated on time and is due most of the time to the instrumental measurements (altimeter).
- Short-time temporal error (< 10 days) : these errors includes all the error uncorrelated and correlated on time for time scales lower than 10 days. It is important to define these errors for oceanographic applications in relationship with mesoscale or sub-mesoscale studies.
- Medium temporal errors (2 months – 1year) : these errors include all correlated temporal errors at medium scales such as for instance periodic signals (annual, semi-annual,..). The description of these errors is useful for climate application.
- Long-term errors (> 1 year) : these errors include inter-annual and drift. It is the most important for climate applications as the global mean sea level evolution (see also **??**).

The purpose of this document is not to describe all these errors although it would be very useful. On the one hand, currently, we are not able to describe the errors at all these temporal scales and on the other hand there is not a clear way to merge all these errors together to calculate the average error. Therefore, our concern hereafter is to focus only on short-time temporal errors (< 10 days) and provide a synthetic view of these errors. Indeed the Jason-2 cycle duration is about 10 days (like it was already the case for Jason-1 and Topex/Poseidon). The ocean is therefore globally covered within the 10 days period. Several diagnostics based on almost 10 days periods were already developed in the frame of the validation of the altimeter data (see chapter "Method to determine the error" in [17]) and can be used for the estimation of the error budget. Furthermore, the ocean state varies only slightly within a 10 days period (except for high variability regions, such as the Gulf Stream). Notice also, that the spatial repartition of these errors has not been described. Only the global mean error have been calculated in order to simplify the approach.

The method used is detailed in [17].

8.3.3. Description of the error budget

Description of the level-2 Product

All products for Jason-2 (OGDR, IGDR, and GDR) are generated using the MLE4 (maximum likelihood estimator) ground retracking algorithm (note that the MLE3 parameters also available in the products are not analyzed hereafter). Therefore, the figures concerning the altimeter parameters derived from waveforms are identical whatever type (OGDR, IGDR, GDR) of product is used. In reality, this could slightly be different as time differences may occur between 1 Hz OGDR and IGDR data. OGDR, IGDR, and GDR products differ mainly by the orbit, as well as some corrections coming from models (using either predicted or analyzed fields). For these corrections, the performance results are discussed separately for the three product types. The whole GDR data are homogeneous in version D. OGDR and IGDR data have been disseminated in product version D since August 2012.

Description of the parameters/corrections analyzed

The analyzed parameter/corrections have either directly or indirectly an impact on the sea surface height. Hereafter we divide the parameters/corrections in 3 groups. The first group contains the parameters/ corrections for the raw sea-level height calculation. Raw sea surface height is here defined as: Orbit – range – corrections which have a direct impact on the path delay. The second group contains corrections which have not an impact on the path delay, but are used in the final sea surface height computation. Indeed it is necessary to apply them when looking on meso-scale features. The third group contains parameters which have not direct impact on the path delay, but are inputs for corrections used in the sea surface height computation. Hereafter a short description of the analyzed parameters and corrections:

- Parameters and corrections for raw sea surface height calculation:

- Altimeter range. This is the distance from the satellite to the surface of the Earth measured by the altimeter. It's derived from the waveforms. Only its white noise is easily accessible.
- Altimeter Ionosphere correction. The ionosphere correction is necessary to correct for the path delay due to the free electrons of the Earth's Ionosphere. It is computed by using the dual-frequency measurements of the altimeter (Ku- and C-band). This correction is also dependent on the sea state bias.
- Sea state bias. This correction encloses corrections for the electromagnetic bias (troughs of waves tend to reflect altimeter pulses better than do crests, which overestimates the range), skewness bias and tracker bias. The sea state bias correction is highly dependent on significant wave height, but shows also a dependency on wind speed.
- Dry troposphere correction. This correction is necessary to account for path delay due to "dry" gases of the Earth's troposphere. This correction comes from models.
- Wet troposphere correction derived from radiometer. This correction is necessary to account for path delay due to water vapor in the Earth's troposphere. It is derived from radiometer measurements.

- Orbit. It corresponds to the distance of the satellite above the reference ellipsoid. Several techniques to determine the satellite ephemeris exist. The orbit solutions are different for the three products.

- Corrections for final sea-level height:
The following corrections are not actual corrections to the altimeter measurement itself, but they are necessary to apply, when computing meso-scale sea surface height (for example to analyze geostrophic currents). Tides are significant contributors to the observed sea surface height. In order to observe ocean circulation, tides have to be removed as otherwise they dominate the ocean signal. This is possible, as they are nowadays very good modeled.

- Geocentric Ocean tide. The geocentric ocean tide provided in the products is the sum of the ocean tide and the load tide. The ocean tide is related to the luni-solar forcing. The load tide is forced by the ocean tide.
- Pole tide. The pole tide is due to variations in the Earth's rotation and is unrelated to luni-solar forcing.
- Terrestrial tide. The solid earth tide is also related to luni-solar forcing of the earth. In the Jason-2 products the solid earth tide is computed as a purely radial elastic response of the solid Earth to the tidal potential.
- Dynamic Atmosphere Correction (DAC). The Dynamic Atmosphere Correction is the combination of the inverted barometer (hydrostatical response of the sea surface to the atmospheric pressure variation) and the barotropic/baroclinic response to atmospheric forcing (response of the sea surface due to high frequency wind and pressure).

- Altimeter parameters not directly involved in sea-level height calculation:

- Significant Wave Height (SWH). The significant wave height is derived from the waveforms measured by the altimeter. It is an input for the sea state bias correction computation.
- Altimeter Backscattering coefficient (Sigma-0). This coefficient is also retrieved from the altimeter waveforms. It corresponds to the power of the returned radar signal. It is important for the computation of the altimeter wind speed.
- Altimeter wind speed. The altimeter wind speed is derived from the backscattering coefficient, as well as (in a minor proportion) from significant wave height. The wind speed is an input for the sea state bias correction.

Error bugdet
Table 82 shows the specifications and determined errors for each of the three Jason-2 products (O/I/GDR). The studied parameters/ corrections are divided into three groups described in previous part. Furthermore, the specifications and errors of the raw and final sea surface height are shown.
The specifications of the error budget are taken from the Jason-2 handbook ([52]). These specifications seem not always correct, especially when showing different figures (for example for altimeter derived ionosphere correction) between the three product types for altimeter parameters. As mentioned previously, these specifications should be the same for the altimeter parameters, as all three products (O/I/GDR) are generated using the same ground retracking algorithm. Furthermore

some specification figures seem to concern errors and some only the noise part of the error.
Hereafter we choose to show in a first table (Table 82) the errors (noise estimation of the different corrections and parameters). Remind that errors described here do not take into account long-term errors impacting climate implications as long-term drift, periodic signals (annual, semi-annual or 60-day signals) and isolated jumps for instance. For most of the parameters presented in the table, the errors have been averaged spatially and temporally over a short period (10 days). In a second table (Table 83), the white noise (when useful) is shown.
Historically, these figures are specified for 1 Hz measurements with 2 m significant wave height. This is an average situation (the majority of data has wave height around 2 m). Nevertheless, in the following document, this is not always the case (depending on the method used for the error determination).
For some corrections, several error figures are given. This is the case when different methods were used to determine the errors. Furthermore most errors are given as a minimum threshold. **Figures for each parameter/ correction are explained in [17].** For some corrections (the second group concerning corrections for final sea surface height), no figures are given. They did not appear in current altimeter error budgets. But we think, that they also can contain errors when computing sea surface height. The estimation of errors of these corrections will be addressed in the future.

Outlook
GDR-D data have been used for the error budget estimation of Jason-2. Further work will include estimation of errors of corrections such as tides. Furthermore, noise estimation could be extended to sea state bias and altimeter wind speed. A new approach using spectral analysis (not used here) is presented in [69].

	Error budget	Specifications			Error (<10 days)			GOAL
		OGDR	IGDR	GDR	OGDR	IGDR	GDR	
Parameters and corrections for raw sea surface height calculation	Altimeter range	>1.7 cm[a,b,c]			>1.6 - 1.7 cm			1.5 cm[a,b,c]
	Ionosphere	1 cm[d,c]	0.5 cm[d,c]		>1 cm[h] / >0.2 cm[i]			0.5 cm[d,c]
	Sea State Bias	3.5 cm	2 cm		>0.4 cm			1 cm
	Dry troposphere	1 cm	0.7 cm		0.4-0.7 cm	0.3-0.7 cm		0.7 cm
	Wet troposphere	1.2 cm			>0.2 cm			1 cm
	Rms Orbit (radial component)	10 cm[e]	2.5 cm	1.5 cm	>3.7 cm	>1.7 cm	>1.0 cm	1.5 cm
Corrections for final sea surface height	Ocean tide	?			?			?
	Polar tide	?			?			?
	Terrestrial tide	?			?			?
	DAC	?	?		?	?		?
Altimeter parameters	Significant wave height	10% or 50 cm[f]	10% or 50 cm[f]		13 cm			5% or 25 cm[f]
	Wind speed	1.6 m/s	1.5 m/s		1 m/s			1.5 m/s
	Sigma0 (absolute)	0.7 dB			0.11 dB			0.5 dB
Raw sea surface height		11 cm[A]	3.9 cm[A]	3.4 cm[A]	> 4.2 cm[A]/ -	> 2.6 cm[A] - 2.8 cm[B]	>2.1 cm[A] - 2.4 cm[B]	2.5 cm[A]
Final sea surface height		?	?	?	< 5.0 cm[C]	< 4.1 cm[C]	< 4.0 cm[C]	

[a] Ku-band after ground retracking

[b] Averaged over 1 sec

[c] Assuming 320 MHz C-bandwidth

[d] Filtered over 100 km

[h] Non filtered value

[i] Filtered over 300 km

[e] Real time DORIS onboard ephemeris

[f] whichever is greater

[A] Computed with $\sqrt{\sum_i \sigma_i}$ Assuming that errors in the table are uncorrelated (which is not the case).

[B] from formation flight phase (Jason-2/Jason-1)

[C] from cross-over computations of Jason-2 data

Figure 82: Jason-2 Error budget including white noise and correlated errors for timescales less than 10 days

	White noise budget	Specifications			Error (<10 days)			GOAL
		OGDR	IGDR	GDR	OGDR	IGDR	GDR	
Parameters and corrections for raw sea surface height calculation	Altimeter range	1.7 cm[a,b,c]			1.6-1.7 cm			1.5 cm[a,b,c]
	Ionosphere	<1 cm[d,c]	<0.5 cm[d,c]		0.7 cm[h] / 0.1 cm[i]			<0.5 cm[d,c]
	Sea State Bias	<3.5 cm	<2 cm		?			<1 cm
Altimeter parameters	Significant wave height	<10% or 50 cm[f]	<10% or 50 cm[f]		11.2 cm			<5% or 25 cm[f]
	Wind speed	<1.6 m/s	<1.5 m/s		?			<1.5 m/s
	Sigma0 (absolute)	<0.7 dB			0.08 dB			<0.5 dB

[a] Ku-band after ground retracking

[b] Averaged over 1 sec

[c] Assuming 320 MHz C-bandwidth

[d] Filtered over 100 km

[h] Non filtered value

[i] Filtered over 300 km

[f] whichever is greater

Figure 83: Jason-2 Error budget including only the white noise error

8.4. Comparison between DEM and Median tracking modes

The objective of this section is to provide a validation and an evaluation for the Jason-2 DEM mode performance on cycles 209 (March 2014) and 220 (June 2014). This performance is compared to neighboring cycles acquired by Median mode tracking, in the open ocean as well as in coastal areas.

8.4.1. Editing overview

First of all, the quality of the altimeter data is studied and non-valid measurements are removed with the usual standards (see section 3.2.1.).
On this study, two different editing techniques are considered:

- with restrictive threshold values (Flag Open Ocean);
- with threshold values less restrictive only for data close to coast (Flag Coast).

As expected, differences between both flag computation lead to an increased number of valid points with Flag Coast because of the thresholds which are more permissive close to coastal zones.

Cycle	208	209	210	219	220	221
Editing by threshold (open ocean)	2.75%	2.78%	2.77%	3.57%	3.56%	3.28%
Editing by threshold (coastal)	0.84%	0.77%	0.81%	0.94%	0.96%	0.95%
Global Editing	8.36%	8.60%	8.71%	15.23%	16.04%	16.07%

Table 12: Editing summary of the cycle 208, 209, 210, 219, 220 and 221 of Jason-2

Table 12 displays results for the editing of DEM mode cycles 209 and 220 and neighboring cycles in median mode (208,210,219,221). Results are quite similar. Results on the different criteria are higher for cycles 219-221 (June/July 2014) than for cycles 208-210 (February/March 2014), due to the ice coverage evolution during the year.

8.4.2. Ocean Monitoring

The standard deviation of Sea Level Anomaly difference between two successive cycles is represented on figure 84 for cycle 209 (DEM mode) and cycle 208 (Median mode). Theses maps are very similar and do not show neither improvement, nor degradation due to DEM mode. Similar results are obtained in comparison with cycle 210, or comparing cycles 219 and 221 to cycle 220. The Sea Level Anomaly variability seems to be the same, using one mode or the other.
On figure 85 is displayed the mean per pass of the 20 Hz range standard deviation of each cycle. Results are quite similar. As a conclusion, the DEM mode exhibits similar performances with the Median mode over open ocean.

8.4.3. Interest of the DEM mode in coastal zones

One of the improvements of the DEM mode compared to the Median mode should be observed in coastal areas. Since the DEM tracking mode is based on a digital elevation model, the instrument will better detect ocean surfaces in case of land to sea transition. Figure 86 illustrates this behavior. Indeed, histograms of the number of elementary measurements in coastal zones for cycle 209

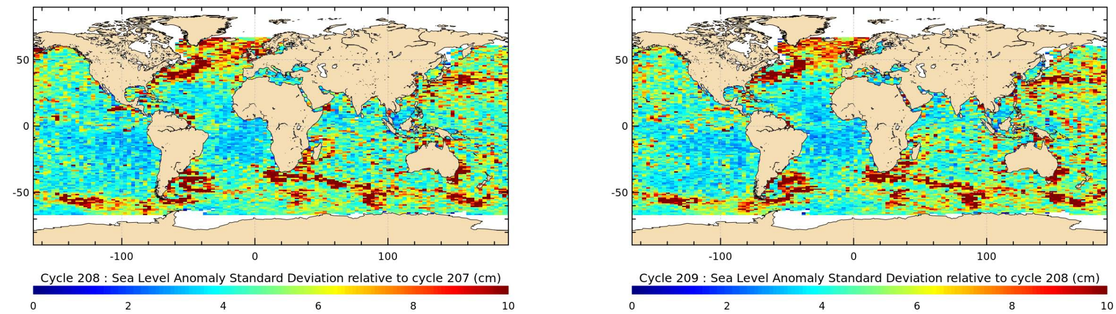

Figure 84: Cartography of the standard deviation of Sea Level Anomaly Difference between two successive cycles. Left : between 208 and 207. Right : between 209 and 208

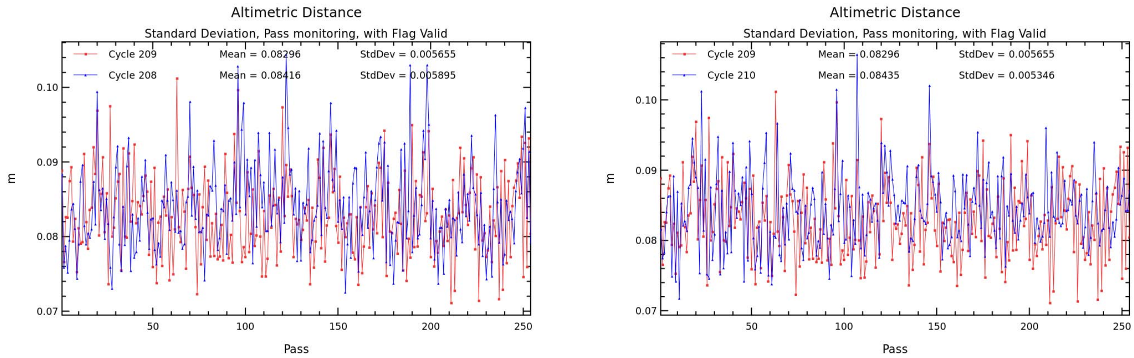

Figure 85: Mean per pass of 20 Hz range standard deviation. Left : cycles 209 and 208. Right : cycles 209 and 210

compared to cycles 208 and 210 show that the DEM mode has between 500 and 1000 more valid points than the Median mode, in agreement with the specification.

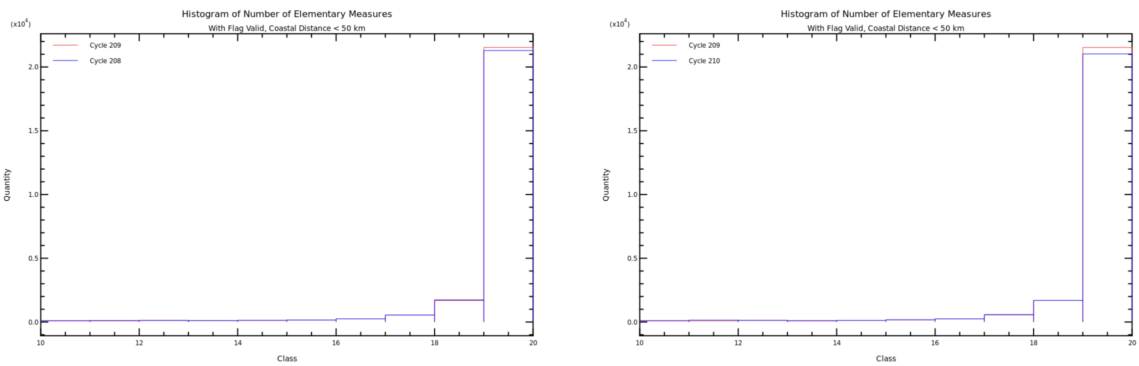

Figure 86: Histograms of the number of Elementary Measurements in coastal zones. Left : comparison between cycles 209 and 208. Right : comparison between cycles 209 and 210

Figure 87 illustrates the percentage of valid points gained by the DIODE/DEM mode over the Median mode, when approaching the coast. This percentage is always positive and confirms that the DEM mode helps to retrieve more observations in coastal zones by 2 or 3%.

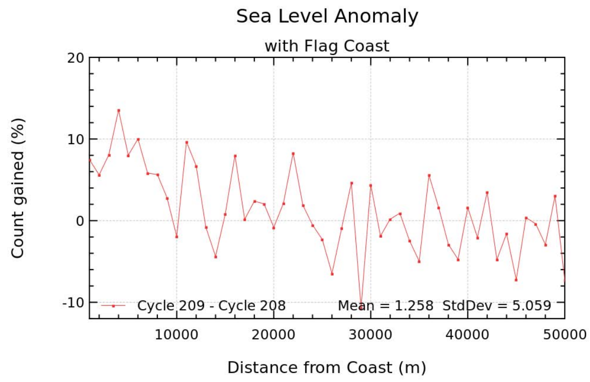

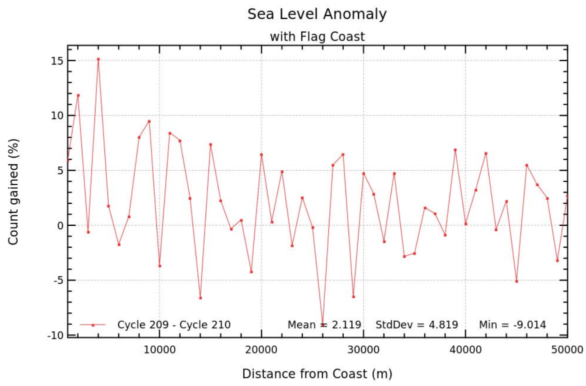

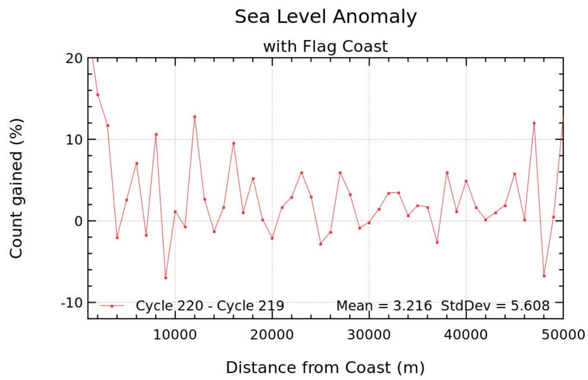

Figure 87: Percentage of Gained points by the DEM mode over Median mode depending on the distance from coast. Left : Comparison between cycles 209 and 208. Right : Comparison between cycles 209 and 210. Bottom : Comparison between cycles 220 and 219

The quality of the gained measurements for cycles 209 and 220 is studied on figures 88, 89 and 90, where the 20 Hz standard deviation of the Range and of the Backscatter Coefficient and the variability of the Sea Level Anomaly is displayed. Results are available for cycle 209 and cycle 220 and respectively compared to cycle 208 and cycle 219. Again, for each parameter, results are similar between both modes and no significant improvement nor degradation can be highlighted. This confirms that the DEM tracking mode allows recovering more data in coastal regions with a quality equivalent to the Median tracker mode.

In conclusion, DEM mode and Median mode have similar results on open ocean, and DEM mode has the same quality in coastal zones but with more valid points than Median mode. So, DEM mode seems to be better than Median mode.

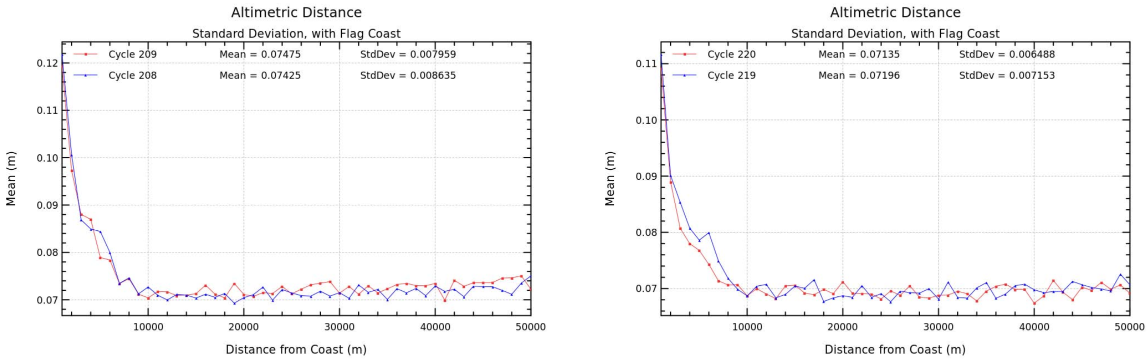

Figure 88: Mean of 20 Hz range standard deviation in function of distance from coast. Red : cycle with DEM mode. Blue : cycle with Median mode

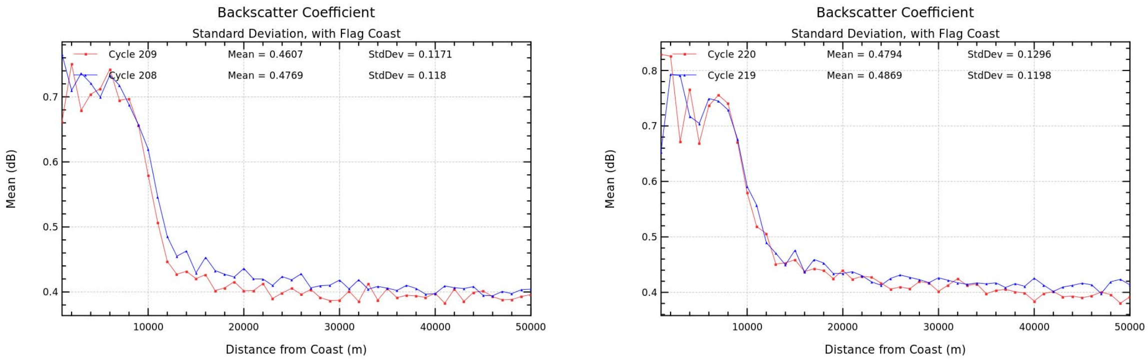

Figure 89: Mean of 20 Hz backscatter coefficient standard deviation in function of distance from coast. Red : cycle with DEM mode. Blue : cycle with Median mode

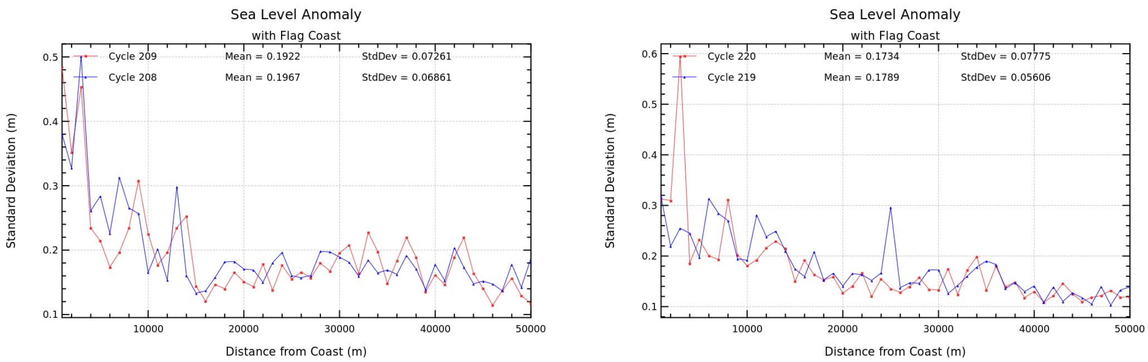

Figure 90: Standard deviation of Sea Level Anomaly depending on the distance from coast. Red : cycle with DEM mode. Blue : cycle with Median mode

8.5. Sensibilty of Jason-2 altimeter during meteorological events

For cycle 216, a large rain event was detected in the altimeter data in the south of Indian Ocean. This event is due to a strong depression, as confirmed by cloud liquid water content measured by the satellite SSMI (see figure 91). Rain events occur very frequently and can alter Ku-band radar altimeter but this one was particularly wide spread, resulting in rain presence along 1000 km of Jason-2 track. The analysis of such an event was motivated by the need to verify how the altimeter data are impacted and how the data are discarded from the products available to the users.

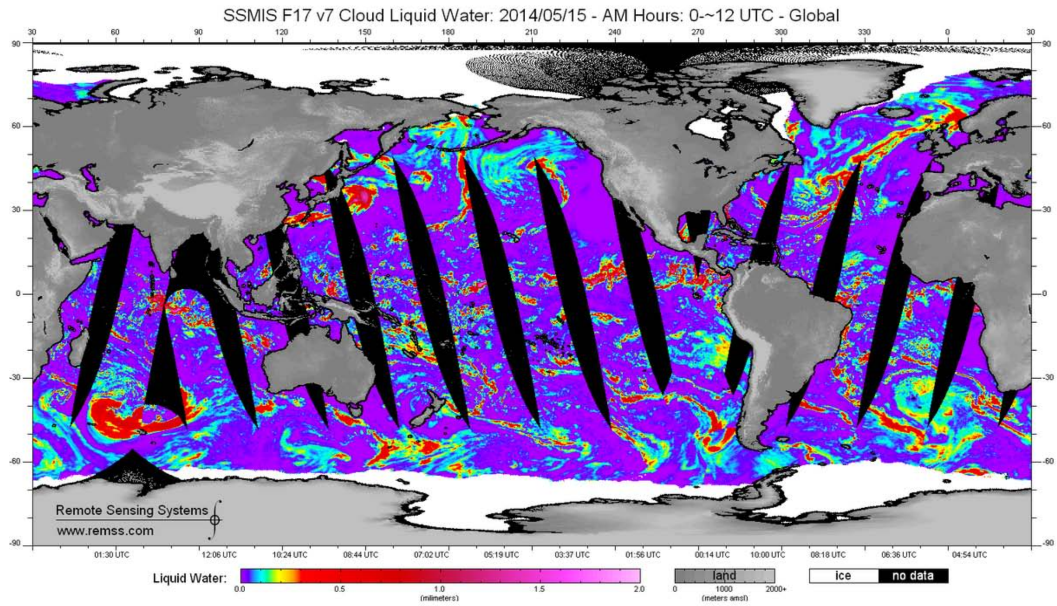

Figure 91: Cartography of cloud liquid water on 2014-05-15 between 00h and 12h

For the detection of rain events, a rain flag is provided in the GDR products. It shows that a large portion of the track was detected as being corrupted by rain, between 34S and 50S (see figure 92 on left). However, we know that this flag is sometimes too restritive. The profile of the SLA is shown for cycle 216, the cycle before and the cycle after the event, after selection of the data without using the rain flag (see figure 92 on right). It confirms that the SLA for cycle 216 is meaningful, the large scale content being quite close from the ones observed 10 day apart, even where the flag is set to rain (Value 1). Even if most of selected data appears to be not impacted by the rain at large scales, some outliers are still present, mainly located in the yellow strip. The Level 3 products distributed on AVISO are shown for the same track (see figure 93). These products are further edited and more filtered than the native GDR 1 Hz data, but the same outliers are also present in the yellow strip, suggesting that the processing used to discard outliers could be further refined.
This analysis shows that the detection of data impacted by rain events could be further improved for Jason-2 in order to find the good trade off between our current processing which is slightly too permissive and the rain flag which is too stringent. One possible outcome could be to make use of several altimeter parameters, such as the waveform mispointing which is disturbed during the strongest rain events (see figure 94 on left) and possibly coupled with cloud liquid water content measured by the AMR (see figure 94 on right).

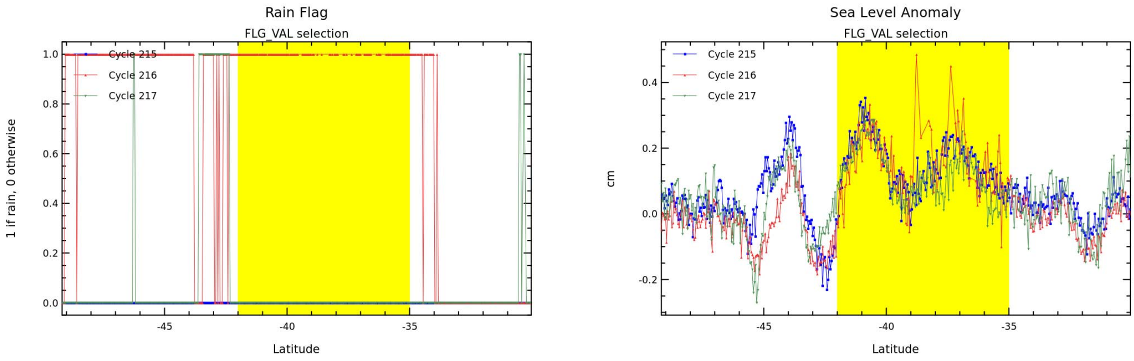

Figure 92: On Left : Monitoring along track of the Flag for rain detection. Right : Monitoring along track of Sea Level Anomaly on the rain zone event for cycles 215 (blue), 216 (red) and 217 (green). The event is highlighted by the yellow strip.

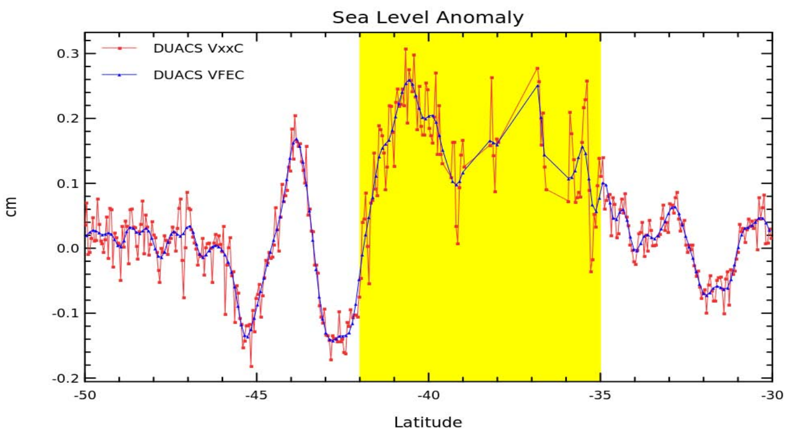

Figure 93: Monitoring along track of Sea Level Anomaly on the rain zone event for cycle 216 in DUACS products, non filtered (red) and filtered (blue). The event is higlighted by the yellow strip.

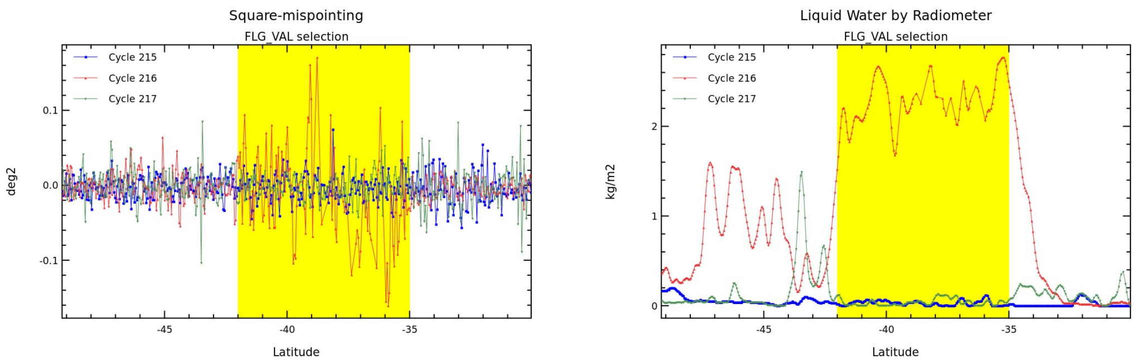

Figure 94: Monitoring along track of some parameters on the rain zone event for cycles 215 (blue), 216 (red) and 217 (green). The event is highlighted by the yellow strip. Right : Mispointing. Left : Quantity of atmospherical liquid water. The event is highlighted by the yellow strip.

8.6. Wind evolution in comparison with models during the period 2011 2013

The detection of long-term instabilities on altimeter backscattering coefficient thanks to wind speed data comparisons from altimeters and models was analyzed by Ablain et al ([3]). On the first hand, this study led to analyze the accuracy of the wind speed evolution over ocean derived from altimeter between 1993 and 2011. On the other hand, the accuracy of the Sigma-0 deduced from the wind speed stability was described for the main altimeter mission (<0.05 dB/year for Jason-1 and 0.2 dB/year for TOPEX). These uncertainties also provide an estimation of the error on the global mean sea level variations.
The Ablain's study has been here updated until 2013 included until the end of Envisat and Jason-1 mission, and for all available period on Jason-2. The same methodology has been applied in order to compare different altimeters and models : global mean wind speed was calculated by box of 2° of latitude and 2° of longitude, with a 10 days averaging and between 66° North and 66° South; then, each box was weighted depending on its area; afterwards, the temporal evolution of global mean wind speed was performed filtering annual signal. Concerning the analysis of Jason-2 data, a drift of 20 cm/s over a 2,5 year period is observed between Jason-2 altimeter and the ECMWF/ERA reanalysis (see figure 95 on left). It is equivalent to a drift of 5 cm/s/year. If this drift was an error on Jason-2, it might correspond to a drift of 0.06 dB on the backscatter coefficient over a 2,5 year period an it would impact the Global Mean Sea Level measurement (via the Sea State Bias) by about 1 mm. However, this potential drift on Jason-2 is currently not demonstrated. First of all, the other altimeter missions are not relevant on this period : Envisat ended in March 2012 thus the period is too short, Jason-1 sigma-0 is impacted by some instability problems on this period maybe in relationship with the end of life, the period covered by SARAL/Altika is too short to be relevant and the Cryosat-2 sigma-0 data are impacted by a strong drift. Therefore, although the operational and reanalysis ECMWF wind speed have a similar behavior on this period (see figure 95 on right), the differences between wind speed derived from altimeters and models can't bring us to a conclusion, and in particular to the detection of a drift of a Jason-2 sigma-0. In addition, the small impact on the Mean Sea Level (about 1 mm) is not detectable by comparison with in-situ measurements. In the next future, it will be important to continue these analyses to pay a great attention on the Jason-2 sigma-0 stability.

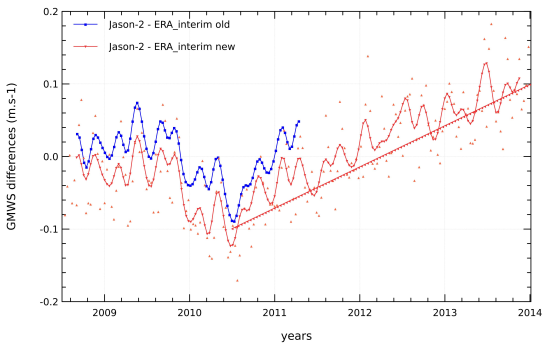

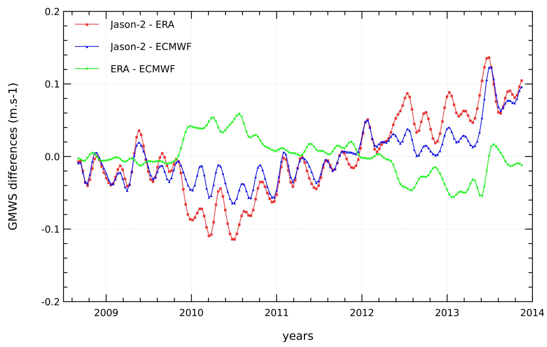

Figure 95: Difference of Global Mean Wind Speed between Jason-2 Altimeter and ERA model (centered). Right : results from the paper [3] (blue) and updated results (red). Left : Jason-2 altimeter - ERA model (red), Jason-2 altimeter - ECMWF model (blue) and ERA model - ECMWF model (green)

8.7. Reduction of the 58.77-day signal in Jason-2 MSL with the latest ocean tide models

Recent works on Global MSL time series highlight a strong 58.77-days signal on Jason-1 and Jason-2 whereas it is smaller on TOPEX/Poseidon.
Results of [Ablain et al., OSTST 2010] show this signal is the aliasing of a higher frequency error inherited from the tide model correction: the semi-diurnal wave S2. They also suggest TOPEX/Poseidon SSH -without tide corrections- contains an error due to the semi-diurnal wave S2. It is then assimilated in tide model corrections using TOPEX/Poseidon data: GOT (Goddard/Grenoble Ocean Tide, GSFC/NASA) and FES (Finite Element Solution, LEGOS / Noveltis / CLS).
When these corrections are used in the computation of TOPEX/Poseidon MSL, most of the error cancels. However, this error is communicated to Jason-1 and Jason-2 MSLs, which explains why it is stronger for these missions than for TOPEX/Poseidon.

With the conclusions of [Ablain et al., OSTST 2010], efforts have been made to improve GOT and FES S2 waves. The present study quantifies the improvements of the latest GOT and FES releases in Jason-2 MSL.

8.7.1. GOT ocean tide model

In the latest GOT release, GOT4.10, TOPEX/Poseidon measurements were not used in the computation of the S2-wave. Instead, Jason-1 and Jason-2 measurements were assimilated. This is actually the only difference with GOT4.8. Fig. 96 shows the amplitude of the 58.77-day signal in the Global MSL of TOPEX/Poseidon and Jason-2 for 3 GOT releases. Results obtained with GOT4.10 clearly show the diminution of the 58.77-day error in Jason-2 GMSL from 3mm to 0.4mm. This goes along with a rise of this error for T/P GMSL, from 1.2 to 2.3 mm. This rise was expected because T/P MSL error is not compensated by the ocean tide error anymore.

The local analysis, see Fig. 97, show the error is located in the Atlantic and Indian oceans at low latitudes, with amplitudes of 1cm, when the SLA is corrected by GOT4.7. With GOT4.10, the 58.77-day error is reduced to 3mm.

Results suggest GOT4.10 is a tremendous improvement - with regard to the 58.77-day signal - for the computation of Jason-2 MSL.

8.7.2. FES ocean tide model

FES ocean tide model, contrary to GOT, is a hydrodynamic model which assimilates altimetric data. GOT, however, is a stochastic model based on altimetric data. This difference implies that FES is less sensitive to altimetry errors.
The latest FES release will be FES2014. However, as it is not available yet, the study is based on a preliminary version. Improvements, by comparison to the previous version FES2012, include a new meshgrid, new standards (PVA2014), assimilation of tide gauges measurements. TOPEX, Jason-1 and Jason-2 are assimilated in the S2-wave.

The Global analysis, see Fig. 98, shows the amplitude of Jason-2 GMSL 58.77-day error remains below 0.6mm while it remains above 1.7mm for TOPEX. These amplitudes are comparable to results obtained with GOT4V10, see Section 8.7.1.. Even though no significant improvement or regression

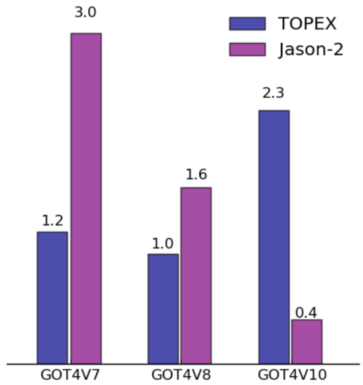

Figure 96: Global MSL 58.77-day signal amplitudes for TOPEX and Jason-2 with GOT ocean tide corrections (mm)

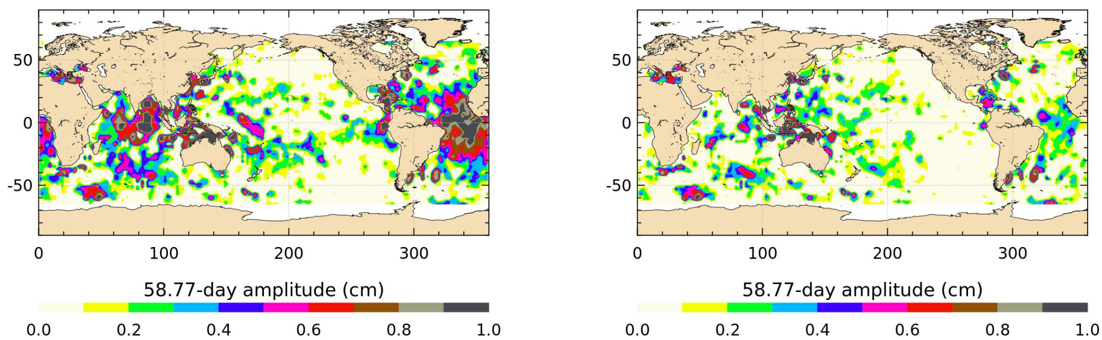

Figure 97: Local amplitude of Jason-2 SLA 58.77-day signal with GOT ocean tide corrections. Right: GOT4.7 ocean tide. Left: GOT4.10 ocean tide.

may be observed in the latest preliminary release FES2014, the error remains low for Jason-2 GMSL.

The local analysis, see Fig. 99, however, shows local 58.77-day error amplitude is significantly reduced in the Indian and the Atlantic oceans, dropping from 6mm to 3mm.

Paradoxically, results suggest no improvement on Jason-2 GMSL 58.77-day error (even though it remains very low), but strong improvements locally. This is due to the local phases of the signal. Hence, FES2014 preliminary version is an improvement for Jason-2 MSL with regard to the 58.77-day error.

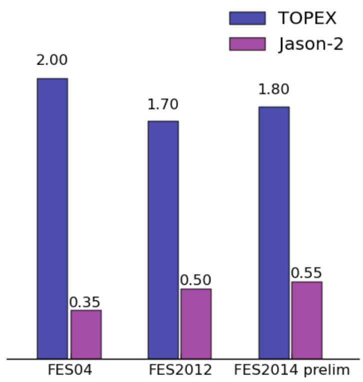

Figure 98: Global MSL 58.77-day signal amplitudes for TOPEX and Jason-2 with FES ocean tide corrections (mm)

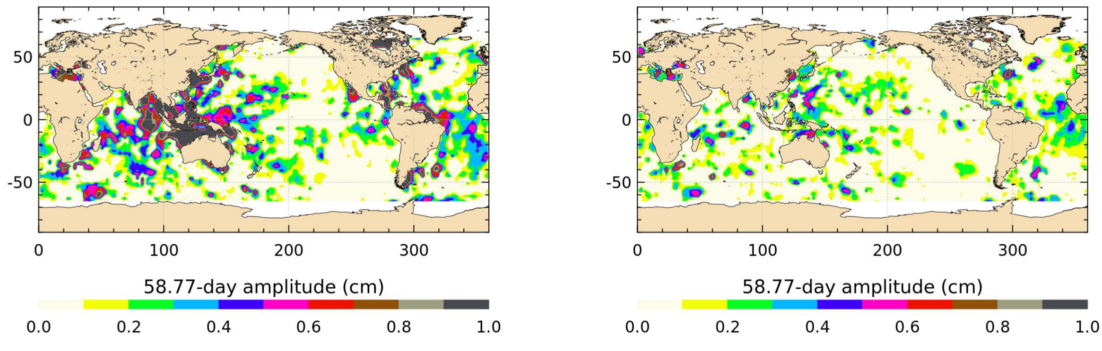

Figure 99: Local amplitude of Jason-2 SLA 58.77-day signal with FES ocean tide corrections. Right: FES04 ocean tide. Left: FES2014 prelim ocean tide.

9. Conclusion

Jason-2 is in orbit since 20th of June, 2008. During the flight formation phase, which lasted 20 cycles (till 2009-01-26), Jason-2 flew with Jason-1 (55s apart) over the same historical TOPEX/Poseidon ground track. This allowed extensive verification and validation of the data, as both satellites observed the same geophysical phenomena. OGDR and IGDR data quality was already approved during OSTST 2008 meeting in Nice. OGDR products were distributed to users since mid-December 2008 and IGDR since mid-January 2009. The GDR production started end of February 2009 and was released in version T to users since August 2009. More than 5 years of GDR data are now available. Note that during 2012, the whole mission was reprocessed in standard GDR-D. During 2013, Jason-2 entered Safe Hold Mode by three times (in February, March and September).

The flight formation phase has shown that Jason-2 data quality is excellent, at least of the same order as the Jason-1 one. The raw data coverage is similar to Jason-1's over ocean and improved in coastal areas. Thanks to the new altimeter tracking modes, the availability of land measurements is significantly improved. The valid data coverage is similar since the additional Jason-2 raw measurements over land are removed by the editing procedure. The additional measurements in coastal areas and over rivers and lakes benefit to projects such as PISTACH (see PISTACH handbook http://www.aviso.oceanobs.com/fileadmin/documents/data/tools/hdbk_Pistach.pdf).

The altimetric parameter analysis has shown a similar behavior compared to Jason-1. Some biases exist as between dual-frequency ionosphere correction, but they are stable. Though Jason-2 radiometer performances are improved especially near coasts, stability problems are observed in Jason-2 IGDR product (small jumps (versus JMR or ECMWF model) occurred in 34 GHz channel). During 2011, these stability problems became more frequent leading to jumps and drifts also in the 18.7 GHz channel. These stability problems are mostly corrected thanks to the ARCS system applied for GDR. For the GDR-D reprocessing, new calibration coefficients were used. According to the JPL, cycles 001 to 113 have climate data record quality calibrations, cycles 114 to 140 have intermediate quality calibrations and cycle 141 and onwards have operational (ARCS) quality calibrations. But even the new calibration coefficients are not able to correct rapid drifts which occur within a cycle (as happened around cycle 120).

The SSH performances analyzed at crossovers or along-track highlight similar performances between Jason-1 and Jason-2. The consistency between both SLA is remarkable with a small geographically correlated signal lower than 1 cm. This signal is removed using GSFC orbits proving the sensibility of the orbit calculation for the detection of geographically correlated biases. The fact that several production centers (CNES, JPL, GSFC) compute different kinds (tri-technic, GPS only, Doris+SRL) of Jason-2 precise orbit solutions, gives also a great opportunity to understand more about the impact of orbit on altimetry data and to explain some of the observed signals.

The flight formation phase between Jason-1 and Jason-2 allowed us to check accurately the Jason-2 mission. As during the Jason-1/TOPEX flight formation phase, we also learned a lot from Jason-1 measurement quality. To balance all these excellent results and especially the quasi-perfect SSH consistency between both missions, both systems can contain similar errors undetectable with the analyzes performed here. Comparisons with external and independent datasets (Tide gauges, Temperature/Salinity profiles, ...) are thus essential to detect potential errors.

The more of 6 years of Jason-2 data show excellent quality. Scientific studies and operational applications therefore benefit from the combination of altimeter data from several missions. The 2012 reprocessing of the whole mission in GDR-D standard has improved the dataset in comparison to the GDR-T standard for meso-scales (improved coherence at crossover points), as well as on longer time scales (coherence between ascending and descending passes is improved).
The Jason-1 mission ended on 21st June 2013, so that cross calibration between Jason-1 and Jason-2 are no longer possible. The whole Jason-1 data will be reprocessed during 2015.
Finally, the launch of the AltiKa mission on 25th of February 2013 allows to complete the altimetry constellation from 2013 onwards, re-occupying the long-term ERS and Envisat ground track. Comparisons between AltiKa and Jason-2 data are available in [22].

The remaining open points which needs further investigation or surveillance are:

- the stability of the AMR
- the monitoring of the backscattering coefficient, as comparison between altimeter wind speed (computed from backscattering coefficient) and ERA-interim wind speed model seems to show a drift
- the remaining signal of approximately 120 days in the monitoring of the ascending/descending crossover differences, though using preliminary POE-E standard seems to strongly reduce them
- the excessive altimeter rain flag
- the sea state bias, which is quite different from the one of Jason-1 (nevertheless new sea state bias look-up tables (presented at OSTST 2012 by Tran et al.[[85]]) are available for Jason-1 and Jason-2)
- the radiometer processing is different between Jason-1 and Jason-2
- there remains a hemispherical bias between Jason-2 and Jason-1 linked to orbit solutions (see Special Investigations chapter in [12]).

10. References

References

[1] Ablain, M., A. Cazenave, G. Valladeau, and S. Guinehut. 2009 : A new assessment of the error budget of global mean sea level rate estimated by satellite altimetry over 1993-2008. *Ocean Sci*, **5, 193-201**. Available at http://www.ocean-sci.net/5/193/2009/os-5-193-2009.pdf

[2] Ablain, M., S. Philipps, 2006, Topex/Poseidon 2005 annual validation report, Topex/Poseidon validation activities, 13 years of T/P data (GDR-Ms).

[3] Ablain, M., S. Philipps, M. Urvoy, N. Tran, and N. Picot (2012) Detection of Long-Term Instabilities on Altimeter Backscattering Coefficient Thanks to Wind Speed Data Comparisons from Altimeters and Models, *Marine Geodesy*, **35:S1, 258-275**. Available at http://www.tandfonline.com/doi/pdf/10.1080/01490419.2012.718675

[4] Ablain, M., G. Larnicol, Y. Faugère, A. Cazenave, B. Meyssignac, N. Picot, J. Benveniste, 2012. Error Characterization of altimetry measurements at Climate Scales. Oral presentation at OSTST meeting, Venice, Italy, 27-28 September 2012. Available at: http://www.aviso.altimetry.fr/fileadmin/documents/OSTST/2012/oral/02_friday_28/04_errors_uncertainties_I/03_EU1_Ablain.pdf

[5] AVISO and PODAAC User Handbook. IGDR and GDR Jason-1 Products. Edition 4.1, October 2008. SMM-MU-M5-OP-13184-CN (AVISO), JPL D-21352 (PODAAC). Available at http://www.aviso.oceanobs.com/fileadmin/documents/data/tools/hdbk_j1_gdr.pdf.

[6] Beckley, B. D. , Zelensky, N. P. , Holmes, S. A. , Lemoine, F. G. , Ray, R. D. , Mitchum, G. T. , Desai, S. D. and Brown, S. T. (2010) Assessment of the Jason-2 Extension to the TOPEX/Poseidon, Jason-1 Sea-Surface Height Time Series for Global Mean Sea Level Monitoring, *Marine Geodesy*, **33:1, 447 - 471**. Available at http://pdfserve.informaworld.com/96442__925511460.pdf

[7] Bertiger, Willy , Desai, Shailen D. , Dorsey, Angie , Haines, Bruce J. , Harvey, Nate , Kuang, Da. , Sibthorpe, Ant and Weiss, Jan P. (2010) Sub-Centimeter Precision Orbit Determination with GPS for Ocean Altimetry. *Marine Geodesy*, **33:1, 363 - 378**. Available at http://pdfserve.informaworld.com/858128__925510150.pdf

[8] Bertiger, Willy , Desai, Shailen D. , Haines, Bruce J., R. DeCarvalho, and A. Dorsey (2010) Jason-2/OSTM Precision Orbit Determination with GPS *Oral presentation at OSTST meetting, Lisbon, Portugal*, Available at http://www.aviso.oceanobs.com/fileadmin/documents/OSTST/2010/oral/19_Tuesday/bertiger.pdf

[9] E. Bronner and G. Dibarboure, May 24th, 2012: Technical Note about the Jason-1 Geodetic Mission. *SALP-NT-MA-EA-16267-CNv1.0*. Available at: http://www.aviso.oceanobs.com/fileadmin/documents/data/duacs/Technical_Note_J1_Geodetic_Mission.pdf

[10] Valladeau, G., S. Philipps. Jason-1 validation and cross calibration activities (Annual report 2009).SALP-RP-MA-EA-21795-CLS, CLS.DOS/NT/10-005.

[11] Valladeau, G., S. Philipps. Jason-1 validation and cross calibration activities (Annual report 2010).SALP-RP-MA-EA-21903-CLS, CLS.DOS/NT/10-332.

[12] Roinard H., Philipps S., Ablain M., Valladeau G., and Legeais J.-F., Jason-1 validation and cross calibration activities (Annual report 2013). Reference: CLS.DOS/NT/13-226. Nomenclature: SALP-RP-MA-EA-22269-CLS. Available at http://www.aviso.oceanobs.com/fileadmin/documents/calval/validation_report/J1/annual_report_j1_2013.pdf.

[13] Philipps, S., M. Ablain, G. Valladeau, and J.-F. Legeais. Jason-2 validation and cross calibration activities (Annual report 2011). Reference: CLS.DOS/NT/12-005. Nomenclature: SALP-RP-MA-EA-22042-CLS. Available at http://www.aviso.oceanobs.com/fileadmin/documents/calval/validation_report/J2/annual_report_j2_2011.pdf.

[14] Philipps, S., M. Ablain, G. Valladeau, and J.-F. Legeais. Jason-2 validation and cross calibration activities (Annual report 2012). Reference: CLS.DOS/NT/12-223. Nomenclature: SALP-RP-MA-EA-22141-CLS. Available at http://www.aviso.oceanobs.com/fileadmin/documents/calval/validation_report/J2/annual_report_j2_2012.pdf.

[15] Roinard, H., Philipps S., Jason-2 reprocessing impact on ocean data (cycles 001 to 020). Comparison of Jason-2 Gdr-D with Gdr-T, as well as with Jason-1 Gdr-C. SALP-RP-MA-EA-22118-CLS. CLS.DOS/NT/12.138. Available at ftp://avisoftp.cnes.fr/AVISO/pub/jason-2/documentation/gdr_d_calval_report/JA2_GDR_D_validation_report_cycles1to20_V1_1.pdf

[16] Roinard, H., S. Philipps. Jason-2 reprocessing impact on ocean data (cycles 001 to 145). Comparison of Jason-2 Gdr-D with Gdr-T, as well as with Jason-1 Gdr-C and Envisat Gdr v2.1. SALP-RP-MA-EA-22140-CLS. CLS.DOS/NT/12.222.

[17] Philipps, S., H. Roinard, M. Ablain, G. Valladeau, and J.-F. Legeais. Jason-2 validation and cross calibration activities (Annual report 2013). Reference: CLS.DOS/NT/13-227. Nomenclature: SALP-RP-MA-EA-22270-CLS. Available at http://www.aviso.oceanobs.com/fileadmin/documents/calval/validation_report/J2/annual_report_j2_2013.pdf.

[18] Ollivier A., M. Guibbaud. Envisat RA2/MWR ocean data validation and cross-calibration activities. Yearly report 2012. SALP-RP-MA-EA-22163-CLS, CLS.DOS/NT/12-292.

[19] A. Ollivier. M. Guibbaud. Envisat RA2/MWR ocean data validation and cross calibration activities (Yearly report 2013). Reference: CLS.DOS/NT/13-290. Nomenclature: SALP-RP-MA-EA-22293-CLS.

[20] M. Guibbaud. A. Ollivier. Envisat RA2/MWR ocean data validation and cross calibration activities (Yearly report 2014). Reference: CLS.DOS/NT/14-253. Nomenclature: SALP-RP-MA-EA-22396-CLS.

[21] S. Philipps. Saral/AltiKa validation and cross calibration activities (Annual report 2013). Reference: CLS.DOS/NT/13-228. Nomenclature: SALP-RP-MA-EA-22271-CLS.

[22] P. Prandi. Saral/AltiKa validation and cross calibration activities (Annual report 2014). Reference: CLS.DOS/NT/14-234. Nomenclature: SALP-RP-MA-EA-22418-CLS.

[23] Valladeau, G.. Validation of altimetric data by comparison with tide gauge measurements for TOPEX/Poseidon, Jason-1, Jason-2 and Envisat. SALP-NT-MA-EA-22157-CLS, CLS.DOS/NT/12-259.

[24] Legeais J.-F. and S. Dupuy. 2012 annual report: Validation of altimeter data by comparison with in-situ T/S Argo profiles for T/P, Jason-1, Jason-2 and Envisat missions. CLS-DOS/NT/12-261. SALP-RP-MA-EA-22176-CLS.

[25] Valladeau G. and Prandi P., 2013:Validation of altimeter data by comparison with tide gauge measurements for TOPEX/Poseidon, Jason-1, Jason-2 and Envisat (Annual report 2013). [CLS.DOS/NT/13-262].

[26] Legeais J.F. and Ablain M., 2013: Validation of altimetric data by comparison with in-situ T/S Argo profiles (Annual Report 2013) [SALP-RP-MA-EA-22281-CLS, CLS.DOS/NT/13-256]

[27] Prandi P., Valladeau G., 2014:Validation of altimeter data by comparison with tide gauge measurements for TOPEX/Poseidon, Jason-1, Jason-2 and Envisat (Annual report 2014). [SALP-RP-MA-EA-22419-CLS, CLS.DOS/NT/15-020].

[28] Prandi P., Legeais J.F. and Ablain M., 2014: Validation of altimetric data by comparison with in-situ T/S Argo profiles (Annual Report 2014) [SALP-RP-MA-EA-22406-CLS, CLS.DOS/NT/15-007]

[29] Boening, C., J. K. Willis, F. W. Landerer, R. S. Nerem, and J. Fasullo (2012), The 2011 La Niña: So Strong, the Oceans Fell, *Geophys. Res. Lett.*, doi:10.1029/2012GL053055, in press.

[30] John T. Fasullo , C. Boening, F. W. Landerer, R. S. Nerem (2013), Australia's Unique Infuence on Global Sea Level in 2010-2011, doi:10.1002/grl.50834, in press.

[31] Boy, François and Jean-Damien Desjonqueres. 2010. Note technique datation de l'instant de reflexion des échos altimètres pour POSEIDON2 et POSEIDON3 *Reference: TP3-JPOS3-NT-1616-CNES*

[32] Brown G.S., "The average impulse response of a rough surface and its application", *IEEE Transactions on Antenna and Propagation*, Vol. AP 25, N1, pp. 67-74, Jan. 1977.

[33] Brown S., S. Desai, and W. Lu "Initial on-orbit performance assessment of the advanced microwave radiometer and performance of JMR GDR-C", *Oral presentation at OSTST meeting, Nice, France, 9-12 november 2008*. Available at http://www.aviso.oceanobs.com/fileadmin/documents/OSTST/2008/oral/brown_calval.pdf

[34] Brown, S., S. Desai, W. Lu, and A. Sibthorpe. 2009. Performance Assessment of the Advanced Microwave Radiometer after 1 Year in Orbit. *Oral presentation at OSTST meeting, Seattle, USA*. Available at: http://www.aviso.oceanobs.com/fileadmin/documents/OSTST/2009/oral/Brown.pdf

[35] S. Brown. 2010. A Novel Near-Land Radiometer Wet Path-Delay Retrieval Algorithm: Application to the Jason-2/OSTM Advanced Microwave radiometer. *IEEE TGRS vol. 48 n °4*. Available at ftp://podaac.jpl.nasa.gov/allData/ostm/preview/L2/AMR/docs/Brown_TGARS_2010.pdf

[36] Cerri, L. , Berthias, J. P. , Bertiger, W. I. , Haines, B. J. , Lemoine, F. G. , Mercier, F. , Ries, J. C. , Willis, P. , Zelensky, N. P. and Ziebart, M. (2010) Precision Orbit Determination Standards for the Jason Series of Altimeter Missions, *Marine Geodesy*, **33:1, 379 - 418**. Available at http://pdfserve.informaworld.com/816985__925509111.pdf

[37] Cerri, L., A. Couhert, S. Houry, F. Mercier. 2011. Improving the long-term stability of the GDR orbit solutions. *Oral presentation at OSTST meeting, San Diego, USA*. Available at http://www.aviso.oceanobs.com/fileadmin/documents/OSTST/2011/oral/02_Thursday/Splinter3POD/05_Cerri.pdf.

[38] Chambers, D., P., J. Ries, T. Urban, and S. Hayes. 2002. Results of global intercomparison between TOPEX and Jason measurements and models. *Paper presented at the Jason-1 and TOPEX/Poseidon Science Working Team Meeting, Biarritz (France), 10-12 June.*

[39] Collard, F. (2005). Algorithmes de vent et période moyenne des vagues JASON à base de réseaux de neurons. BO-021-CLS-0407-RF. Boost Technologies.

[40] Commien, L., S. Philipps, M. Ablain and N. Picot. 2009. SSALTO CALVAL Performance assessment Jason-1 GDR "C"/GDR "b". *Poster presented at OSTST meeting, Seattle, USA*. Available at: http://www.aviso.oceanobs.com/fileadmin/documents/OSTST/2009/poster/commien.pdf

[41] Couhert, A., L. Cerri, F. Mercier, S. Houry. 2010. Status of Jason-1 and Jason-2 GDR orbits. *Talk presented at OSTST meeting, Lisbon, Portugal*. Available at: http://www.aviso.oceanobs.com/fileadmin/documents/OSTST/2010/oral/couhert.pdf

[42] DeCarvalho, R., S. Brown, B. Haines and S. Desai. 2009. Global cross calibration and validation of the Jason-1 and Jason-2/OSTM data products. *Oral presentation at OSTST meeting, Seattle, USA*. Available at: http://www.aviso.oceanobs.com/fileadmin/documents/OSTST/2009/oral/deCarvalho.pdf

[43] Desjonqueres, J.-D., G. Carayon, J.-L. Courriere, and N. Steunou "POSEIDON-2 In-Flight results", *Oral presentation at OSTST meeting, Nice, France, 9-12 november 2008.* Available at http://www.aviso.oceanobs.com/fileadmin/documents/OSTST/2008/oral/desjonqueres.pdf

[44] Desjonquères, J. D. , Carayon, G. , Steunou, N. and Lambin, J. (2010) Poseidon-3 Radar Altimeter: New Modes and In-Flight Performances, *Marine Geodesy*, **33:1, 53 - 79**. Available at http://pdfserve.informaworld.com/542982__925503482.pdf

[45] Dettmering, Denise and Bosch, Wolfgang (2010) Global Calibration of Jason-2 by Multi-Mission Crossover Analysis, *Marine Geodesy*, **33:1, 150 - 161**. Available at http://pdfserve.informaworld.com/315039__925510361.pdf

[46] Dorandeu.,J., M. Ablain, Y. Faugère, F. Mertz, 2004 : Jason-1 global statistical evaluation and performance assessment. Calibration and cross-calibration results. *Marine Geodesy* **27: 345-372.**

[47] Faugère, Y. et al. 2009. The SLOOP project: preparing the next generation of altimetry products for open ocean. *Poster presented at OSTST meeting, Seattle, USA*. Available at: http://www.aviso.oceanobs.com/fileadmin/documents/OSTST/2009/poster/Faugere2.pdf

[48] Faugère, Y. et al. 2010. CROSS-CALIBRATION between ENVISAT and JASON-1/2. *Oral presentation at OSTST meeting, Lisbon, Portugal*. Available at: http://www.aviso.oceanobs.com/fileadmin/documents/OSTST/2010/oral/19_Tuesday/Tuesday_afternoon/faugere.pdf

[49] Jason-2 Version "T" Geophysical Data Records : Public Release, August 2009. Available at : http://www.aviso.oceanobs.com/fileadmin/documents/data/products/Jason-2_GDR_T_disclaimer.pdf

[50] Renaudie C., S. Philipps, 2014: Comparison of the latest GSFC SLR/DORIS std1204 orbits with current orbits for TP,J1 and J2. CLS Ramonville St Agne.

[51] Gourrion, J., Vandemark, D., Bailey, S., Chapron, B., Gommenginger, G.P., Challenor, P.G. and Srokosz, M.A., 2002: A two-parameter wind speed algorithm for Ku-band altimeters, *Journal of Atmospheric and Oceanic Technology.* **19(12) 2030-2048**.

[52] Dumont, J.-P., V. Rosmorduc, N. Picot, S. Desai, H. Bonekamp, J. Figa, J. Lillibridge, R. Sharroo, 2011: OSTM/Jason-2 Products Handbook. CNES: SALP-MU-M-OP-15815-CN. EUMETSAT: EUM/OPS-JAS/MAN/08/0041. JPL: OSTM-29-1237. NOAA/NESDIS: Polar Series/OSTM J400. Available at http://www.aviso.oceanobs.com/fileadmin/documents/data/tools/hdbk_j2.pdf

[53] Hernandez, F. and P. Schaeffer, 2000: Altimetric Mean Sea Surfaces and Gravity Anomaly maps inter-comparisons. AVI-NT-011-5242-CLS, 48 pp. CLS Ramonville St Agne.

[54] Huffman, G. and D.T.Bolvin, 2009: TRMM and Other Data Precipitation Data Set Documentation. Available at ftp://precip.gsfc.nasa.gov/pub/trmmdocs/3B42_3B43_doc.pdf

[55] Imel, D.A. 1994. Evaluation of the TOPEX/POSEIDON dual-frequency ionospheric correction. *J. Geophys. Res.*, **99, 24,895-24,906**.

[56] Lemoine, F.G., Zelensky N.P., Chinn, D.S., et al. (2010), Towards development of a consistent orbit series for TOPEX, Jason-1, and Jason-2 Adv. Space Res., 46(12), 1513–1540, doi: 10.1016/j.asr.2010.05.007 (updated).

[57] Lemoine, F., N.P. Zelensky, S. Melachroinos, D.S. Chinn, B.D. Beckley, D.D. Rowlands, and S.B. Luthcke. 2011. GSFC OSTM (Jason-2), Jason-1 & TOPEX POD Update. *Oral presentation at OSTST meeting, San Diego, USA*. Available at http://www.aviso.oceanobs.com/fileadmin/documents/OSTST/2011/oral/02_Thursday/SplinterPOD/03Lemoine_etal_SWT2011_v01.pdf.

[58] Lemoine F., N.P. Zelensky, D.S. Chinn, B.D. Beckley, D.E. Pavlis, J. Wimert, O. Bordyugov. 2014 : New GSC POD Standards for TOPEX/Poseidon, Jason-1, Jason-2 (OSTM). *Oral presentation at OSTST meeting, Konstanz, Germany.* Available at http://www.aviso.altimetry.fr/fr/coin-utilisateur/equipes-scientifiques/sci-teams.html.

[59] Le Traon, P.-Y., J. Stum, J. Dorandeu, P. Gaspar, and P. Vincent, 1994: Global statistical analysis of TOPEX and POSEIDON data. *J. Geophys. Res.*,**99, 24619-24631.**

[60] MSEs (CNES, NASA, NOAA, EUMETSAT). 2011. GDR Status. *Oral presentation (by N. Picot) at OSTST meeting, San Diego, USA*. Available at http://www.aviso.oceanobs.com/fileadmin/documents/OSTST/2011/oral/03_Friday/Plenary/GDRProducts/02PicotGDR_status_2011.pdf.

[61] Aviso one-satellite-based Mean Sea Level reprocessing, http://www.aviso.altimetry.fr/fileadmin/documents/data/products/indic/msl/MSL_reprocessing_201402.pdf.

[62] Moyard J., E. Jalabert, A. Couhert, S. Rios-Bergantinos, F. Mercier, S.Houry. 2014 : Jason-2 POD status. *Oral presentation at OSTST meeting, Konstanz, Germany.* Available at http://www.aviso.altimetry.fr/fr/coin-utilisateur/equipes-scientifiques/sci-teams.html.

[63] Obligis, E., L. Eymard, M. Ablain, B. Picard, J.F. Legeais, Y. Faugere and N. Picot, 2010. The wet tropospheric correction for altimetry missions: A mean sea level issue.*Oral presentation at OSTST meeting, Lisbon, Portugal.* Available at http://www.aviso.oceanobs.com/fileadmin/documents/OSTST/2010/oral/19_Tuesday/OBLIGIS.pdf.

[64] Ollivier A., Faugere Y., Granier N., 2008: Envisat RA-2/MWR ocean data validation and cross-calibration activities. Yearly report. Technical Note CLS.DOS/NT/09.10, Contract N° SALP-RP-MA-EA-21633-CLS http://www.aviso.oceanobs.com/fileadmin/documents/calval/validation_report/EN/annual_report_en_2008.pdf

[65] Ollivier A., Faugere Y., P. Thibaut, G. Dibarboure, and J.-C. Poisson, 2008: Investigation on the high frequency content of Jason-1 and Jason-2. CLS.DOS/NT/09-027

[66] Ollivier A., M. Guibbaud, Faugere Y. Envisat RA2/MWR ocean data validation and cross-calibration activities. Yearly report 2011. SALP-RP-MA-EA-22062-CLS, CLS.DOS/NT/12-021.

[67] Ollivier A., A. Couhert, V. Pignot, C. Renaudie, S. Phillips, N. Picot, 2014 : Assessment of orbit quality through the SSH calculation towards GDR-E standards. *Oral presentation at OSTST meeting, Constance, Germany*. Available at http://www.aviso.altimetry.fr/fr/coin-utilisateur/equipes-scientifiques/sci-teams.html

[68] Ollivier A., S. Philipps, M. Ablain, A. Edwell, L. Cerri, N. Picot, 2013 : Assessment of Orbit Quality through the Sea Surface Height calculation, New insight in resolving long term and inter-annual signal for climate studies. *Oral presentation at OSTST meeting, Boulder, USA*. Available at http://www.aviso.altimetry.fr/fr/coin-utilisateur/equipes-scientifiques/sci-teams.html

[69] Ollivier A., Dibarboure G., Picard B., Ablain M., OSTST2014, Konstanz - Germany, "Spectral analysis of altimetric signal and errors Towards a spectral error budget of Nadir Altimetric missions" http://meetings.aviso.altimetry.fr/fileadmin/user_upload/tx_ausyclsseminar/files/30Ball0900-2_Pres_OSTST2014_J2_ErrorBugdet_Spectra_Ollivier.pdf

[70] Otten M., C. Flohrer, T. Springer, and W. Enderle. 2011. Generating precise and homogeneous orbits for Jason-1 and Jason-2. *Oral presentation at OSTST meeting, San Diego, USA*. Available at http://www.aviso.oceanobs.com/fileadmin/documents/OSTST/2011/oral/03_Friday/Splinter6POD/01_Otten.pdf.

[71] Peltier, 2004, Global Glacial Isostasy And The Surface of The Ice-Age Earth: The ICE-5G (VM2) Model and GRACE. *Annual Review of Earth and Planetary Sciences*, May 2004, **Vol. 32, Pages 111-149**, doi: 10.1146/annurev.earth.32.082503.144359

[72] Philipps, S., M. Ablain, J. Dorandeu, P. Thibaut, N. Picot and J. Lambin. 2006. SSALTO CALVAL Performance assessment Jason-1 GDR 'B'/GDR 'A'. *Poster presented at OSTST meeting, Hobbart, Australia*. Available at: http://www.aviso.oceanobs.com/fileadmin/documents/OSTST/2006/ablain1.pdf

[73] Picot, N., P. Thibaut, N. Tran, S. Philipps, J.C. Poisson, T. Moreau, and E. Bronner. 2010. New Jason-2 GDR-C standards. *Oral presentation at OSTST meeting, Lisbon, Portugal*. Available at http://www.aviso.oceanobs.com/fileadmin/documents/OSTST/2010/oral/PThibaut_Jason2.pdf.

[74] Picot, N., P. Thibaut, N. Tran, S. Philipps, J.C. Poisson, E. Bronner, C. Garcia and many others. 2011. Jason-2 GDR-D standards. *Oral presentation at OSTST meeting, San Diego, USA*. Available at http://www.aviso.oceanobs.com/fileadmin/documents/OSTST/2011/oral/02_Thursday/Splinter5IP/05NPicot_et_al_OSTST_2011_J2-GDRD-Standards.pdf.

[75] Schaeffer, P., A. Ollivier, Y. Faugere, E. Bronner, and N. Picot. The new CNES CLS 2010 Mean Sea Surface. *Oral presentation at OSTST meeting, Lisbon, Portugal, 18-20 october 2010*. Available at http://www.aviso.oceanobs.com/fileadmin/documents/OSTST/2010/oral/19_Tuesday/Schaeffer.pdf.

[76] Schaeffer, P., Y. Faugere, J.-F. Legeais, A. Ollivier, T. Guinle, and N. Picot (2012). The CNES_CLS11 Global Mean Sea Surface Computed from 16 Years of Satellite Altimeter Data. *Marine Geodesy* **35: sup1, 3-19**. Available at http://www.tandfonline.com/doi/abs/10.1080/01490419.2012.718231

[77] Scharroo, R., J. Lillibridge, and W.H.F. Smith, 2004: Cross-calibration and long-term monitoring of the Microwave Radiometers of ERS, Topex, GFO, Jason-1 and Envisat. Marine Geodesy, 97.

[78] Solar Radio Flux (10.7cm) (daily solar data). Available at http://www.swpc.noaa.gov/ftpmenu/indices/old_indices.html

[79] Thibaut, P. O.Z. Zanifé, J.P. Dumont, J. Dorandeu, N. Picot, and P. Vincent, 2002. Data editing: The MQE criterion. *Paper presented at the Jason-1 and TOPEX/Poseidon Science Working Team Meeting, New-Orleans (USA), 21-23 October*.

[80] Thibaut, P., J.-C. Poisson, A. Ollivier, S. Philipps, and M. Ablain: "Jason-2 waveforms, tracking and retracking analysis", *Oral presentation at OSTST meeting, Nice, France, 9-12 november 2008*. Available at http://www.aviso.oceanobs.com/fileadmin/documents/OSTST/2008/oral/thibaut.pdf

[81] Moreau, T., P. Thibaut, 2009. Etude dépointage Poseidon-3: optimisation de l'angle d'ouverture d'antenne. CLS-DOS-NT-09-028. 15 pp, CLS Ramonville St. Agne.

[82] P. Thibaut. Bilan des activités d'expertise altimétriques menées en 2009 : Lot 2D. SALP-RP-MA-EA-21808-CLS, CLS-DOS-NT-10-029.

[83] Tran, N. , Labroue, S. , Philipps, S. , Bronner, E. and Picot, N. (2010) Overview and Update of the Sea State Bias Corrections for the Jason-2, Jason-1 and TOPEX Missions, *Marine Geodesy*,**33:1, 348 - 362**. Avialable at http://pdfserve.informaworld.com/804727__925502357.pdf

[84] Tran, N., P. Thibaut, J.-C. Poisson, S. Philipps, E. Bronner, and N. Picot. Jason-1, Jason-2 and TOPEX Sea State Bias. Overview and Updates. *Oral presentation at OSTST meeting, Lisbon, Portugal, 18-20 october 2010*. Avialable at http://www.aviso.oceanobs.com/fileadmin/documents/OSTST/2010/oral/TRAN.pdf

[85] N. Tran, S. Philipps, J.-C. Poisson, S. Urien, E. Bronner, and N. Picot. Impact of GDR_D standards on SSB corrections. *Oral presentation at OSTST meeting, Venice, Italy, 27-28 September 2012*. Available at http://www.aviso.oceanobs.com/fileadmin/documents/OSTST/2012/oral/02_friday_28/01_instr_processing_I/01_IP1_Tran.pdf.

[86] World Meteorological Organization. 2010. El Nino/ La Nina Update (30 March 2010). Available at http://www.wmo.int/pages/prog/wcp/wcasp/documents/El_Nino_Mar10_Eng.pdf.

[87] World Meteorological Organization. 2011. El Nino/ La Nina Update (17 November 2011). Available at http://www.wmo.int/pages/prog/wcp/wcasp/documents/El_Nino_Nov11_Eng.pdf.

[88] Zlotnicky, V. 1994. Correlated environnemental corrections in TOPEX/POSEIDON, with a note on ionomospheric accuracy. *J. Geophys. Res.*, **99, 24,907-24,914**

[89] Zawaszki, L., M. Ablain, A. Cazenave, B. Meyssignac. 2014. Confidence envelop of the Global MSL time-series deduced from Jason-1 and Jason-2 altimetric missions. *Poster presentation at OSTST meeting, Constance, Germany, 28-31 October 2014*, Available at http://meetings.aviso.altimetry.fr/fileadmin/user_upload/tx_ausyclsseminar/files/Poster_OSTST14_GMSLUncertainty.pdf